Annex 49

Heat pump prototype developments and testing for nZEB application

Final Report Part 4

Editor:
Carsten Wemhoener
Institute for Energy Technology
Eastern Switzerland University
of Applied Sciences, Rapperswil
carsten.wemhoener@ost.ch

December 2020
Report no. HPT-AN49-5

Published by Heat Pump Centre
c/o RISE – Research Institutes of Sweden
Box 857, SE-501 15 Borås
Sweden
Phone +46 10 16 53 42
Website https://heatpumpingtechnologies.org

Production Heat Pump Centre, Borås, Sweden

ISBN 978-91-89385-31-3
Report No. HPT-AN49-5

Preface

This project was carried out within the Technology Collaboration Programme on Heat Pumping Technologies (HPT TCP), which is a Technology Collaboration Programme within the International Energy Agency, IEA.

The IEA

The IEA was established in 1974 within the framework of the Organization for Economic Cooperation and Development (OECD) to implement an International Energy Programme. A basic aim of the IEA is to foster cooperation among the IEA participating countries to increase energy security through energy conservation, development of alternative energy sources, new energy technology and research and development (R&D). This is achieved, in part, through a programme of energy technology and R&D collaboration, currently within the framework of nearly 40 Technology Collaboration Programmes.

The Technology Collaboration Programme on Heat Pumping Technologies (HPT TCP)

The Technology Collaboration Programme on Heat Pumping Technologies (HPT TCP) forms the legal basis for the implementing agreement for a programme of research, development, demonstration and promotion of heat pumping technologies. Signatories of the TCP are either governments or organizations designated by their respective governments to conduct programmes in the field of energy conservation.

Under the TCP, collaborative tasks, or “Annexes”, in the field of heat pumps are undertaken. These tasks are conducted on a cost-sharing and/or task-sharing basis by the participating countries. An Annex is in general coordinated by one country which acts as the Operating Agent (manager). Annexes have specific topics and work plans and operate for a specified period, usually several years. The objectives vary from information exchange to the development and implementation of technology. This report presents the results of one Annex.

The Programme is governed by an Executive Committee, which monitors existing projects and identifies new areas where collaborative effort may be beneficial.

Disclaimer

The HPT TCP is part of a network of autonomous collaborative partnerships focused on a wide range of energy technologies known as Technology Collaboration Programmes or TCPs. The TCPs are organised under the auspices of the International Energy Agency (IEA), but the TCPs are functionally and legally autonomous. Views, findings and publications of the HPT TCP do not necessarily represent the views or policies of the IEA Secretariat or its individual member countries.

The Heat Pump Centre

A central role within the HPT TCP is played by the Heat Pump Centre (HPC).

Consistent with the overall objective of the HPT TCP, the HPC seeks to accelerate the implementation of heat pump technologies and thereby optimise the use of energy resources for the benefit of the environment. This is achieved by offering a worldwide information service to support all those who can play a part in the implementation of heat pumping technology including researchers, engineers, manufacturers, installers, equipment users, and energy policy makers in utilities, government offices and other organisations. Activities of the HPC include the production of a Magazine with an additional newsletter 3 times per year, the HPT TCP webpage, the organization of workshops, an inquiry service and a promotion programme. The HPC also publishes selected results from other Annexes, and this publication is one result of this activity.

For further information about the Technology Collaboration Programme on Heat Pumping Technologies (HPT TCP) and for inquiries on heat pump issues in general contact the Heat Pump Centre at the following address:

Heat Pump Centre
c/o RISE - Research Institutes of Sweden
Box 857, SE-501 15 BORÅS, Sweden
Phone: +46 10 516 53 42
Website: https://heatpumpingtechnologies.org

Design and Integration of heat pumps for nearly Zero Energy Buildings

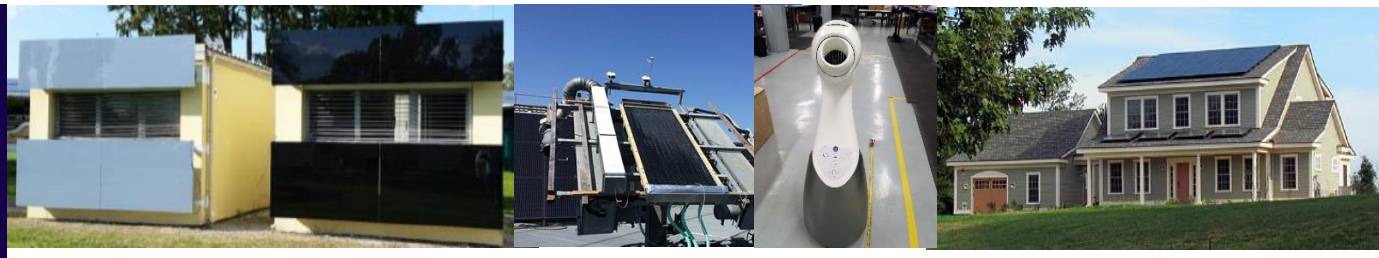

Final report IEA HPT Annex 49 part 4

Heat pump prototype developments and testing for nZEB application

Carsten Wemhoener (Editor)
IET Institute for Energy Technology
OST - Eastern Switzerland University of Applied Sciences, Rapperswil
carsten.wemhoener@ost.ch

Report Annex 49 part 4 Prototypes

December 2020

International Energy Agency
Heat Pumping Technologies

Imprint

IEA HPT Annex 49 "Design and integration of Heat pump for nearly Zero Energy Buildings"

The work presented here is a contribution to the Annex 49 in the Heat Pumping Technologies (HPT) Technical Collaboration Programme (TCP) of the International Energy Agency (IEA)

Operating Agent (Switzerland):
IET Institute for Energy Technology, HSR University of Applied Sciences Rapperswil (now: OST – Eastern Switzerland University of Applied Sciences, Rapperswil)
Prof. Carsten Wemhöner, carsten.wemhoener@ost.ch, Lukas Rominger

Austria:
Unit for energy efficient building UIBK, University of Innsbruck, Austria
Dr. Fabian Ochs Fabian.Ochs@uibk.ac.at, Mara Magni Mara.Magni@uibk.ac.at
IWT Institute of Thermal Engineering, Graz Technical University, Austria:
DI Dr. tech. Andreas Heinz andreas.heinz@tugraz.at
AIT Austrian Insitute of Technology
Philip Horn, Philip.Horn@ait.ac.at, Tim Selke, tim.selke@ait.ac.at

Belgium:
Institute of Aeromechanics, Free University of Brussels, Brussels, Belgium
Prof. Dr. Patrick Hendrick, patrick.hendrick@ulb.ac.be

Germany:
Technical University Georg-Simon Ohm, Nuremberg
Prof. Dr. Arno Dentel, Arno.Dentel@th-nuernberg.de,
Christina Betzold, Christina.Betzold@th-nuernberg.de
Institute of Building Services and Energy Design IGS, University of Braunschweig (now Steinbeis-Innovationszentrum Energie+ (SIZ energie+))
Franziska Bockelmann, franziska.bockelmann@stw.de
TEB GmbH, Vaihingen/Enz
Dr. Thomas Dippel, dippel@teb-online.de

Norway:
SINTEF Community, Trondheim, Norway
Oystein Rønneseth, oystein.ronneseth@sintef.no, Maria Justo Alonso, maria.j.alonso@ntnu.no
NTNU
Prof. Dr. Laurent Georges, laurent.georges@ntnu.no, Dr. John Clauß, john.clauss@ntnu.no
COWI AS
Dr. Ing. Jørn Stene, jost@cowi.no

Sweden
SP Technical Research Institute of Sweden, Borås
Ola Gustafsson, ola.gustafsson@ri.se

United Kingdom:
Renewable Energy, Glen Dimplex, UK
Martin Betz, martin.betz@glendimplex.co.uk

USA:
Oak Ridge National Laboratory, Oak Ridge, Tennessee, United States of America
Van D. Baxter, baxtervd@ornl.gov
National institute of Standards and Technology (NIST)
Vance Payne, Ph.D., vance.payne@nist.gov, Harrison Skye
Center for Environmental Energy Engineering (CEEE), University of Maryland, Maryland, USA
Prof. Reinhard Radermacher, Ph.D., raderm@umd.edu

Abstract

The IEA HPT Annex 49 "Design and integration of heat pumps for Nearly Zero Energy Buildings" deals with the heat pump application as core component of the HVAC system for Nearly or Net Zero energy buildings (nZEB/NZEB) and is structured in the following Tasks:

- Task 1. State of the art in different countries
- Task 2: Integration options for multifunctional heat pumps in nZEB
- Task 3: Field monitoring of marketable and prototype heat pumps in nZEB
- Task 4: Design and control of integrated heat pumps for nZEB

Besides the monitoring of marketable heat pumps treated in the Annex 49 report part 2, also prototype heat pumps for the application in nearly Zero Energy Buildings have been developed and tested in Annex 49, which are treated in this report.
Thereby, the developments were dedicated to highly integrated heat pumps developments, on the one hand regarding the functionality of the heat pump, i.e. multiple building integrated services in one packaged unit, and on the other hand regarding compactness of the components/unit. Moreover, the integration of cooling function has been a focus of the developed prototypes:
At IWT of TU Graz, a façade integrated cooling device with 2 kW cooling capacity has been developed by simulations, prototyping and monitoring in two test cells of the campus of Graz Technical University. The prototype heat pump is covered by façade integrated PV-modules, which are sufficient to supply the module during summer cooling operation due to good load match. The unit can cover about 40% of the space heating demand of the adjacent room for Graz climate data. Different operation modes like grid independent and grid coupled operation, with and without battery storage as well as different cooling options by fan coils or cooling ceiling have been investigated. Further developments encompass façade integration of larger units.
At the OST Eastern Switzerland University of Applied Sciences, an unglazed absorber component has been tested for night time cooling application. The components is already market available for space heating and DHW application, and the objective is to integrated free cooling function in the system configuration. Cooling capacities, though, are strongly depending on the weather conditions. At clear sky and moderate nighttime temperatures between 23-13 °C, cooling capacities up to 250 W/m^2 have been measured, while for cloudy sky values are in the range of 100 W/m^2 were measured.
At the CEEE of the University of Maryland, a roving comforter (RoCo) unit, which is a personal-sized heat pump that cools indoor air to guarantee occupants comfort has been developed as several prototypes and is now in the market introduction. Energy analysis in office buildings for 9 climates revealed that RoCo can provide up to 49% energy savings in mild climate, such as San Francisco, CA, and 9% energy savings in hot climate, such as Phoenix, AZ. PCM development is another focus of the project, both regarding good latent heat capacity and thermal conductivity as well as regarding lowering costs and VCC integration. Field testing showed that RoCo can provide 10 W effective cooling, reducing body temperature by 1 K and heart rate by 9 BPM. Most people expressed a better thermal sensation with RoCo.
At the ORNL a long-term development of the Integrated Heat Pump (IHP) for the space heating and cooling as well as DHW and dehumidification function has been carried out. A ground-source and three air-source variants have been designed, lab tested and simulated and subsequently field testing. Field tests results for the different prototypes variant are summarised with implications to market state and introduction. While the ground-source variant is already on the market for several years, for the gas-driven air-source variant, a value engineering is carried out in order to improve cost-competitiveness.
At NIST campus the Net Zero Energy Residential Testing Facility (NZERTF) has been designed and operated for several years. The test house with tuneable loads is a dedicated testing platform for nZE technologies. As contribution to the Annex 49 two air source heat pumps, a conventional ducted system and a small duct high velocity system has been extensively testing in space heating and cooling mode. Further testing incorporate among other also the ground-source IHP variant.

Contents

1 Prototype heat pump developments and monitoring

Prototype developments of heat pumps for nZEB application mainly focus on highly integrated heat pump system layout, which can serve multiple building functions. This is partly dedicated to layout and design of the prototype itself, and partly also to the testing and monitoring of already developed prototypes, e.g. for the Integrated Heat Pump (IHP) prototype developed in frame of IEA HPT Annex 32 and Annex 40. On the other hand, also testing on the test rigs are reported, as for the Net Zero Energy Residential Testing Facility at NIST, which was developed as dedicated testing facility for nZEB technologies on the NIST campus, and component test rig measurements performed at the solar test rig of the University of Applied Sciences Rapperswil. In the following an overview of the prototype development, testing and monitoring of prototypes is given.

1.1 Overview

The **façade-integrated heat pump prototype at the IWT at TU Graz, Austria,** is intended as self-sustained cooling device covered by a PV façade module, with delivers enough cooling capacity for the respective office room behind the facade. The prototype has been modelled and investigated by simulations for different design and operational boundary conditions.Furthermore, the prototype systems have been built and monitoring in two test cells at the campus of Graz University of Technology. Different options are integrated in the prototype, e.g. a use of different cooling systems like air-based fan coils or water based TABS or grid independent operation with or without an electric battery storage vs grid-connected operation. Both simulation and monitoring show a feasible operation of the prototype development, while also further optimisation can be applied for future designs.

A **prototype solar absorber component with surface wetting** has been tested on the **test rig of HSR Rapperwil, Switzerland** in order to integratea radiative and evaporative free-cooling operation into solar source heat pump systems. In Switzerland so-called solar ice systems, which include and ice storage with solar thermal regeneration as only heat source are on the market and several installation are spread around Switzerland. However, currently the system is only used in space heating and DHW application, while the system configuration would allow the integration of the freecooling operation, addressing growing cooling requests also in residential buildings. Test rig measurement have been carried out to characterise the cooling capacities at different weather boundary conditions in order to evaluate freecooling shares for different applications. As variant the system can also be used for recooling operation of an active cooling mode for the heat pumps in reverse operation as chiller.

The **Roving Comforter (RoCo) development at CEEE, University of Maryland, College Park, MD, USA** is a personal cooling device dedicated for the application in office buildings. The development was started in 2015 with a roving function, which, however, has been removed in later prototypes. The report shortly introduces the latest prototype version, which is close to commercialisation. For this version, on the one hand energy saving compared to common reference cooling systems are reported, and on the other hand, the development and linked material research of the integrated PCM recooler are described.

The PCM recooler absorbs the waste heat from the active cooling by the heat pump chiller and enables longer operation of the RoCo device without a regeneration of the stored waste heat from the cooling. In order to combine good latent heat capacity with good heat conduction in the material, a graphite enhanced PCM was investigated by lab testing and in prototype application.

The field monitoring of **ground-source integrated heat pump (IHP) in Knoxville, TN, and Oklahoma, USA**. The IHP development at the Oak Ridge National Laboratory already started in the frame of IEA HPT Annex 32 with conceptual and design studies and lab and field testing in Annex 40, and was continued in IEA HPT Annex 49. In Annex 32 two principle prototype variants have been develop, a ground-to-air variant and an air-to-air variant. In the frame of two field monitoring campaign is Knoxville and Oklahoma, the IHP has been monitored in two institutional/ commercial buildings. The ground-to-air prototype is already on the market by the manufacturer Climate Master and one of the most efficient heat pumps for nZEB application.

For the **air-source integrated heat pump (IHP)** prototype three embodiments have been developed with manufacturing partners, of which are two electric-driven and one natural gas engine-driven. All three AS-IHP developments have reached the prototype packaged system stage and have completed field evaluation. Electric AS-HP Concept 1 is suited for residential applications with R410A and a 10.6 kW has been designed. Field test took place in **Knoxville TN.** Electric AS-HP Concept 2 is a two box system, which separates the DHW and dehumidification function from the space heating and cooling in a separate unit and has also been field tested in Knoxville, TN. The gas engine-driven concept has been field tested for a commercial unit in Las Vegas, NE. A prototype for residential application has also been developed, but production cost turned out to be too high. Therefore, currently, a value engineering is ongoing to reduce cost and enhance market competitiveness.

The **Net Zero Energy Residential Testing Facility NZERTF at NIST, Gaithersburg, MD, USA** is a testing facility for dedicated nZE System Technology. In IEA HPT Annex 49 two different air-to-air heat pumps were intensively tested in the NZERTF, a conventional ducted air-to-air system as a reference and a high velocity small duct air-to-air heat pumps system. The first heat pump was a two-stage, 7 kW (2 ton) system having a rated seasonal energy efficiency ratio (SEER) of 15.8, and a rated heating seasonal performance factor (HSPF) of 9.05. This air-source heat pup (ASHP) utilized a conventional the central air-duct system for distribution of conditioned air. The second HP was a variable-speed, 10.6 kW (3 ton) system with rated SEER of 14 and HSPF of 8.35. This ASHP used a smaller size, high velocity central air-ducted distribution. These two systems operated side-by-side, using separate supply ducts and a common return duct, on a weekly alternating schedule. The systems have been compared for both space heating and cooling application and thoroughly documented in this report. Further investigation will comprise among other also the detailed testing of the ground-source integrated Trilogy heat pump of Climate master, which is market available.

2 Façade integrated cooling device – Graz, AT

The cooling demand of buildings is constantly increasing. The predominant architectural style with large-scale glazing, increasing comfort requirements and changing climatic conditions are the driving forces behind this trend. Currently, common cooling systems consume large amounts of mostly fossil energy and are often unsatisfactory in their technical planning and implementation as well as in their architectural integration. On the one hand, this is due to the system configuration, which has to be developed individually from case to case, and on the other hand it is caused by the limited production possibilities on-site. In contrast, decentralized systems offer the possibility of a high degree of prefabrication, quick and easy installation and low error-proneness.
The aim of the project COOLSKIN was to design decentralised façade-integrated systems for space cooling. Due to the very good temporal coincidence of available solar radiation and the cooling load occurring in the building, as well as decreased costs for photovoltaic modules over the last ten years, the use of solar energy for such kind of systems seems obvious. The solar radiation onto the façade surface is converted directly or with a time delay into cooling energy and released to the adjacent room. Energetically the system should be as self-sufficient as possible thus require as little energy supply from external sources as possible. In contrast to conventional cooling systems, not only the system components, but the entire system can be configured and prefabricated industrially.
The COOLSKIN project was subdivided into several phases:

1. Evaluation of promising system configurations
2. Dimensioning and construction of a functional model
3. Implementation and monitoring in an outdoor test under real operating conditions

In the first project phase, a comparison of different possible variants of decentralised PV-driven façade-integrated compression cooling systems was carried out under defined boundary conditions with regard to climate, geometry and use by means of detailed system simulations. This work is documented in this report together with results from a monitoring of the functional model that was built within the project.

2.1 Evaluation of System configurations

2.1.1 Boundary conditions and simulation setup

2.1.1.1 Building and climate

An office room with an occupancy of three persons was defined and built as a thermal building model in the simulation environment TRNSYS 17 (Solar Energy Lab, 2017) The room has a net floor area of 25 m², with the facade facing south, see Figure 1. The used wall constructions and U-values are summarized on the right side of the Figure. It is assumed that the room is located in an intermediate floor, so that there is no heat exchange via floor and ceiling. The same applies to the partition walls, as it is assumed that an equally conditioned room is adjacent to the left and right. Behind the room, as shown in Figure 1 on the left, there is an additional corridor zone which is not conditioned but is in thermal contact with the offices via the interior walls and doors.
A façade configuration was defined in terms of the arrangement and dimensions of the glazing surfaces, as shown in Figure 1 (left, bottom). Assuming that the total façade area minus the window area is covered with PV, the total PV area is 10 m², whereby in the simulations the PV area was varied from 2 to 10 m².
External shading was assumed for the windows, which is activated with a shading factor of 0.75, if the room temperature rises above 24 °C, and deactivated again, if it drops below 22 °C. Ventilation was defined with 90 m³/h in the presence times from 8:00 to 18:00 hours from Monday to Friday. A typical occupancy profile according to (SIA, 2015) was assumed, with heat gains of 70 W and a moisture input of 80 g/h per person present. Heat gains for appliances were set at a maximum of 15 W/m², again assuming a typical hourly profile on working days according to SIA 2024 (2015), resulting in an annual sum of 36 kWh/m².

The lighting is switched on from 8:00 to 18:00 on working days with heat gains of 7 W/m², when the solar radiation on the horizontal is lower than 120 W/m², and switched-off again, when the radiation exceeds 200 W/m². This results in a heat gain of 10 kWh/(m²a).

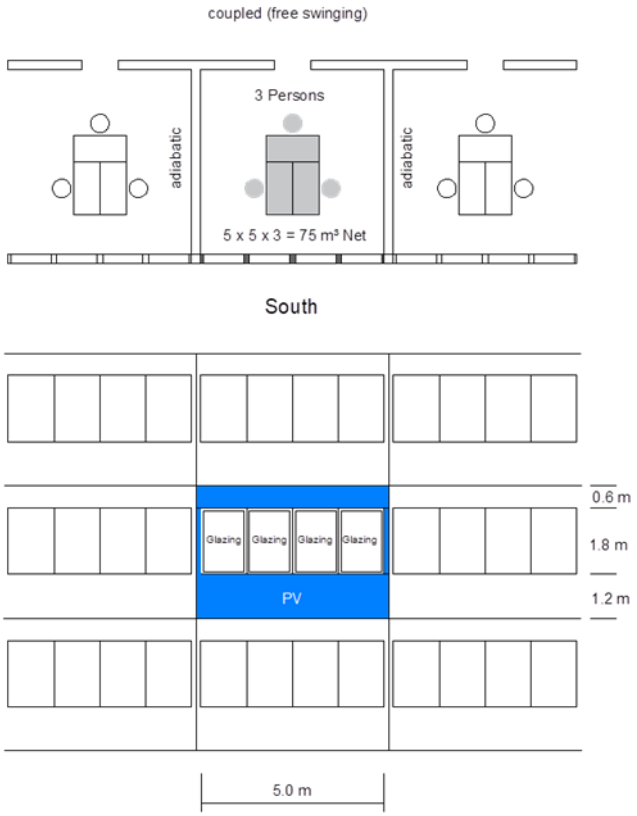

Fassade, opaque	d [m]	λ [W/(mK)]	R [m²K/W]	
steel	0.008	15.00	0.001	
insulation	0.033	0.04	0.825	
steel	0.008	15.00	0.001	
		Σ	0.826	[m²K/W]
		h i	0.130	[m²K/W]
		h e	0.040	[m²K/W]
		Rges	0.996	[m²K/W]
		Uges	1.004	[W/m²K]

Partition wall, adiabatic	d [m]	λ [W/(mK)]	R [m²K/W]	
plasterboard	0.030	0.21	0.142	
insulation	0.140	0.04	3.500	
plasterboard	0.030	0.21	0.142	
		Σ	3.784	[m²K/W]
		h i	0.130	[m²K/W]
		h e	0.040	[m²K/W]
		Rges	3.954	[m²K/W]
		Uges	0.253	[W/m²K]

Partition wall	d [m]	λ [W/(mK)]	R [m²K/W]	
plasterboard	0.020	0.21	0.095	
insulation	0.109	0.04	2.725	
plasterboard	0.020	0.21	0.095	
		Σ	2.914	[m²K/W]
		h i	0.130	[m²K/W]
		h i	0.130	[m²K/W]
		Rges	3.174	[m²K/W]
		Uges	0.315	[W/m²K]

Ceiling, adiabatic	d [m]	λ [W/(mK)]	R [m²K/W]	
wallboard	0.050	0.17	0.295	
air (massless layer)	0.250		0.169	
concrete	0.300	2.10	0.143	
		Σ	0.607	[m²K/W]
		h i	0.130	[m²K/W]
		h i	0.130	[m²K/W]
		Rges	0.867	[m²K/W]
		Uges	1.154	[W/m²K]

Window				
g-value			0.59	[-]
U glazing			0.59	[W/m²K]
U frame			2.08	[W/m²K]

Figure 1: Office room: floor plan (top left), front view / facade configuration (bottom left), details of wall construction (right)

The building is located in Graz (latitude 47.07°), and an average climate data set of the years 2001-2010, which was generated with the software METEONORM (Meteotest, 2015) is used. The most important data of the climate used are: average / min / max ambient temperature: 10.7/-12.3/32.7 °C, heating degree days HDD20/12: 3102 Kd, cooling degree days CDD18.3: 256 Kd, global radiation on the horizontal: 1206 kWh/a. Based on these assumptions, an ideal heating and cooling of the office space results in an annual maximum heating load of 975 W and a maximum cooling load of 978 W (sum of sensitive and latent).

2.1.1.2 PV-HP system concept

The system concept under consideration consists of a PV system, a DC/AC inverter, a battery, a grid connection and a reversible compression heat pump. Depending on the system variant under consideration, not all system components are used, as described in section 2.1.1.3. The complete system with all components is shown in Figure 2. The solar power generated by the PV system is converted into alternating current by an inverter, an integrated charge controller feeds the DC PV current into the battery for later use, if required. If the available power from the PV and/or the battery is insufficient to cover the system demand, it is assumed that the remaining power is drawn from the grid. The battery is modelled with a constant efficiency of 0.85 over the whole range of possible charging and discharging capacities and independent of the state of charge.

The efficiency of the DC/AC inverter is assumed to be a constant 0.94. Three different battery capacities (500, 1,000 and 2,000 Wh) are considered in the simulations to evaluate the influence on the system performance. It is assumed that the capacity can be fully utilized in each case. The photovoltaic modules are simulated with the model Type 94a (TRNSYS 17, 2014), the main parameters correspond to the modules used for the field test in the project and are listed in Table 1. Six different sizes of the PV system from 2 to 10 m² were used in the simulations for all considered system variants.

An air-to-air heat pump with a reversible refrigerant circuit is used for heating and cooling. In cooling mode, the room is cooled via the evaporator and the condensation heat is transferred to the ambient air.

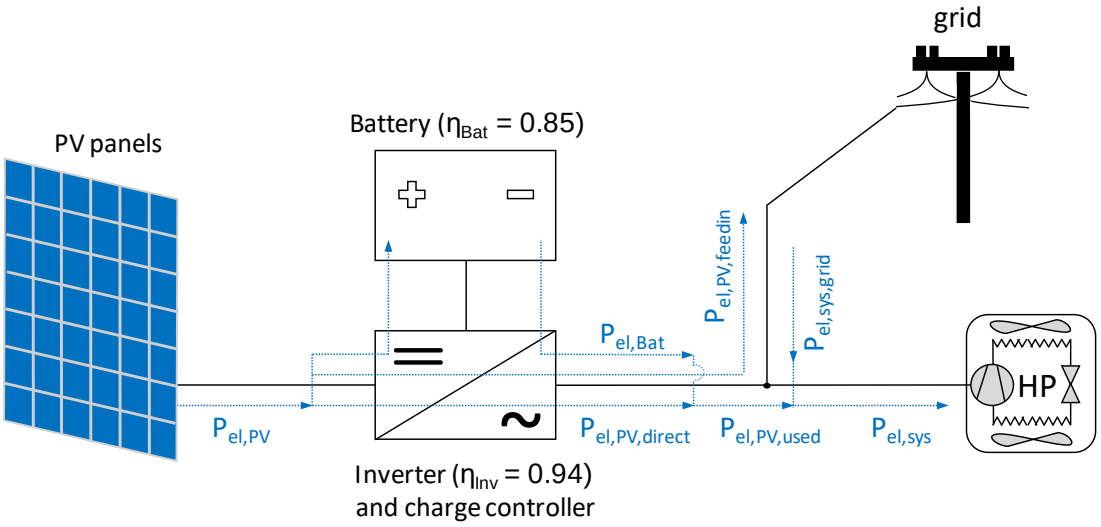

Figure 2: Schematic of the system concept with all components that occur in the different system variants (battery, grid connection)

In heating mode, the ambient air is used as a heat source for the evaporator and the condensation heat is used to heat the room. The refrigerant circuit is modelled with the heat pump model Type 887, which is a further development of the model Type 877 described in Dott et al. (2013) and Hengel, Heinz and Rieberer (2014). The model parameterisation was done out according to the refrigerant circuit built in the project, which fits well for the boundary conditions used here in terms of size. The most important parameters and assumptions used in the simulations are summarized in Table 1. It is assumed that the compressor has a speed range of 12 to 100%, which is advantageous for some of the control strategies considered here, regarding the ability to modulate and adapt the power consumption of the heat pump to the available PV power.

The system was implemented in TRNSYS with the possibility to simulate all system and control variants described in the next section. All simulations were carried out for one year with a time step of one minute, and a pre-simulation time of one month prior to the simulation year to be evaluated.

Table 1: Parameters of the PV and heat pump model

Photovoltaic System (Type 94)	
Power MPP (Maximum Power Point)	137.8 W/m²
Temperature coefficient short circuit current	0.0044 A/K
Temperature coefficient open circuit voltage	-0.1216 V/K
Heat pump (Type 887)	
Refrigerant	R134a
Compressor speed range	12 – 100 %
Heating capacity[1] @ A7A20	1.59 kW
COP[1] @ A7A20	4.04
Cooling capacity[1] @ A35A27	2.31 kW
EER[1] @ A35A27	3.46
Air flow rate, el. consumption fan indoor HX	400 m³/h, 30 W
Air flow rate, el. consumption fan outdoor HX	400 m³/h, 30 W

[1] at max. speed

2.1.1.3 System and control variants

With regard to system configurations and control, different variants were simulated. Figure 3 shows simulation results of five exemplary summer days for illustration and a better comprehensibility of the used system configurations and control strategies, which will be discussed in the following paragraphs.

All variants shown in the figure were simulated with 6 m² of PV and (when using a battery in the respective system) a battery capacity of 2 kWh. The results of the annual simulations for these system and control variants are discussed in section 2.1.3.

No Battery, no Grid connection (nBnG)
In this variant it is assumed that the system is not connected to the grid and that there is no battery installed. Thus system operation is only possible if the electricity consumption is lower than or equal to the current PV electricity yield. This is probably not a very practical case, since a system without grid connection is usually not built without a storage. Nevertheless, it shall be examined here what is possible with such a system compared to the other variants.
In the simulation it is assumed that the compressor speed can be adapted in order to match the system consumption to the PV yield, taking into account the possible compressor speed range. Concerning the room temperature control the system is switched-on and off using a hysteresis of 1 K above and below a set room air temperature, which is chosen with 22 °C for heating and 25 °C for cooling.
In Figure 3 (nBnG) the resulting system behaviour can be seen for five exemplary summer days. In the first half of the first day the system is periodically switched-on and off (control signal CF_{HP}), as the room temperature oscillates around the set temperature $t_{set,c}$. During the rest of the time CF_{HP} remains on, as the room temperature cannot be cooled below the set temperature minus the hysteresis. However, as explained before, the compressor is only switched-on, if enough PV yield is available.

With Battery, no Grid connection (wBnG)
If a battery is installed, the load can be decoupled from the PV yield, meaning the system can be operated whenever the state of charge of the battery or the current PV yield allows it. The system is controlled in a way to reach and hold the set room temperature t_{set} by varying the compressor speed via a PID controller. Figure 3 (wBnG) shows how the system can be operated depending on the battery´s state of charge (1..full, 0..empty). Compared to system nBnG it is possible to maintain lower room temperatures, as the system can also be operated, if sufficient PV yield is currently not available.

No Battery, with Grid connection (nBwG)
In this variant the system is connected to the grid, so it can be operated whenever necessary. The room temperature control is assumed to be the same as for system wBnG, using the same PID controller and set temperatures. Adaptation of the compressor speed in order to match the consumption with the current PV yield like in nBnG is not performed here, so the control can be considered as independent of the PV yield. With this type of control and using no battery the utilization of PV electricity is more or less random, only when there is a coincidence between the PV yield and system operation. As it can be seen in Figure 3 (nBwG), a smaller portion of the available PV electricity can be used compared to nBnG, as system operation is performed independently of the PV yield, leading to significant quantities of electricity drawn from the grid. The energy exchange with the grid is represented by $P_{el,grid}$ ($P_{el,grid} > 0$ ... energy consumption, $P_{el,grid} < 0$ ... energy feed-in).

With Battery, with Grid connection (wBwG)
If the system is connected to the grid and the control is independent of the PV yield, the advantage of using a battery becomes obvious when comparing wBwG with nBwG in Figure 3. Here grid consumption occurs only on day four after the battery is fully discharged, as only low PV yield is available. Compared to nBwG a much lower energy amount is fed into the grid.

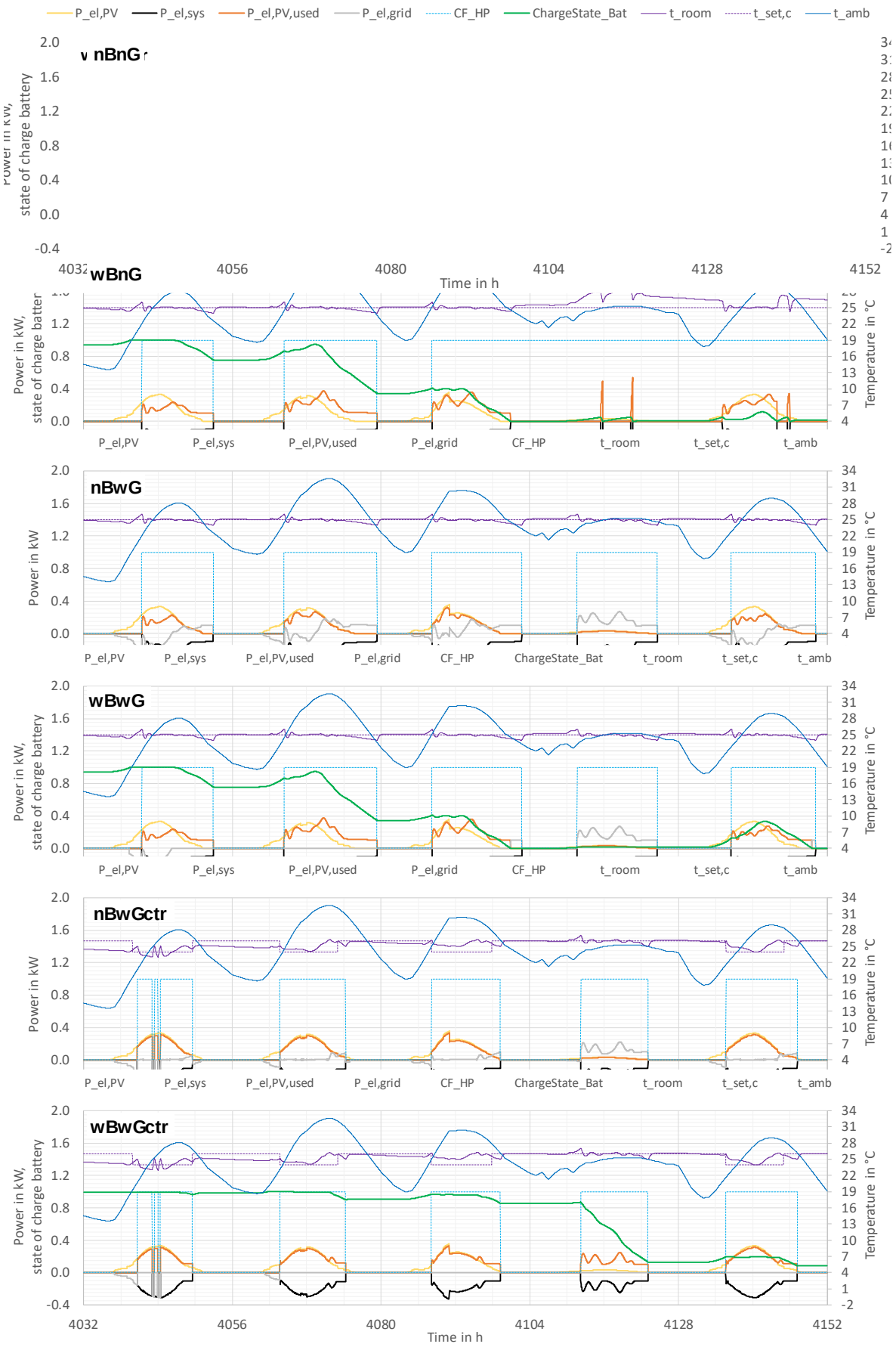

Figure 3: Simulation data of five exemplary summer days to illustrate the various system configurations and control approaches, 6 m² PV, 2 kWh battery capacity (for variants "wB")

No Battery, with Grid connection, adapted control (nBwGctr)
In order to increase the share of electricity from PV, a simple adapted control is implemented, consisting of two parts. Firstly, as already discussed in nBnG the compressor speed is adapted in order to match the system consumption to the PV yield, whenever the yield is larger than 100 W. Secondly, if the system is in cooling mode and if the first criterion is met, the set room air temperature is decreased to 24 °C. If the PV yield is lower than 100 W, the set temperature is increased to 26 °C. In heating mode the set temperature is accordingly increased to 23 and decreased to 21 °C. These measures are intended to shift system operation into times, when PV electricity is available. Comparing nBwG and nBwGctr in Figure 3 shows that this works well with a significant reduction of grid consumption in the considered period. Of course, this type of control causes the room temperature to deviate from the set temperatures defined above, as discussed in the results section.

With Battery, with Grid connection, adapted control (wBwGctr)
The control strategy used in nBwGctr is also applied to further increase the share of PV electricity in Figure 3 the system using a battery. A comparison between wBwG and wBwGctr in shows that the grid consumption can be reduced to zero in the considered period by applying this control. Compared to wBwG the battery is not discharged during night-time, as there is no operation, and on day four still enough capacity is available to bridge a day with very low PV yield.

2.1.2 Performance figures

In order to enable a comparison of the analysed variants of the system the following performance figures were defined, all of them on an annual basis. For better comprehensibility, most of the figures used here are shown graphically in Figure 2. The self-sufficiency ratio SSR that describes what proportion of the electricity consumption can be covered by the PV system, is defined both for heating (h) and for cooling (c), in order to be able to separately assess the system's performance for these two operating modes. For the off-grid systems SSR is 100 % by definition, as the electricity consumption from the grid $W_{el,sys,grid}$ is zero. The self-consumption ratio SCR is used to evaluate the ratio of the actual PV electricity consumed by the system $W_{el,PV,used}$ to the total PV yield $W_{el,PV}$ (including grid feed-in).
For off-grid systems $W_{el,PV}$ is assumed to be the theoretically possible total PV yield, if every kWh would be used. In addition, the room temperatures that can be maintained by the system are evaluated as average hourly values, since continuous operation is not possible independently of available solar radiation.

$$W_{el,sys} = \int \left(P_{el,HP} + P_{el,ventilators}\right) dt \quad \text{Eq. 2.1}$$

$$W_{el,sys,grid} = \int \left(P_{el,sys} - P_{el,PV,used}\right) dt \quad \text{Eq. 2.2}$$

$$W_{el,PV,used} = \int \left(P_{el,PV,direct} + P_{el,Bat}\right) dt \quad \text{Eq. 2.3}$$

$$W_{el,PV,feedin} = \int \left(P_{el,PV}\,\eta_{inv} - P_{el,PV,used}\right) dt \quad \text{Eq. 2.4}$$

$$SSR = 1 - \frac{W_{el,sys,grid}}{W_{el,sys}} \quad \text{Eq. 2.5}$$

$$SSR_c = 1 - \frac{W_{el,sys,grid,c}}{W_{el,sys,c}} \quad \text{Eq. 2.6}$$

$$SSR_h = 1 - \frac{W_{el,sys,grid,h}}{W_{el,sys,h}} \quad \text{Eq. 2.7}$$

$$SCR = 1 - \frac{W_{el,feedin}}{W_{el,PV}\,\eta_{inv}} \quad \text{Eq. 2.8}$$

$P_{el,PV}$	*electricity from PV (before inverter losses)*
$P_{el,HP}$	*electricity consumption heat pump / chiller*
$P_{el,ventilators}$	*electrical consumption of ventilators*
$P_{el,PV,used}$	*PV electricity used by the system*
$P_{el,PV,direct}$	*PV electricity directly used by the system*
$P_{el,Bat}$	*PV electricity used by the system provided by the battery*
SSR	*solar fraction (self-sufficiency ratio)*
SSR_c	*solar fraction (self-sufficiency ratio) for cooling*
SSR_h	*solar fraction (self-sufficiency ratio) for heating*
SCR	*fraction of PV self-consumption*
$W_{el,sys,grid}$	*electricity consumption from grid*
$W_{el,PV,feedin}$	*electricity feed-in into the grid*

2.1.3 Results and Discussion

The simulation results of the six system and control variants discussed in section 2.1.1.3 are shown in Figure 4. With the used configuration and assumptions the total possible yield per m² PV is 125.2 kWh/(m²a) for all systems.

Systems without grid connection

For the off-grid systems (nBnG, wBnG) the amount of thermal energy that can be provided for cooling (Q_c) and heating (Q_h) is increasing with the size of the PV system, which is the only energy source. SCR is decreasing with the PV size as a lower share of the provided electricity can be used. This is actually true for all simulated variants.

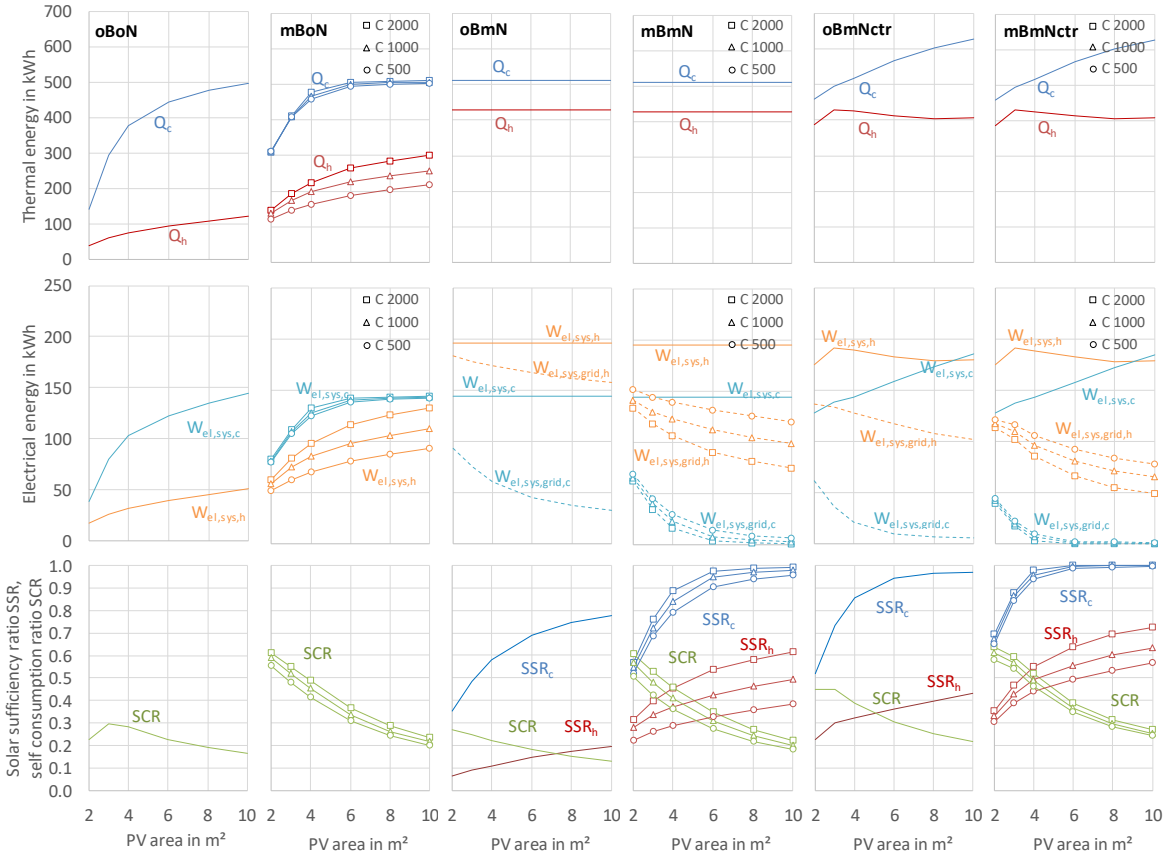

Figure 4: Annual simulation results for all considered variants

Comparing nBnG with wBnG shows significant advantages of the system with battery, especially for smaller PV systems and for heating. Due to the battery significantly more heating energy Q_h can be provided, and depending on the PV size also more cooling Q_c.

Both the system electricity consumption, which is 100 % PV electricity in the off-grid systems, and the SCR show between 1.2 and 3 times more PV utilization for wBnG compared to nBnG, depending on the PV size and the capacity of the battery. For wBnG different battery capacities (C2000, C1000, C500, denoting the capacity in Wh) were evaluated, showing a rather low influence for cooling and larger differences for heating operation. This is due to the fact that the heating demand, unlike the cooling demand, tends to occur during the night hours at low outside temperatures when there is no PV yield, which increases the necessity of a battery with appropriate capacity.
Because operation is not possible, whenever it is necessary for the off-grid systems, it is of interest, which room temperatures can be achieved. Figure 5 shows annual duration curves of the room temperatures for the systems nBnG and wBnG. As expected the set room temperatures of 22 °C for heating and 25 °C for cooling cannot be maintained at all times without grid connection. The smaller the PV area, the larger the deviation from the set temperature and its duration. For the reasons discussed already for Figure 4 the room temperatures in the heating case can be maintained much better, if a battery is used.

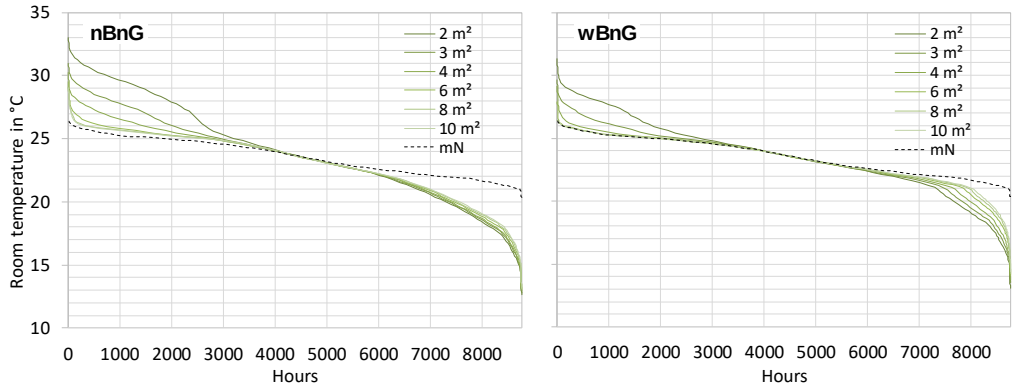

Figure 5: Annual duration curves of room air temperatures for off-grid systems without (nBnG, left) and with battery (wBnG, right) for different PV areas in comparison to a grid-connected system

For comparison Figure 5 also shows a duration curve for a grid-connected system, where the room temperature ranges from 21 to 26 °C. The deviation of -1 and +1 K from the set temperatures 22 and 25 °C can be explained by the hysteresis used for switching heating and cooling on and off (see section 2.1.1.3). For cooling almost the same results as with a grid-connected system can be achieved with nBnG using a PV area of 6 m² or more and wBnG using 4 m² or more.

System with grid connection

For the grid connected systems nBwG and wBwG both the provided heat for heating (Q_h) and cooling (Q_c) are independent of the PV size with the assumed control, the same applies to the electricity demand $W_{el,sys,h}$ and $W_{el,sys,c}$. The resulting total heating demand per m² useful floor area is 17.1 kWh/(m²a) and the cooling demand 20.5 kWh/(m²a). It is noticeable that for cooling there is no major difference between off-grid and grid-connected systems concerning the provided cooling energy Q_c, if the PV area is 6 m² and larger. For heating the off-grid systems can provide considerably less energy also with larger PV sizes.
For the grid connected systems the amount of electricity drawn from the grid is depending on the available PV area and is significantly lower for the system with battery, again especially in heating mode. Depending on the PV area the reduction of $W_{el,sys,grid,h}$ compared to nBwG is 20–26% with a battery capacity of 500 Wh and 30 – 55% with 2000 Wh. As for the off-grid systems (wBnG) the results for cooling are less dependent on the battery capacity. Compared to nBwG SSR_c can be increased by 17-21 percentage points (pp) with 500 Wh and 21-31 pp with 2000 Wh.
Using the adapted control in system nBwGctr results in a strong increase of both SSR_c (17–28 pp) and SSR_h (16-24 pp) compared to nBwG, as the system operation is potentially shifted into times, where PV yield is available (see nBwGctr in Figure 3 and Figure 4). With a PV size of 6 m² 94 % of the cooling electricity demand and 36 % of the heating electricity demand can be covered with PV, whereas it is 69 % and 15 % respectively for nBwG.

However, it has to be mentioned that the adapted control causes an increase of $W_{el,sys,c}$ compared to nBwG for a PV size of 6 m² and larger, which is due to the reduction of the set temperature in times with available PV yield (see section 2.1.1.3) and the adaption of the compressor speed to the available PV yield, which causes the VC system to run increasingly with higher power with increasing PV area. Nevertheless compared to nBwG the grid consumption $W_{el,sys,grid}$ can be reduced in all simulated variants. On the other hand the amount of electricity fed into the grid is also reduced, for PV sizes of 6 m² and larger due to the higher overall electricity consumption even to a larger extent than the grid consumption.
The heating demand Q_h and $W_{el,sys,h}$ are on the other hand hardly influenced by the adapted control. As shown in Figure 6 the applied control strategy tends to cause lower room temperatures in heating mode. This is due to the fact that here increasing the set room temperature in times with PV yield (see section 2.1.1.3) tends not to lead to an increase in the actual room temperature. Instead lowering the set temperature in times with no yield has a stronger effect and causes a temperature decrease, which also does not strongly depend on the PV size.

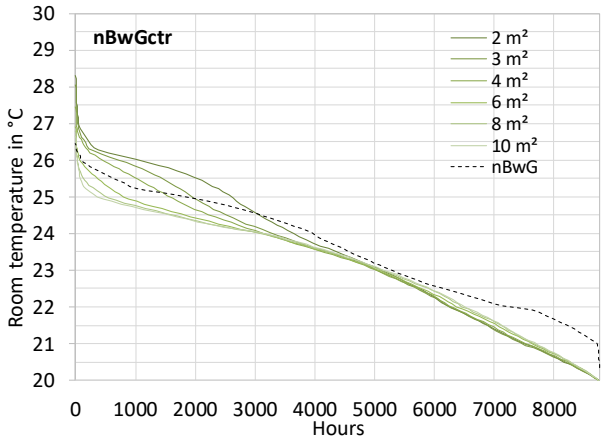

Figure 6: Annual duration curves of room temperatures for system nBwGctr for different PV areas compared to nBwG

For cooling operation this is different. Especially for PV sizes ≥ 6 m² the applied control leads to a temperature decrease of about 0.5-1 K compared to system nBwG with a fixed set temperature of 25 °C. For the smaller PV sizes the room temperature tends to increase, because increasing the set temperature in times with no yield has a stronger effect here.

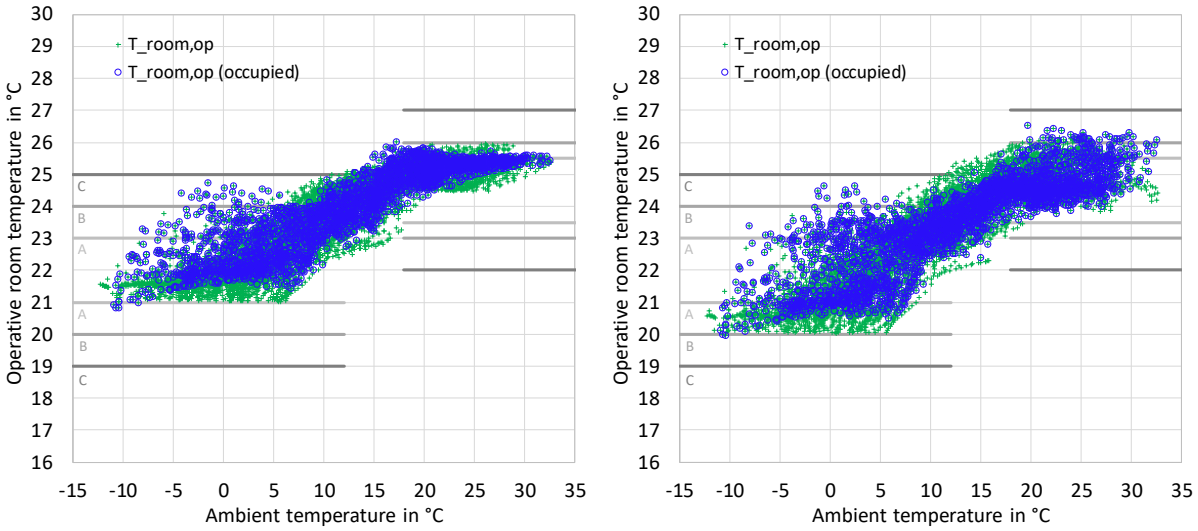

Figure 7: Hourly average values of the operative room temperature for the whole simulation year and only for the hours with office use (occupied) for the systems nBwG (left) and nBwGctr (right) with 6 m² PV

Figure 7 shows hourly average values of the operative room temperature for the entire simulation year and only for the hours with office use (occupied) on weekdays from 8:00 to 18:00 for the system nBwG (left) and nBwGctr (right) with 6 m² PV.

The figure shows the comfort classes A, B and C according to EN ISO 7730 (Austrian Standards Institute, 2006). In heating operation (assumption: outside temperature <12 °C), it can be seen that with nBwGctr the temperature is below 21 °C and thus in category B in approx. 7 % of the times of presence, whereas this is only the case with nBwG at 0.2 %. With regard to higher temperatures that occur in heating mode, both variants are very similar. In cooling mode, temperatures above 25.5 °C (category B) occur in 4 % of the presence time and above 26 °C (category C) in 1 %. In nBwG these percentages are 3 % and 0 %.
Also in the case of the grid-connected system with battery (wBwGctr), the use of the adapted control system leads to a reduction in grid consumption compared to wBwG (Figure 3), which is again higher for heating than for cooling. With the largest PV system and battery, 74% of the electricity consumption for heating can be covered by PV, SSR_c is almost 100% with 4 m² PV.

2.2 Functional model and monitoring

2.2.1 System description

A functional model of a PV-driven façade integrated heat pump system for cooling and heating was developed within the project COOLSKIN. Figure 8 (left) shows a cut-away sketch of the unit and Figure 8 (right) a photo of the system and the test cells for the field monitoring with two different PV panel covers for the unit, each with 1.2 kWp. The unit has different options that were tested: the cooling distribution and emission can be accomplished by a water-driven thermally-activated building system (TABS) or air-driven by the integrated fan-coil unit (green). The core component is the reversible heat pump cycle (blue). A battery (blue green) with a capacity of 2 kWh was integrated in order to enable storage of PV electricity. The system was designed for a monitoring, in which an autarkic operation without grid connection was tested.

The unit was installed in one of two small identical test buildings available at the Campus of TU Graz (Figure 8, bottom right). The buildings have an effective floor area of 13.49 m², windows oriented to the south and an almost identical thermal behaviour. The COOLSKIN system was implemented in the eastern building (cooled/heated box) below the windows. The western building was used as a reference without cooling and heating.

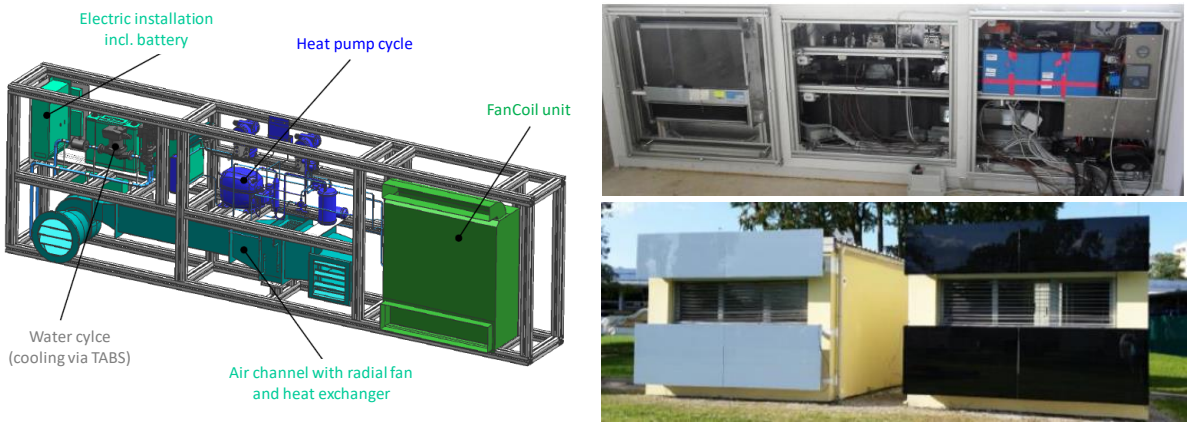

Figure 8: Cut-away of the prototype (left) and photo of the prototype (top right) and test cells for the field monitoring (bottom right)

In the monitoring the differences of the interior temperatures and the resulting thermal comfort between the building with the integrated cooling system and the reference building were analysed over a period of 1.5 years.
Both buildings are equipped with an internal heat load (dummy) in order to simulate the internal thermal loads over the day due to persons and equipment of an office room. Internal heat loads of 300 W were activated on working days between 8:00 and 16:00. Mechanical ventilation was used in both rooms (room volume app. 30 m³) ensuring an air exchange of 60 m³/h during assumed working hours.

2.2.2 Monitoring results

Exemplary monitoring data for three days of **cooling** operation in August 2018 are shown in Figure 9. Essentially three operating characteristics occurred in this period. On/off operation (1) occurred from about 08:00 to 10:00 and from 16:00 to 20:00 due to relatively low cooling loads. Between 10:00 and 16:00, the refrigerant cycle was continuously on (2) on all days in this period, as neither of the two limit temperatures used to switch the compressor on and off (Temp. limit on and off) was reached. The operative room temperature in the conditioned room (op. Temp.) was always between 23 and 25 °C, whereas in the unconditioned room (op. Temp. uncond.) it was between 29 and 32.5 °C. Even in this rather hot period, energy remained in the battery at the end of each day (battery voltage is plotted in Figure 9), which would have been available for other purposes during office operation. The average cooling capacity during this period was 1014 W.

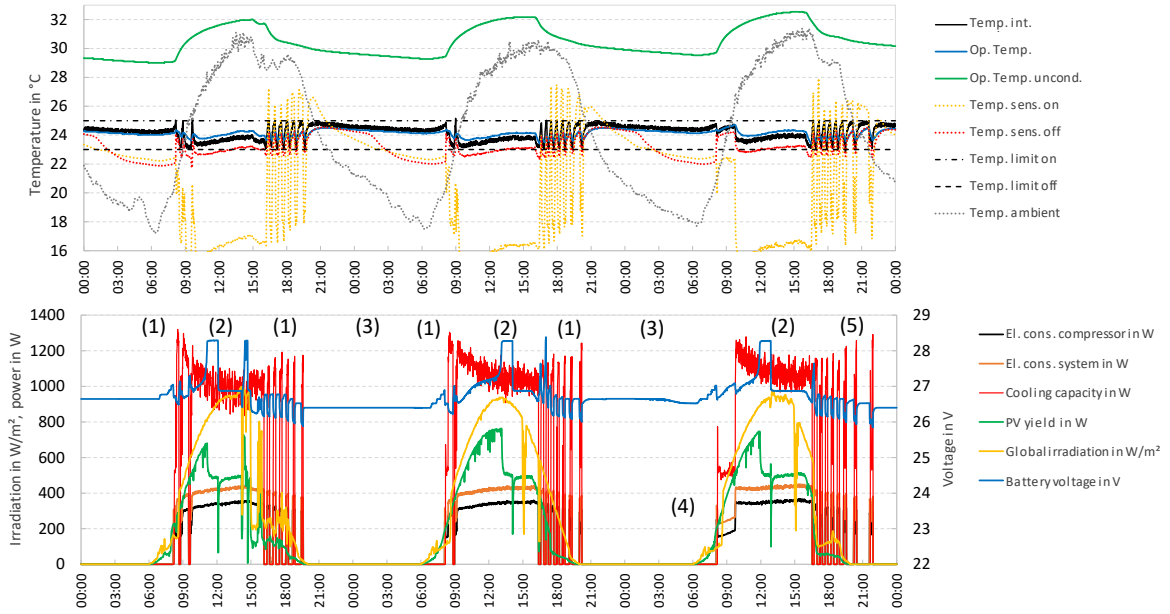

Figure 9: Exemplary monitoring data for cooling operation (air/air)

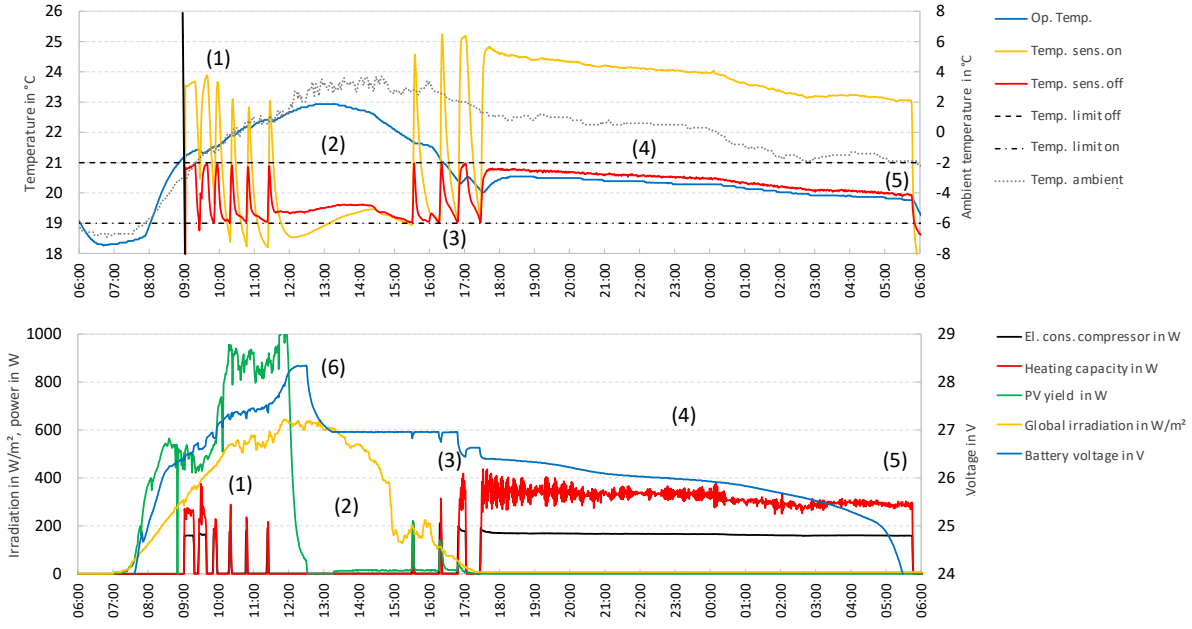

Figure 10: Exemplary monitoring data for heating operation (air/air)

An exemplary day of **heating** operation is shown in Figure 10. The measured outdoor air temperature in the considered period wass between -7 and 4 °C, the maximum measured global radiation (onto the horizontal) was approx. 600 W/m². Operation of the heating system started at about 09:00. In the period until 11:30 on/off operation occurred (1), as the room temperature was fluctuating between the on- and off-limit. From 11:30 to 15:30 (2) the heat pump was off because of a low heat load due to internal and solar gains.
The battery voltage shows that the battery was empty in the morning and was then recharged by PV until it was fully charged at about 12:30. After charging stopped the voltage in the battery dropped to approx. 27 V (6) and remained constant from then on until the heat pump was switched on again. From 15:30 to 17:30 (3) the heat pump went back into alternating operation, the room temperature oscillated back and forth between on and off limits. From 17:30 on (4), as the outside temperature dropped, the system was continuously in operation. The temperatures then dropped steadily overnight. On the next day, shortly before 06:00 (5), the heat pump was switched off because the battery was fully discharged again.

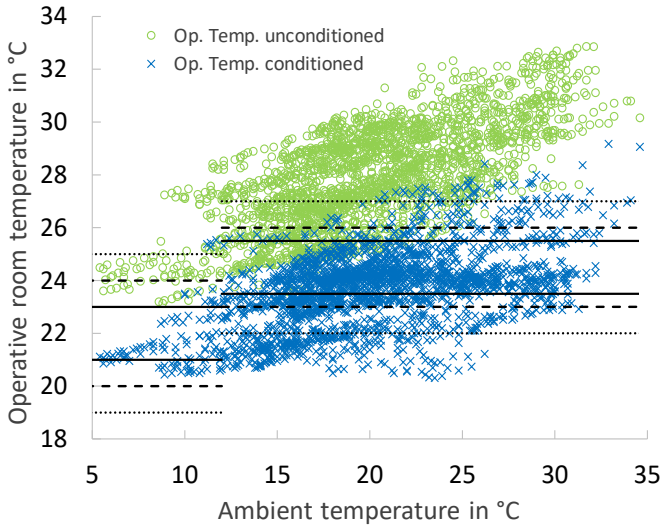

Figure 11: Comparison of operative room temperatures as a function of outside air temperature during the whole monitoring period

These results show that, as expected from the beginning, for heating a purely photovoltaic supplied operation is not possible on cold days or during the entire heating period. Nevertheless, year-round operation makes sense, if the system is connected to the grid and can therefore also be operated when there is not enough solar energy available.

A comparison of the operative room temperatures in the conditioned and the unconditioned room in cooling operation, depending on the outside air temperature, are shown in Figure 11 for the whole monitoring period of 1.5 years. The temperature in the cooled test room was almost continuously 3-6 K lower than in the unconditioned room. Even without any connection to the grid it was possible to maintain temperatures of mostly < 27 °C.

2.3 Conclusions and Outlook

For different system and operating constellations of façade-integrated, decentralised cooling (and heating) systems, detailed simulations were carried out for a typical office room under defined boundary conditions. Both off-grid and grid-connected systems and systems with and without battery storage were considered, and the Self Sufficiency Ratio (SSR), depending on the PV area installed in the façade, was evaluated.
The results show that even the considered off-grid systems are able to sufficiently cool the assumed office room, even if no battery is installed and ≥6 m² of PV is available on the facade. In heating mode without grid connection, the use of a battery offers clear advantages, as considerably higher room temperatures can be maintained in heating mode than it is possible without a battery. In grid-connected systems, the use of a battery also leads to a significant improvement in the degree of self-sufficiency SSR, both in cooling and heating mode.
In order to increase the degree of self-sufficiency or to reduce the amount of electricity drawn from the grid, an adapted control strategy was investigated in which the set room air temperature is varied depending on the availability of PV yield. This leads to a significant increase in the PV electricity share for both systems with and without battery. With regard to thermal comfort, this control strategy has minor disadvantages, but overall the room temperatures remain within an acceptable range.

The simulation results show, as well as the field test carried out in the project (not described here), that a complete off-grid mode of operation has significant disadvantages. On the one hand, potential PV yields remain unused in times of high solar radiation. On the other hand, in periods of low radiation, often only small amounts of electrical energy are needed to maintain comfort in the room, which could also be obtained from the grid.
The use of a battery has proven to be particularly advantageous in heating operation, as the heating load and the solar yield naturally do not coincide well in time. However, the simulation results show that the system could also work well without the use of a battery. This is of particular interest because a battery is not economically viable given the energy savings it can achieve and the current investment costs (approx. 600 to 1000 €/kWh) and electricity prices. The space required for a battery in the façade and safety aspects are additional arguments against the integration of an electrical storage unit.

3 Absorber freecooling - Rapperswil, Switzerland

3.1 Introduction

Currently, residential buildings are seldom cooled actively in central European countries like Switzerland, while in office buildings, there is already a cooling demand due to higher internal gains. However, recent studies indicate, that due to increasing outdoor air temperatures, rising number of electric devices and higher comfort requirements, also residential cooling demands will increase notably until the mid of the 21st century.
In Settembrini et al. (2017) an increase of the cooling demand in residential buildings in Switzerland of 300% to 700% for the reference year of 2060 has been evaluated by simulations, see Figure 12. Since buildings have a long life cycle, it is thus important to consider changing boundary conditions already in the planning phase. In addition to purely passive measures regarding the design of the building envelope, efficient cooling processes must also be developed in order to maintain comfort conditions, but limit the electrical expenditure for the cooling function.
Free cooling methods have already been introduced, but mainly in non-residential buildings. In residential buildings free cooling methods are often limited to nighttime ventilation or ground-coupled free cooling when a ground-coupled heat pump is used as heat generator. A possibility of free cooling in residential buildings, which is not much applied so far, is the heat dissipation by activated outer surfaces of the building envelope, e.g. those installed with solar thermal components. These components, which are designed to generate heat, can also reject heat to the ambiance during nighttime operation, under the condition that there is a good thermal connection to the ambiance.

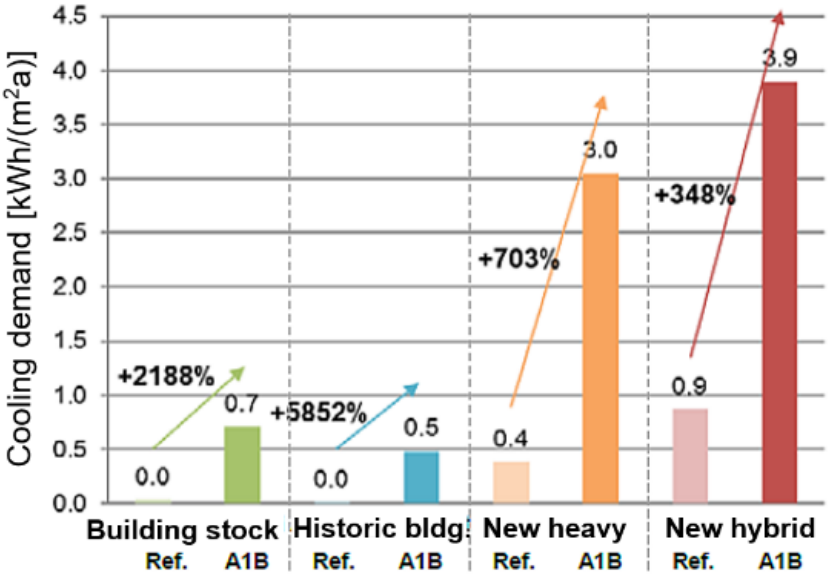

Figure 12: Long-term evolution of residential cooling demands in Switzerland to the reference year 2060 for different building types (Settembrini et al., 2017)

In addition to pure heat dissipation to the outside air by convection, heat dissipation by infrared radiosity to the ambiance and particularly to the sky is used, since a cloudless night sky has a significant lower equivalent sky temperature that is up to 20 K colder than the outdoor air temperature.
shows the cooling mechanisms that can be used for nighttime cooling on the outer surfaces of buildings. The heat emission is especially favourable for uncovered solar components, which are in direct contact to the ambiance. An increase in the cooling capacity of these components can be achieved by an additional evaporative cooling, if the surface of the components is wetted with water. In order to have a sustainable water source, reuse of decentralized treated grey- and wastewater is investigated as water for wetting the absorber.

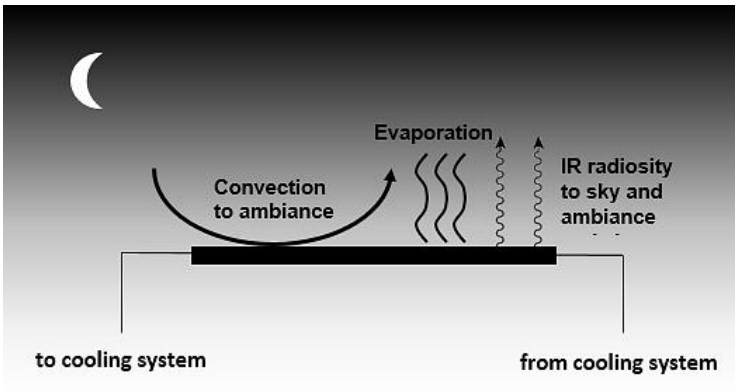

Figure 13: Different cooling mechanisms on building outer surfaces

3.2 Test rig results for the space cooling operation

In order to further characterise the space cooling operation with test rig results, measurement have been performed on a selectively coated unglazed solar collector on the accredited test rig of the HSR Institute SPF, which is the national test centre of Switzerland for solar thermal collector. Figure 14 left shows the unglazed solar collector on the test rig and Figure 14 right depicts a sketch of the measurement system including a legend of the measurement points. In order to determine the capacity of the absorber in free cooling mode, the inlet and outlet temperatures of the absorber fluid are measured.

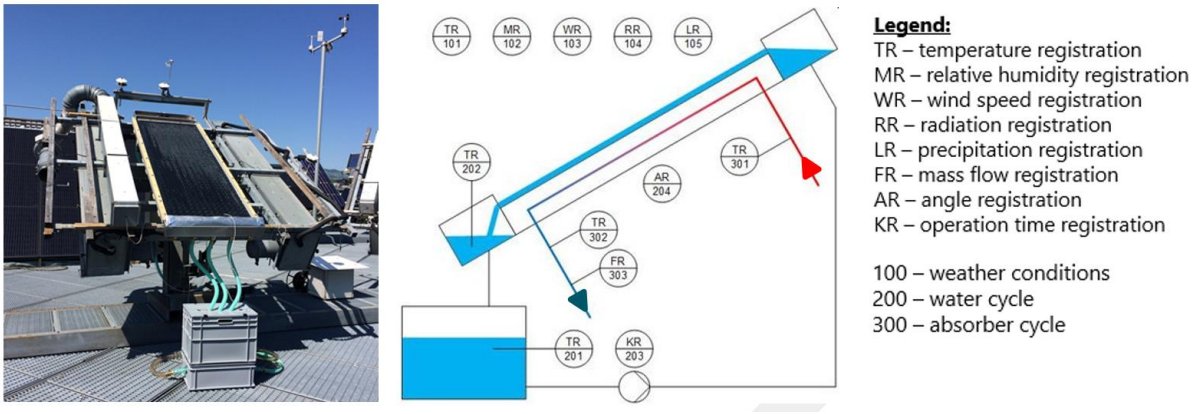

Figure 14: Unglazed solar collector on the test rig (left) and sketch of the test rig with measurement points including the legend of the measurement points (right)

With the measured volume flow the enthalpy change on the fluid side and thereby the cooling capacity can be evaluated. The fluid is a water-glycol mixture.
Additionally, the weather boundary conditions of the short wave solar irradiation, the downward long wave radiation, the ambient temperature and relative humidity as well as the wind speed and precipitation are measured in order to characterize the impact on the cooling capacity. As expenditure for the free cooling operations the electricity input to the pump is measured. For the operation of the system, continuous and cyclic operation can be run. During continuous operation, the absorber surface is continuously wetted by a water film running down on the absorber surface. In cyclic operation, the film is only continued for 10 seconds every 2 minutes, which saves pump electricity.
In the following figures, the cooling capacity for different weather boundary conditions is depicted. Fig. 7 left shows the temperatures linked to the nighttime absorber operation in cooling mode. The inlet and outlet temperature are decisive for the evaluation of the cooling capacity. The inlet temperature is kept constant at about 20 °C. By the high volume flow rate of 200 l/h, the temperature difference between inlet and outlet is limited to 2 K. With a lower mass flow rate, the temperature difference can be increased, but the capacity is reduced, since the average temperature difference to the ambient is decreased. Thus, as in space heating, a lower mass flow decreases the outlet temperature, but also the cooling capacity.

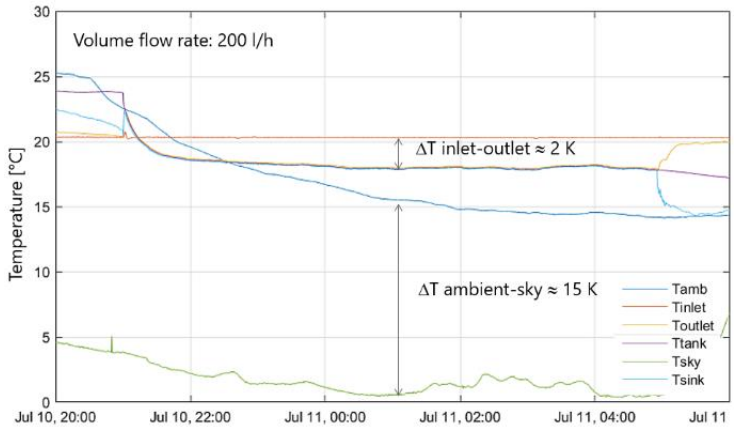

Figure 15: Temperatures of the unglazed solar collector on the test rig at favourable nighttime ambient conditions with clear sky and moderate ambient temperature

The temperature of the tank characterizes the temperature of the water film on the absorber. In this case, a night with a moderate ambient temperature and a clear sky is depicted. This can be seen at the temperature difference to the (fictive) sky temperature that characterizes the long wave radiation exchange between the absorber and the sky.

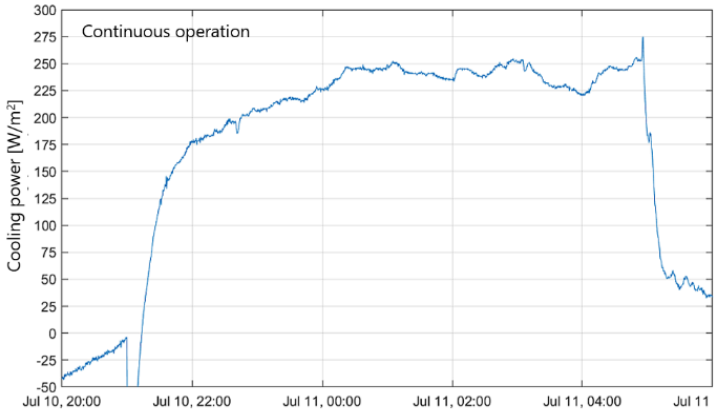

Figure 16: Cooling capacity of the unglazed solar collector on the test rig at favourable nighttime ambient conditions with clear sky and moderate ambient temperature

Since the water vapour in the atmosphere absorbs long wave radiation and reemits it as long wave downward radiation, a clear sky is a more favourable weather condition than a cloudy sky and the sky temperature reaches values up to 20 K lower than the ambient air temperature. Figure 16 depicts the cooling capacity of the absorber. At favourable conditions a cooling capacity in the range of 250 W/m^2 is reached. Until about 10 p.m., the ambient temperature is still higher than the average absorber temperature, which limits the cooling capacity.

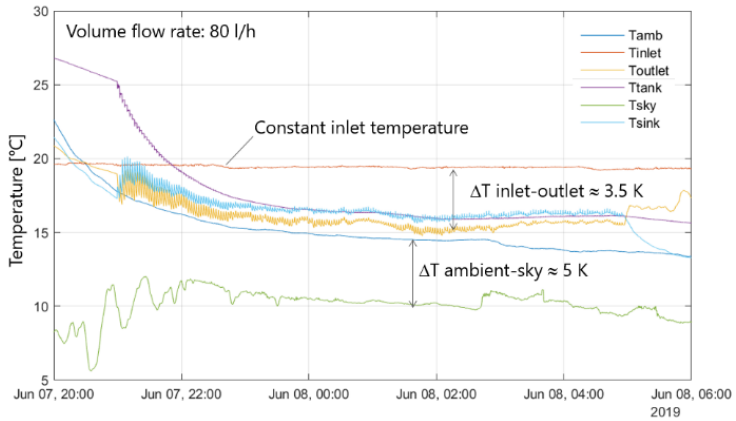

Figure 17: Temperatures (left) and cooling capacity (right) of the unglazed solar collector on the test rig at moderate nighttime ambient conditions with cloudy sky and moderate ambient temperature

Figure 17 depicts a cyclic operation with cloudy sky conditions and a lower mass flow rate of 80 l/h, which is the nominal mass flow of the collector at heating conditions. In this case, the temperature difference between the ambient and the sky temperature decreases to only 5 K, which is due to a higher long wave downward radiation from the sky.

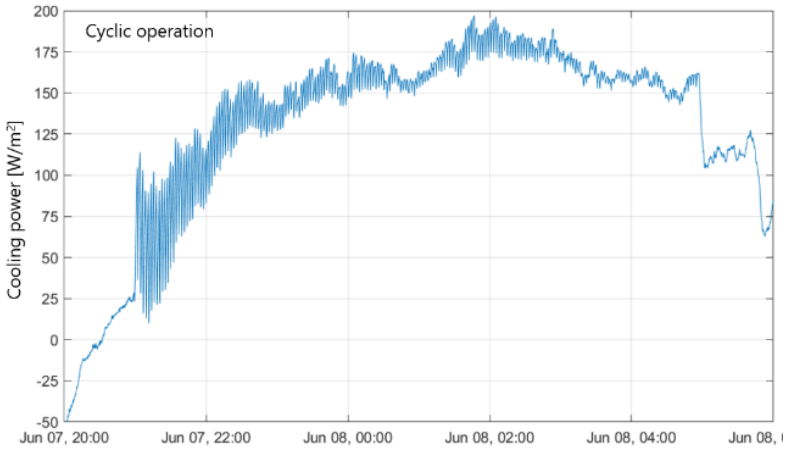

Figure 18: Cooling capacity of the unglazed solar collector on the test rig at moderate nighttime ambient conditions with cloudy sky and moderate ambient temperature

Despite the lower cooling capacity, which is depicted in Figure 18, a temperature difference for 3.5 K over the absorber is reached due to the lower mass flow rate.
The cooling capacity is not constant due to the cyclic operation. The water on the collector surface is partly evaporating, which has also influence on the radiation properties, since the collector has a selective coating. If water is on the collector, the long-wave emissivity in the infrared spectrum ε_{IR} is defined by the water to values around ε_{IR}=0.95. However, if the water is evaporated, the emissivity changes to the one of the selective coating, which has an emissivity around ε_{IR}=0.15. Thus, the evaporative and radiative cooling capacity is reduce at dry parts of the collector surface, which leads to a decrease of the cooling capacity in cyclic operation.

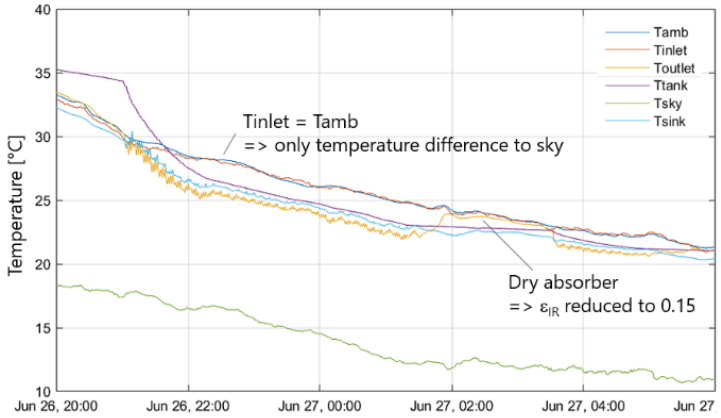

Figure 19: Temperature difference for wet and dry absorber (left) and respective cooling capacity (right)

In the beginning of the night, the water for the wetting of the absorber is still warm, which leads to the higher swing in the temperatures. The swing is successively reduced down to differences of about 20 W/m^2. This effect of the selective coating is depicted in Figure 19. In this case, the inlet temperature to the collector is adapted to the ambient temperature. Until about 1:30 am the collector is wetted. Then, the water film is stopped for two hours until 3:30 am, and the collector is drying completely. In the drying process cooling capacity successively decreases, as shown in Figure 20 and for the dry collector, the cooling capacity is strongly decreased from initially 125 W/m^2 before the drying process down to values around 10 W/m^2 after complete drying of the collector surface.

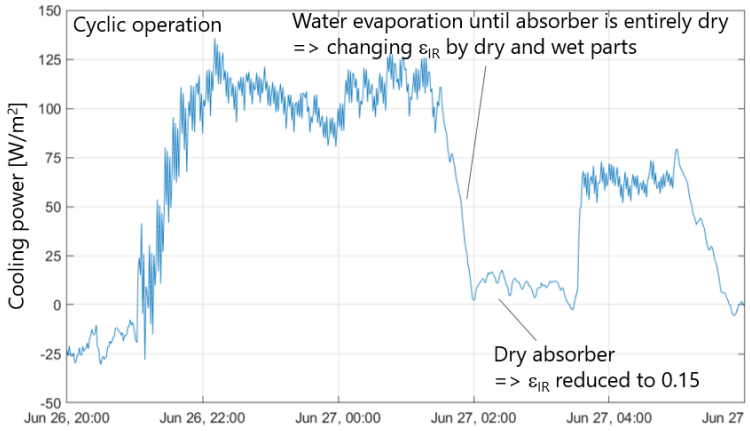

Figure 20: Cooling capacity for wet and dry absorber

At the test rig, there is also the option to switch-on artificial wind in the range of wind speed of 1-3 m/s. The ventilator is located directly along the long side or the absorber and shown as a white box in Figure 14. As the wind changes both the convective and evaporation heat transfer coefficients, a significant increase of the cooling capacity is measured with artificial wind.

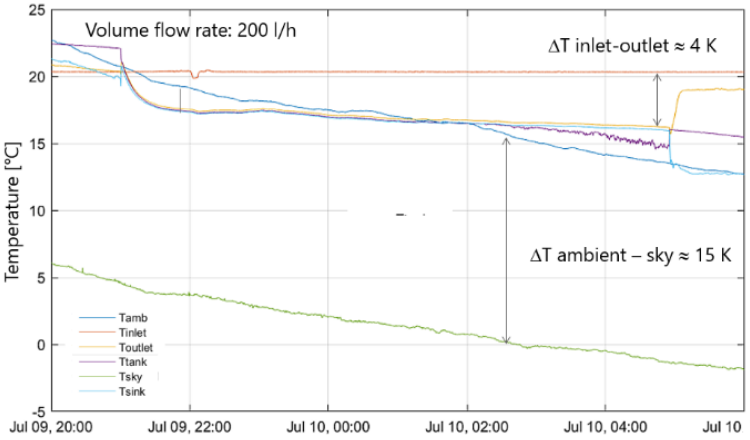

Figure 21: Temperatures with 3 m/s artificial wind on the absorber surface at clear sky conditions

Figure 21 depicts the temperatures and Figure 22 the cooling capacity at clear sky conditions and artificial wind of 3 m/s. A cooling capacity up to 450 W/m^2 is measured at ambient temperature of 13 °C and a temperature difference to the sky of 15 K.

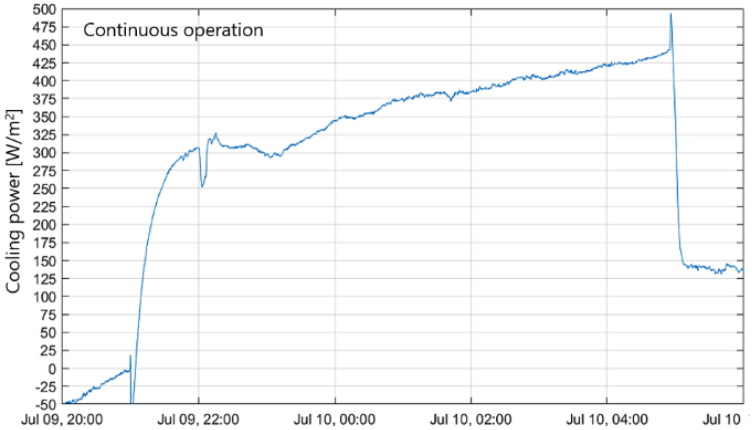

Figure 22: Cooling capacity with 3 m/s artificial wind on the absorber surface at clear sky conditions

3.2.1 Conclusion and Outlook

The investigated unglazed solar collector can also be used for the integration of the freecooling operation during nighttime, where the collector rejects heat by convection, radiation and evaporation, if the collector surface is wetted. Besides the evaporative cooling effect by wetting the collector surface, also radiative properties can be changed in case of a selective coating of the collector. Thereby, a selective coating helps to reach higher temperature in the DHW operation during daytime due to a reduction of the radiative losses, while it enhances radiation losses due to the high emissivity of water up to 95% in nighttime of the freecooling operation.
Test rig measurements have been carried out at the accredited test rig of the national Swiss solar test center for solar thermal systems at the HSR Rapperswil, which confirm good specific cooling capacities in the range of 100 – 250 W/m^2_{abs} depending on the ambient conditions, which are even higher than the values used in the feasibility study. Wind on the collector surface enhances the convective and evaporative heat transfer to the ambiance and values up to 450 W/m^2_{abs} have been measured at a wind speed of 3 m/s at the collector surface. However, in summer, usually lower wind speeds at night are predominant, thus the potential for higher cooling capacities by wind is limited.
In the frame of the project, also the application of treated greywater as water source for the space cooling operation is investigated in collaboration with the Institute of Ecopreneurship of the University of Applied Sciences Northwestern Switzerland FHNW in the frame of the Swiss Competence Centre for Energy Research, Efficiency of Industrial Processes (SCCER-EIP). First results indicate that fouling and scaling on the collector surface can be effectively managed by the water treatment in a decentral membrane bioreactor (MBR) water treatment process, and cooling capacities are not affected. Also, bacteria growth meets the requirements for evaporative cooling, so treated wastewater can be a sustainable water source for the evaporative free cooling. A problem regarding scaling can be the hardness of the water, which however, can be reduced during water treatment.

4 Personal cooling devices – Maryland, US

4.1 Introduction

RoCo (Roving Comforter) is a personal-sized HP that cools indoor air to maintain occupants' thermal comfort. The latest version of RoCo has a stylish appearance, is 30 in. tall, and weighs ~40 lb., Figure 2.1 (Deru et al, 2011). The top of RoCo is an intelligent air nozzle that automatically locks onto its user and directs the airflow to the desired parts of the body. RoCo can operate for up to 8 hours due to the onboard state-of-the-art phase-change material that stores the waste heat. The novel phase change material (PCM) regeneration process requires only a "one-click" switch and ensures the thermal battery can be recharged in less than 40% of its operating time. Initial experimental work shows that RoCo's cooling capacity, which is around 150 W, successfully provides thermal comfort without rejecting waste heat or requiring wires and ducts during operation. This cooling capacity sets RoCo apart from other conditioning devices (e.g., fans, ice coolers) that are currently on the market. Therefore, RoCo was designed with the vision of opening the market for new technology in the space conditioning and thermal comfort field.

Figure 23: Progression of RoCo prototypes (left) and latest version of RoCo (right).

RoCo is equipped with unmatched comfort technology. Some of its features are described as follows. **Intelligent nozzles:** RoCo's intelligent nozzle(s) deliver conditioned air to the parts of the body that need it most. Thermal comfort studies reveal that various parts of the body have different sensitivity levels for thermal sensation. RoCo ensures that users receive most of the cooling/ heating where it is most needed through flexible nozzles that adjust air supply locations and supply air conditions (temperature, RH, etc.). The high-end module saves personal preference data, such as air temperature and velocity, for different human metabolic rates. RoCo knows users' thermal requirements better than anyone else.

Highly efficient thermal management module: The primary feature of this personal cooling/heating device is the next-generation miniature HP system with built-in PCM storage. Benefiting from linear mini-compressor and next-generation air-to-refrigerant heat exchangers, the system delivers cooling and heating at minimum power consumption without releasing waste heat. With the help of RoCo, building operators and homeowners can extend HVAC setpoints and achieve considerable energy savings without compromising occupants' thermal comfort.Through the project, the University of Maryland team developed three generations of RoCo, creating a total of seven devices. RoCo reaches an overall coefficients of performance (COP) of 3.54 (project goal of vapor compression cycle (VCC) coefficient of performance (COP) is ≥ 3.0) with a measured evaporator capacity of 150 W. The overall cycle COP with the total power consumption from cooling and PCM recharging is 1.6. Forty human subject (HS) tests were conducted to measure RoCo's thermal comfort. Overall, all participants in the experiment reported comfortable and very comfortable comfort levels while using RoCo, which are correlated to target predicted percent dissatisfied (PPD) values (<10%).

The effective cooling range attributed to RoCo is 2 to 13 W, which— although short of Advanced Research Projects Agency – Energy goals of 23 W — is a sufficient cooling rate for HS to accomplish savings in energy consumption for overall building cooling. The difference between cooling delivered from RoCo (in the range of 100 W) and effective cooling represents the fact that, even for a localized thermal management device, a majority of generated cooling is used to condition air that is directly circulated to provide personal cooling. However, this difference is one order of magnitude smaller than traditional air conditioners.

4.1.1 Potential Energy Savings with RoCo for Different Climate Conditions

This study assesses the potential energy savings for personalized cooling with RoCo for a time period typically requiring central cooling in the US office buildings. This study considered different climate types, and the selected time period includes May 15–September 15.

Office Building ✓	Warehouse Building	Midrise Apt Building	Manufacturing Building
Area 4892 m^2 (50,000 ft^2) people = 268	Area 4835 m^2 (52,043 ft^2) people = 5	Area 2030 m^2 (21,848 ft^2) people = 58	Area 4892 m^2 (50,000 ft^2) people = 102
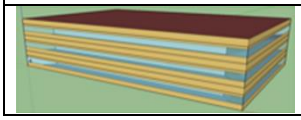	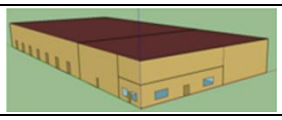	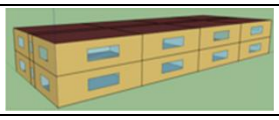	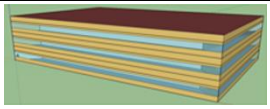

Figure 24: Common building types in the United States.

This investigation used EnergyPlus to simulate the building located in seven different cities across the United States, as shown in Figure 24 and Table 2.

Table 2: Selected cities and climates (Du, 2016)

	City	Climate
1	Austin, Texas	Climate zone 2A: hot/humid (**CDD 18ºC = 441)**
2	Chicago, Illinois	Climate zone 5A: cool/humid (**CDD 18ºC = 199)**
3	Honolulu, Hawaii	Climate zone 1A: very hot/humid (**CDD 18ºC = 408)**
4	Minneapolis, Minnesota	Climate zone 6A: cold/humid (**CDD 18ºC = 185)**
5	New York City, New York	Climate zone 4A: mixed/humid (**CDD 18ºC = 243)**
6	Phoenix, Arizona	Climate zone 2B: dry (**CDD 18ºC = 744)**
7	San Francisco, California	Climate zone 3C: warm/marine (**CDD 18ºC = 30)**

To evaluate the impacts of building construction materials and new building equipment performance when using RoCo for personalized cooling, this study deployed two sets of building energy models covering both the old building and existing building code compliances suggested by the DOE Commercial Reference Buildings (Deru et al., 2011). According to the Commercial Building Energy Consumption Survey, office buildings account for 18.8% of all building spaces in the United States. Consequently, this study aimed to assess the impacts of various scenarios in which RoCo operates in distinct building space types located in different geographic locations.The energy simulation inputs for old building models follow pre-1980 DOE standards, as specified in DOE Commercial Reference Buildings (Deru et al., 2011). The input parameters for existing buildings comply with ASHRAE Std. 90.1-2019 (ASHRAE, 2004).

Table 3: Commercial electricity prices (Heidarinejad et al., 2018)

City	Off-peak	Mid-peak	Peak
Austin, Texas	0.067	3.91	6.54
Chicago, Illinois	6.24	N/A	6.24
Honolulu, Hawaii	16	16.9	16.9
Minneapolis, Minnesota	3.02	N/A	15.13
New York City, New York	1.34	N/A	18.99
Phoenix, Arizona*	5.48/5.15	10.5/10.7	15.41/16.48
San Francisco, California	20.7	23.4	25.8

*Phoenix summer/Phoenix summer peak

The selected cities represent a variety of climate zones in the United States, according to ASHRAE Std. 169-2006 (ASHRAE, 2006). The main objective of this study was to evaluate the impact of introducing RoCo in different climate zones in the United States (Table 1). This assessment used the computer simulation results to summarize the potential savings for adopting RoCo nationwide.

4.2 General descriptions

This study uses DOE Commercial Reference Buildings as the baseline models for the office. For each city, the first simulation represents the current building performance, which serves as the baseline for comparing the potential energy savings associated with RoCo. Additionally, the baseline provides the necessary inputs for the HVAC system—such as system capacity, airflow rate, and duct sizing—which are later used in the simulation models that represent extended setpoint temperatures and RoCo. Specifying these inputs prevents EnergyPlus from downgrading/upgrading the building's HVAC system for the cases with extended temperatures and allows all studied cases to be accurately and fairly compared.
After the baseline models, this study explored the potential energy savings associated with the extended temperature setpoints in each building space. These results led to the potential savings associated with the central temperature setpoint. Furthermore, the results of these simulations provide understanding and later quantify the energy impact associated with RoCo. All distributed heat-rejection systems, such as RoCo, must account for the energy penalties associated with internal equipment and heat-rejection methods, which include infiltration at dedicated openings for heat rejection, a building's HVAC fan power, and space constraints for each RoCo. The building model is fully described in the following section with an example of the energy effects associated with the current RoCo. The current operational characteristics of RoCo include the following (Du, 2016):

- operates 4 hours
- removes 165 W from the space
- consumes 70 W electric load to recharge electric battery
- electrical battery recharges from 22:00 to 4:00 (6 hours)
- requires 10 W fan power to recharge PCM
- PCM recharges from 22:00 to 2:00 (4 hours)
- rejects PCM heat outside the building space
- rejects PCM heat inside the building space

An important aspect of using RoCo for cooling is the potential cost savings due to the peak energy demand shifting. RoCo reduces cooling electricity consumption during the day when electricity costs are the highest based on a local time-of-use program. Many cities across the United States offer time-of-use programs for commercial and residential buildings to regulate energy consumption during high-demand periods. The time-of-use program entails off-peak, mid-peak, and peak hours with associated electricity rates. The most expensive times are the peak hours, followed by the mid-peak hours, and lastly the off-peak hours. Table 3 and Table 4 provides the electricity rates for commercial and residential buildings. The electricity price for the residential sector is more expensive than the commercial sector. The electric company serving Chicago was only able to provide the flat rate price for commercial and residential sectors according to their policy.

Table 4: Residential electricity price, cents/kWh (Heidarinejad et al., 2018)

City	Off-peak	Mid-peak	Peak
Austin, Texas	6.16	9.51	14.98
Chicago, Illinois	6.24	N/A	6.24
Honolulu, Hawaii	18.2	23.7	26.7
Minneapolis, Minnesota	3.02	N/A	20
New York City, New York	13.97	N/A	41.65
Phoenix, Arizona	6.11	N/A	24.47
San Francisco, California	32	N/A	40

Table 5 shows the peak and off-peak hours for each city. Commonly, during the weekends and holidays, the electricity rate falls into the off-peak price for all cities.

Table 5: Peak and off-peak hours for each city (Heidarinejad et al., 2018).

City	Off-peak hours	Mid-peak hours	Peak hours
Austin, TX	22:00 –6:00	06:00–14:00; 20:00–22:00; 06:00–22:00	14:00–20:00
Minneapolis, MI	21:00–09:00	N/A	09:00–21:00
Honolulu, Hawaii	21:00–07:00	07:00–17:00	17:00–21:00
New York City, NY	00:00–08:00	N/A	08:00–24:00
Chicago, IL	N/A	N/A	N/A
San Francisco, CA	21:30–08:30	08:30–12:00; 18:00–21:30	12:00–18:00
Phoenix, AZ	19:00 –24:00	N/A	12:00–19:00

The potential costs savings associated with extended setpoints and RoCo are a combination of electricity prices and cooling degree-days (CDD) 18°C. This study normalizes the electricity price of each city as a ratio between the off-peak to peak price, as shown in Eq. (1). This normalization reveals potential profitable markets for RoCo. In Eq. (1), unity is subtracted to sort each city into an ascending order (Figure 25).

$$Price\ Ratio\ deff = 1 - \frac{off\ peak\ price}{on\ peak\ price}. \quad \text{(eq. 1)}$$

This study proposes that cities with electricity price ratios higher than 0.3 and a CDD 18°C higher than 400 could be the highest profitable markets for RoCo. Cities such as Austin, Minneapolis, New York, and Phoenix have high CDDs and a high electricity price ratio between off-peak and peak, making them a suitable market for systems such as RoCo (Figure 25). On the other hand, cities such as Chicago and San Francisco have low cooling requirements and a low price ratio, which prevents potential cash savings associated with extending temperature setpoints and RoCo. Similarly, Honolulu might not be a potential market due to the small price ratio for the electricity rate.

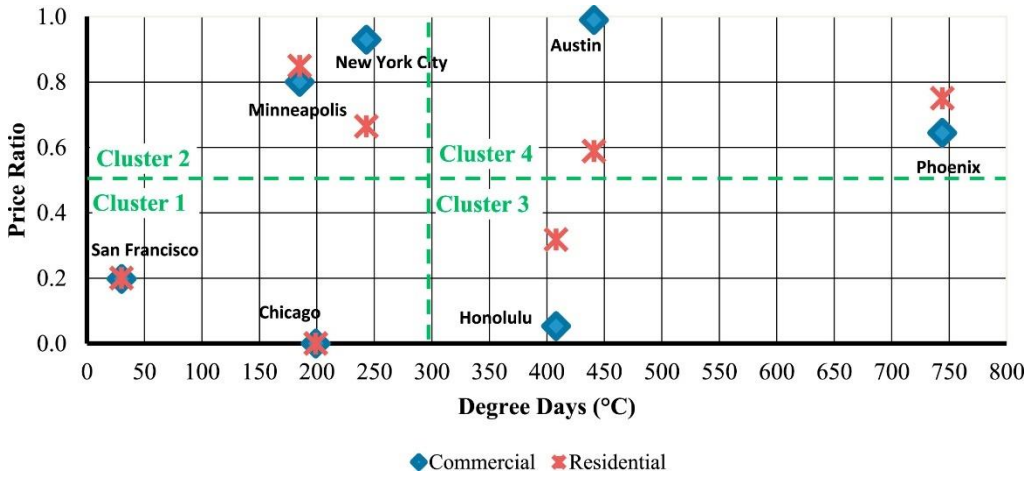

Figure 25: CDDs vs. price ratio (Heidarinejad et al., 2018)

4.2.1 Model Description and Results

The baseline model for this building space assumes a gross floor area of 4,892 m^2 (50,000 ft^2) and 268 occupants. The energy simulation estimates that the cooling season expands from May 15 to September 15 for the old and new office models. The main differences between the old and new office models are construction materials and HVAC systems. Specifically, the new office model has variable air volume, whereas the old office model has a constant air volume. This study considered three different temperature schedules (Figure 26) for each model to compare the building energy consumption. The first temperature schedule is the baseline in which room temperature is 24°C (75.2°F) from 6:00 to 22:00 and 26.7°C (80.6°F) from 22:00 to 6:00 of the following day.

The second temperature schedule (Max80) follows the extended setpoint temperature required by the DELTA program in which room temperature is 26.7°C (80.6°F) (Max80) throughout the day. The third temperature schedule is a combination of the baseline and Max80 schedules in which the temperature setpoint is 24°C (75.2°F) from 6:00 to 13:00 and 26.7°C (80.6°F) from 13:00 to 6:00 of the following day. This study assumes that RoCo operates between 13:00 to 17:00 hours every day to provide cooling during the extended setpoint. According to preliminary results, increasing the daytime (6:00–22:00) temperature more than 26.7°C (80.6°F) increases the fan energy consumption. Additionally, based on experience, building managers would not operate buildings at temperatures higher than 26.7°C (80.6°F) to avoid occupant discomfort. The building's fan increases the energy consumption to satisfy the temperature changes in the space.

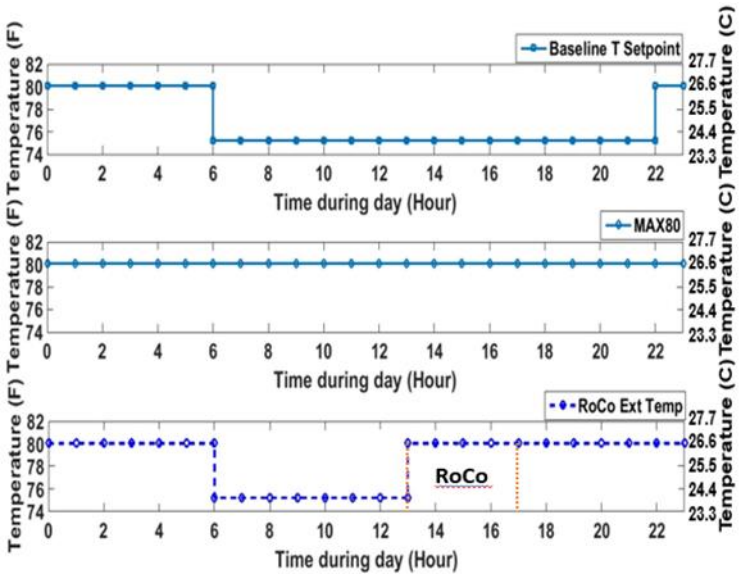

Figure 26: Temperature schedules for office buildings (Heidarinejad et al., 2018)

The simulation results demonstrate that by extending the temperature setpoint to 26°C (80°F), the energy required to cool the building reduces from approximately 20 to 38% for old office models and 7 to 11% for new office models (Figure 27). San Francisco and Chicago are associated with low CDDs in which cooling is a minor portion of the building's total energy. Therefore, the extended temperature setpoint to 26.7°C (80.6°F) in old offices significantly reduces cooling energy by 38% in Chicago and 64% in San Francisco, but it does not affect the building's total energy consumption. The results indicate an increase in the fan energy consumption in the old offices, which limits the total energy savings to 4–5% since fan energy represents approximately 17% (Heidarinejad, 2014) of the total energy in the building.

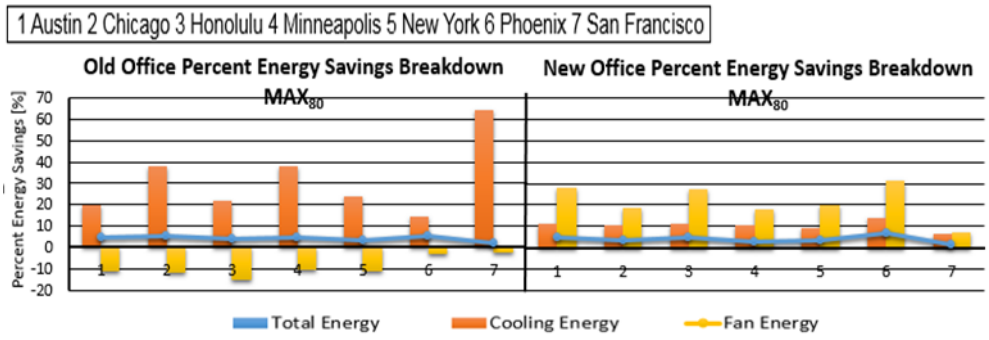

Figure 27: Max80 energy savings for office buildings.

The energy increase is a characteristic of constant volume systems in which the fan operates for longer periods to benefit from free cooling and maintain the desired temperature setpoint of 26.7°C (80°F). In contrast, the results for new offices buildings indicate potential savings in the fan energy ranging from 7 to 32%; however, the fan energy is only 3% of the total energy in the building, which has a negligible impact on the building's overall energy consumption.

The simulation results indicate that the potential savings for cooling energy using the extended setpoint temperature of 26.7°C (80.6°F) are approximately 10%, which represent—depending on the city—approximately 1 to 3% of the building's total energy. For both models, the internal equipment is the same since no additional equipment have been added to the space. An important difference between the old and new building models is the internal equipment energy, which represents 22 and 38%, respectively, of the total energy in the buildings.
Introducing RoCo to the building environment increases the internal equipment energy by 9%. On the other hand, operating RoCo in old offices enables savings in cooling energy that range from 11 (Phoenix) to 51% (San Francisco) (Figure 28). However, as with the previous case, the fan energy in old offices indicates an increase of approximately 8%, which—combined with the internal equipment energy—limit the total energy savings to 2% (Figure 28). The results for the new office models show that cooling energy savings range from 11 (Phoenix) to 5% (San Francisco). Additionally, the results indicate potential savings for the fan energy; however, as explained in the previous section, fan energy does not contribute much to the building's total energy use. For this building model, the total energy does not change compared with the baseline model since the increase in interior equipment energy counterbalances the savings in cooling energy (Figure 28).

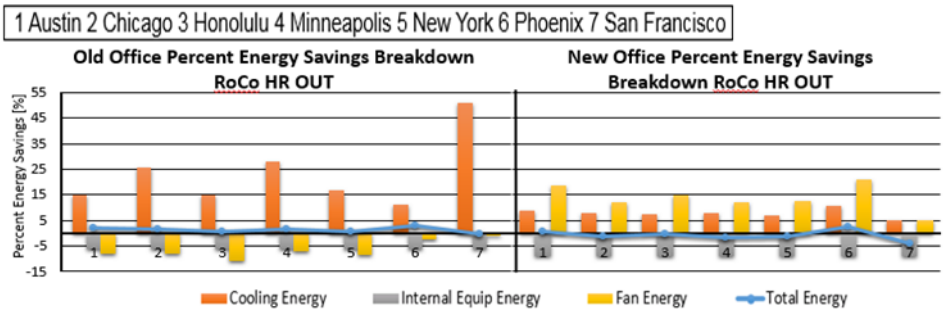

Figure 28: Extended temperature RoCo energy savings in office buildings.

To demonstrate the effect of rejecting RoCo's heat inside a building, this study compares the cooling energy and fan energy for heat rejection outside and inside. Figure 29 shows the cooling energy and fan energy for both cases. The results indicate that the cooling energy savings reduce by ~3% when rejecting heat inside for old and new buildings. Likewise, in the old buildings, the fan energy increases by 7% since it must remove more heat from the space during RoCo's heat rejection process. The fan energy for new office buildings is a small part of the total energy; therefore, its change is negligible. The cooling energy for San Francisco stays the same for both heat rejection processes. The overall energy savings in the building reduces by ~2% when heat is rejected inside.

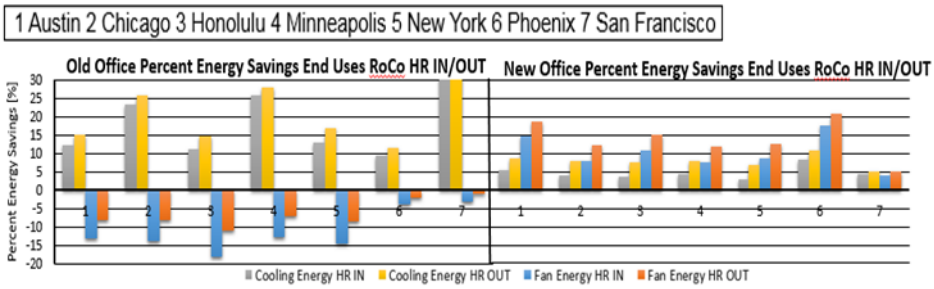

Figure 29: Heat rejection in/out comparison in office buildings.

4.2.2 Cost Analysis

The cost analysis of office buildings reveals higher potential cash savings in the old building compared with the new buildings. Figure 30 shows the cost savings breakdown for each city and each case. Phoenix has the most savings associated with Max80, RoCo (heat rejection outside), and RoCo (heat rejection inside), which escalate up to $3,200. As predicted Chicago, Honolulu, and San Francisco have limited cash savings potential due to the combination of low price ratio and low CDDs. The cash savings for new office buildings are lower than the old

office due to the high internal energy, which offsets the cash savings associated with cooling energy. By rejecting heat inside, the cash savings are limited due to a slight increase in cooling energy added by this process.

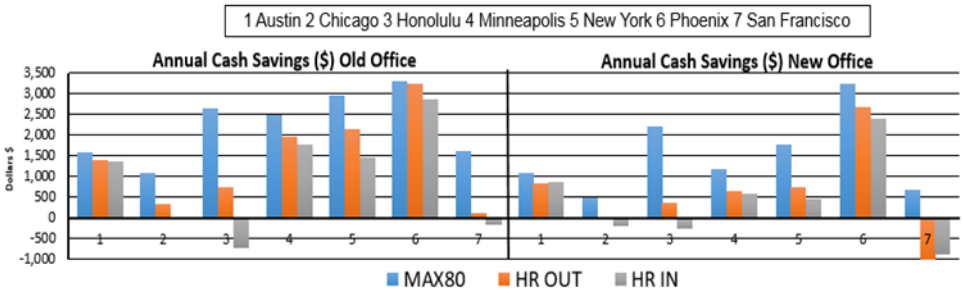

Figure 30: Office buildings cash savings.

4.2.3 PCM Material Development and PCHX Design

This section discusses the development of one of RoCo's most important components: the PCM heat exchanger (HX). The graphite enhanced PCM was an enabling technology for this project. To efficiently store the heat extracted by the HP for multiple hours without releasing waste heat, a high-energy density system capable of accepting the thermal power levels generated was required. To reduce costs, a simple phase change heat exchanger (PCHX) design was needed that must be optimized for integration with the RoCo HP. The compressed expanded natural graphite (CENG)-PCM composite material provided an ideal solution to this challenge, providing high values for the effective thermal conductivity and latent heat.
The selection of the graphite bulk density influences several PCHX design parameters, as shown in the Figure 31 for one of the prototype PCHXs. A bulk density of 50 kg/m^3 was chosen since it minimizes the PCHX mass and volume while requiring a lower limit of refrigerant tubing and charge.

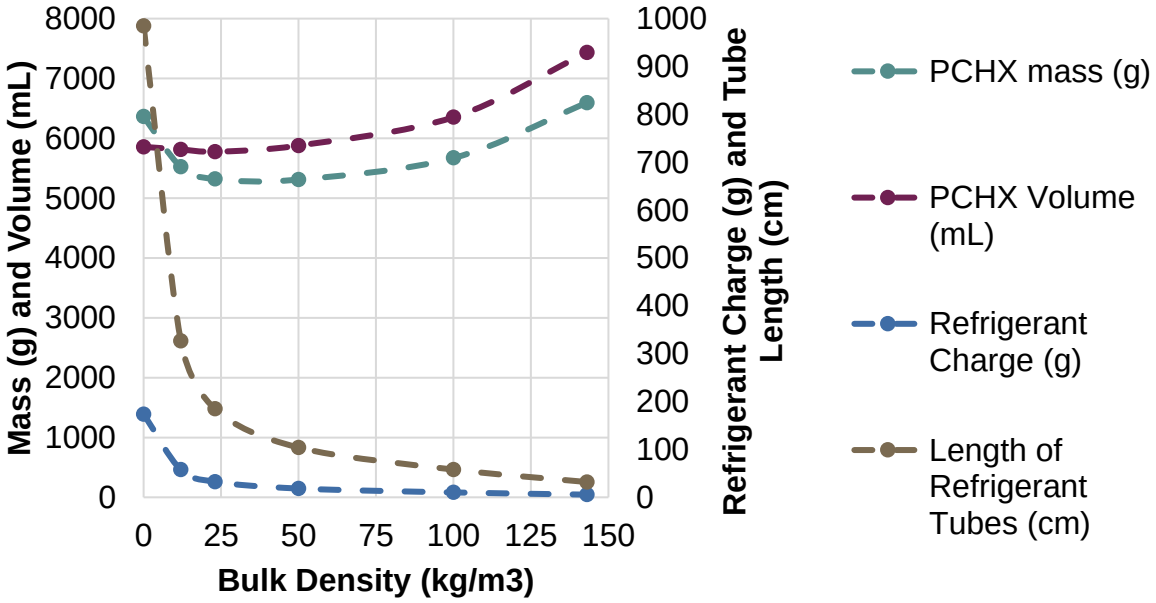

Figure 31: Summary of the impact of graphite foam bulk density on PCHX design parameters.

The PCM-CENG composite material employed for the project used an organic material for the PCM called PureTemp PT37, which has a melting point of 37°C. Composite samples were prepared by different methods, but melting the PCM in a vacuum furnace while maintaining contact with the CENG provided a way to almost completely saturate the CENG with PCM so that void volume was minimal. Percent void was less than 1% using this method. This led to the intimate contact of the PCM with the graphite, yielding optimal heat transfer despite the CENG's low material density and maximizing the system's PCM mass, thus providing the greatest possible latent heat storage capacity.

A thermal conductivity of nearly 5 W/m-K was achieved for the composite, and the PCHX volumetric and gravimetric energy densities were measured at 75.3 Wh/L and 72.9 Wh/kg, respectively. This significantly exceeds the project's target values of 65 Wh/L and 64 Wh/kg for the PCHX.

For the PCHX fabrication approach described previously using sheets of CENG, inserting the refrigerant tubing in the PCHX must be completed after producing the CENG-PCM composite. This requires drilling holes into the composite, inserting tubes, and brazing the required fittings, which is a complicated, time-consuming process. To fabricate the PCHX with this method, small blocks of the CENG-PCM composite material—produced using the same technique as full-sized discs—were poured into a mould in which the fully assembled copper heat exchange tubing network is located, and additional PCM was added to fill the voids.

An optimal distribution of the block sizes can be used to minimize the void space between CENG blocks in the final product. Figure 32 left shows a schematic of this concept, including an approach intended to minimize the contact resistance from the tubing to the PCM.

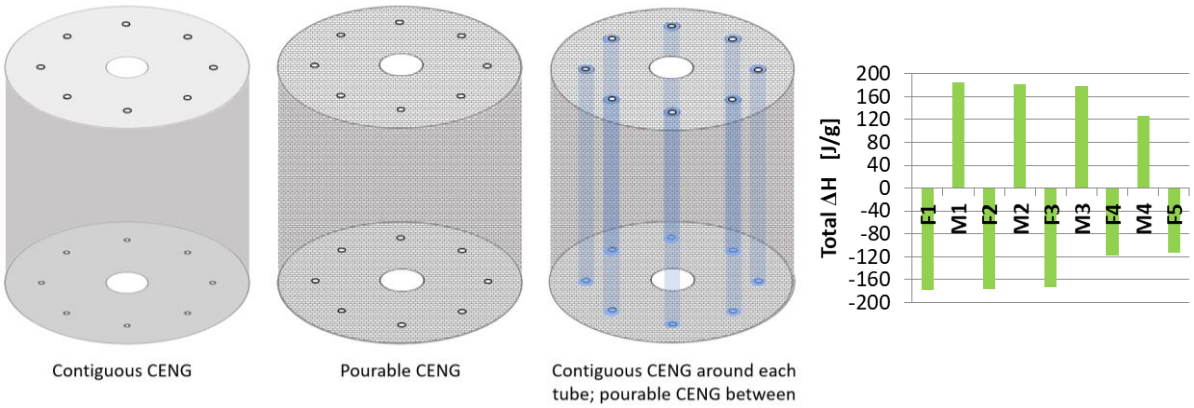

Figure 32: PCM condenser design (left) and CENG-salt hydrate latent heat (right)

Lower cost PCM material development was also pursued as part of the research. Salt hydrates offer the potential for high thermal energy storage capacity at a significantly lower cost than other PCMs. However, salt hydrates have issues with material stability under repeated thermal cycling due to incongruent melting and with the material supercooling before freezing begins. The team conducted a feasibility study of salt hydrate-graphite composites, specifically addressing methods to stabilize salt hydrates by nucleating on expanded graphite and then compressing them into a porous composite. It was demonstrated that incorporating a salt hydrate within a CENG structure can improve the material stability by reducing incongruent melting, thereby improving the cycling performance of the material. A new method for preparing a CENG-salt hydrate PCM composite was developed using a sodium sulphate decahydrate that shows promise as a low-cost PCM material. The data in Figure 32 right shows the measured latent heat from a sample of the CENG-salt hydrate material for five freeze-melt cycles. Considering that this sample did not contain any stabilizing agents except CENG (it was only CENG and sodium sulphate decahydrate), this is a promising result. Pure sodium sulphate decahydrate typically begins to degrade after only the first cycle. Future research is planned to understand the mechanisms at work and improve the stability of CENG-salt hydrate composites for thermal energy storage.

Several factors contributed to the success of this project. Developing the CENG-PCM composite material resulted in a latent heat storage material with relatively high thermal conductivity without significantly reducing thermal storage capacity. The team repeatedly used a combination of thermal modeling and experimentation to improve and validate understanding. Examples include identifying optimal material parameters for the final design through modeling, measuring performances at component and system levels and comparing with model predictions, and validating assumptions such as the magnitude of thermal contact resistance between tubing and the CENG-PCM composite. These proven approaches all contributed significantly to the positive results achieved.

4.2.4 RoCo Power Consumption Measurement

The team also evaluated RoCo power consumption. Table 6 provides the RoCo steady-state power consumption performance. Two cyclic tests were conducted, and the results justify the use of a low-cost PCM material: fatty alcohol. Figure 33 shows the cyclic test results.

Table 6: RoCo steady-state power consumption performance.

System performances	Unit	Results	Uncertainty
Suction pressure	kPa	563.1	1.7
Discharge pressure	kPa	1,188.3	1.7
Evaporating temperature	°C	19.8	--
Condensing temperature	°C	45.9	--
Superheat	K	5.0	0.5
Subcooling	K	1.0	0.5
Refrigerant mass flow rate (MFR)	g/s	0.98	0.001
Evaporator capacity (ref. side)	W	149.9	~0.8
COP	-	3.54 (Y3 goal is >3.0)	0.04
Air inlet temperature	°C	26.0	0.25
Air outlet temperature	°C	21.3	0.25
Evaporator capacity (air side)	W	159.9	~15

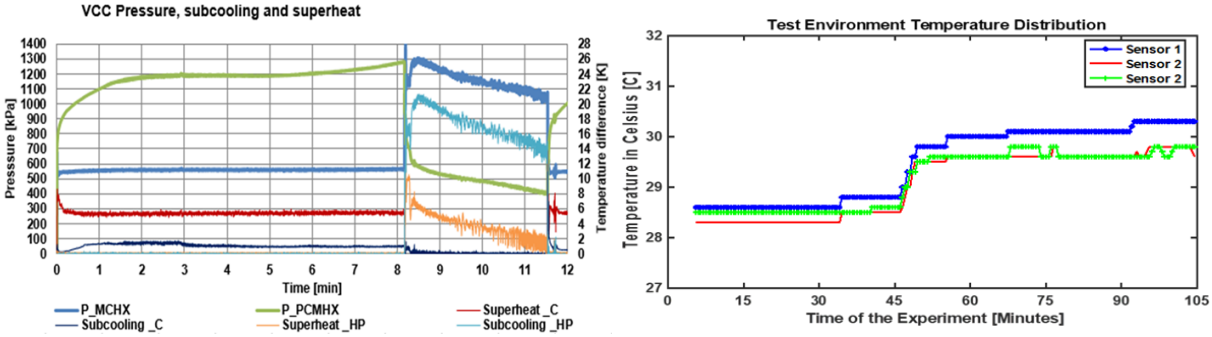

Figure 33: Pressure profile of RoCo under cyclic operation (left) and test environment temperature distribution

4.2.5 RoCo Thermal Comfort Testing

Another important goal for designing RoCo is to achieve good thermal comfort. According to the approved experiment's protocol, the room temperature changes from 27 ± 1°C during the first hour to 29 ± 1°C during the second hour, as shown in Figure 33 right . During the experiment, HS reported their thermal sensation and comfort level based on a seven-point scale and wore a smart bracelet that monitored their heart rate, skin temperature, and galvanic response. Similarly, during the last two rounds of experiments, heat flux sensors and temperature sensors were included in the experiment. Each HS had the option to request, deny, or stop using RoCo at any point during the experiment. Most of the HS chose to position the RoCo to their side (left or right) at approximately 3 ± 0.5 ft. Similarly, the position of the nozzle was consistently maintained toward their upper body, specifically their torso and face. The results indicate that most of the HS request RoCo during the second hour of the experiment when the room temperature reaches 29 ± 1°C. Also, the supply air temperature from RoCo had a consistent differential of 5°C (41°F) compared with the room temperature. Each HS reported comfortable values when using airflow rates between 50 to 60 cfm, and higher flow rates were reported to be uncomfortable due to the noise of the fan and the force of air impacting their bodies. Among the 40 HS, eight did not request RoCo due to their high tolerance to warm-hot environments. These HS reported comfortable values throughout the experiment. Lastly, the approved protocol for the smart nozzle occurred during the last 10 minutes of the experiment.

4.2.6 Experimental Results

RoCo's objective is to allow HS to manage and regulate their personal thermal environment. The results of the HS experiments indicate that RoCo positively impacts HS comfort levels and allows them to maintain their thermal comfortable level. However, the results also demonstrate high variability among HS due to their own individuality. Therefore, the results presented in this section will show the most significant responses obtained in the experiments.

4.2.7 Effective Cooling

RoCo's air jet aims at the upper body (i.e., chest and stomach) since this is the most effective area for heat transfer with the human body. For this reason, heat flux sensors were distributed over the torso to measure the effect of RoCo on the human body heat flux. Thus, the difference of the heat rejected when using RoCo and the heat rejected when NOT using RoCo is the effective cooling. Figure 34 left shows the general trend of measured heat flux over the time of the experiment. As expected, the heat flux when RoCo is operating, represented by the green line, is higher due to a higher temperature difference between the human body and RoCo's air jet. The red line represents the heat flux of the HS when not using RoCo. To estimate effective cooling, the difference of the means between the green and red line were considered. Table 7 shows the effective cooling for some HS during the last two rounds of experiments. The measured effective cooling for this range of experiments was 2–10 W, and the project's target effective cooling is 23 W. The difference between the calculated and target effective cooling is in the ambient temperature difference during the experiment. Nevertheless, the calculated effective cooling shows a linear correlation to the CFD estimation (Zhu et al. 2017), as shown in Figure 34 right.

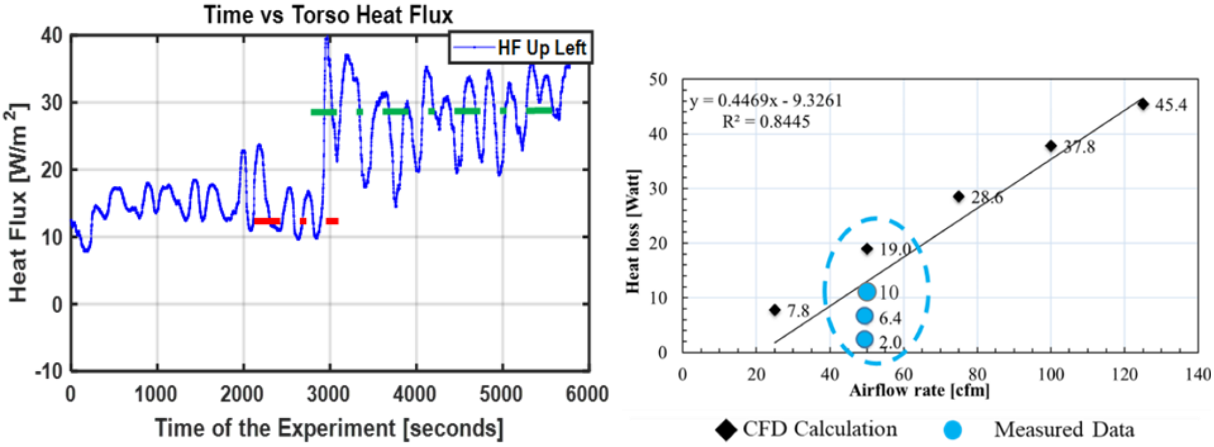

Figure 34: Heat flux measurement for no-RoCo and RoCo (left) and comparison of CFD and experimental data (right)

Table 7: Effective cooling calculations.

ID	CFM	Effective cooling due to RoCo (W)
HS1	50	6.4
HS 2	50	4
HS 3	50	4
HS 4	50	2
HS 5	60	10

4.2.8 Body Temperature Analysis

To regulate the personal space of HS, RoCo helps reduce the human body's skin temperature. As expected, human body temperature follows the temperature profile of the room, and RoCo helps reduce this temperature as soon as it starts operating. The results suggest that RoCo reduces skin temperature by approximately 1 K. An analysis of variance (ANOVA) showed statistically that the differences in skin temperature due to RoCo are significant in the experiments, as demonstrated in Figure 35 left.

4.2.9 Heart Rate Analysis

An important aspect of the human body thermoregulatory system is the heart due to its function to respond to hot or cold environments. The results suggest that the heart rate of most HS reduced or increased its variability. This effect is associated with the reduction of heat stress due to RoCo that allows the human body to ease the process of thermoregulation. An ANOVA analysis shows the statistically significant effect on the heart rate. This is due to RoCo since nothing else during the experiment changed. Figure 35 right shows the statistics obtained from the ANOVA analysis.

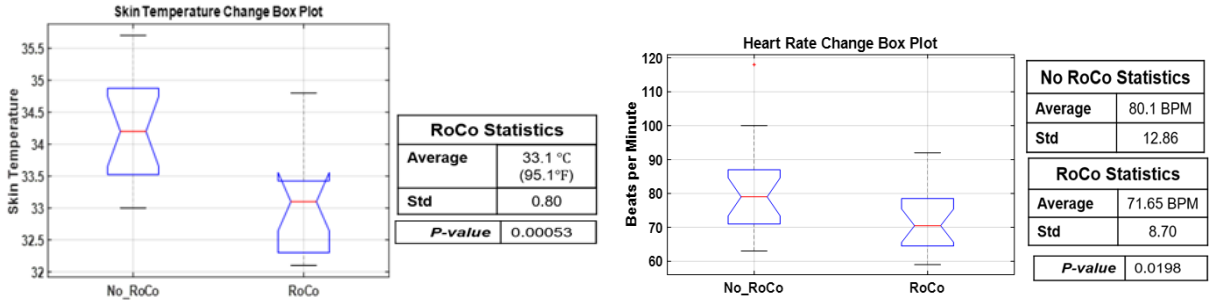

Figure 35: ANOVA skin temperature (left) and ANOVA heart rate (right)

4.2.10 Subjective Response

During the experiment, HS were required to report their thermal sensation and comfort level values every 10 minutes. Figure 36 shows a sample of the subjective response from four HS. Most HS required RoCo during the second hour of the experiment. At that time, all reported to be neutral, uncomfortable, or very uncomfortable when requesting RoCo. Meanwhile, as RoCo started operating, all reported an increase in their comfort level until reaching "very-comfortable," as shown in Figure 36. Therefore, the subjective results demonstrate that the presence of RoCo has a positive effect on the comfort level of HS.

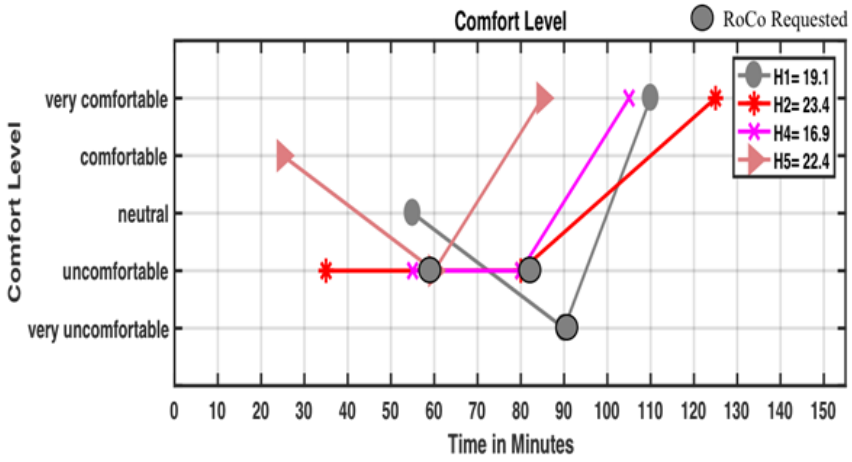

Figure 36: Sample of subjective responses from HS.

4.3 Conclusion Personal Cooling System

An assessment was performed on RoCo energy saving potentials for office buildings in the United States. For seven cities representing various climates, RoCo can provide up to 49% energy savings in mild climate, such as San Francisco, California, and 9% energy savings in hot climate, such as Phoenix, Arizona.

PCM development is another focus of the project. Before starting the project, the team expected the primary challenge to be obtaining a material with both good latent heat capacity and thermal conductivity. The two issues were solved by having a compressed graphite-assisted PCM. The targeted latent heat capacity and thermal conductivity were successfully achieved. However, the PCM research then shifted to lowering costs and VCC integration. To

lower the cost, a compressed graphite disc manufacturing process and alternative PCM materials were investigated. To better integrate the PCM with the VCC, the refrigerant piping and header design of the PCM condenser were investigated.
RoCo also provides good thermal comfort. Field testing showed that RoCo can provide 10 W effective cooling, reducing body temperature by 1 K and heart rate by 9 BPM. Most people expressed a better thermal sensation with RoCo.

4.4 Publications to the RoCo development

Further information on the RoCo development are contained in the following journal publications:

Rohit Dhumane, Yiyuan Qiao, Jan Muehlbauer, Jiazhen Ling, Vikrant Aute & Yunho Hwang (2019) Evaluating Recharge Options for Phase-Change Material Storage of a Personal Conditioning System, Science and Technology for the Built Environment, 25:10, 1337-1351, DOI: 10.1080/23744731.2019.1667699

Rohit Dhumane, Jiazhen Ling, Vikrant Aute, Reinhard Radermacher, Modeling Heat Pump Recharge of a Personal Conditioning System with Latent Heat Storage, Proceedings of the 13th International Modelica Conference, Regensburg, Germany, March 4–6, 2019

Rohit Dhumane, Yiyuan Qiao, Jiazhen Ling, Jan Muehlbauer, Vikrant Aute, Yunho Hwang, Reinhard Radermacher, Improving system performance of a personal conditioning system integrated with thermal storage, Applied Thermal Engineering, Volume 147, 2019, Pages 40-51, ISSN 1359-4311, https://doi.org/10.1016/j.applthermaleng.2018.10.004

Rohit Dhumane, Anne Mallow, Yiyuan Qiao, Kyle R. Gluesenkamp, Samuel Graham, Jiazhen Ling, Reinhard Radermacher, Enhancing the thermosiphon-driven discharge of a latent heat thermal storage system used in a personal cooling device, International Journal of Refrigeration, Volume 88, 2018, Pages 599-613, ISSN 0140-7007 https://doi.org/10.1016/j.ijrefrig.2018.02.005.

Rohit Dhumane, Jiazhen Ling, Vikrant Aute, Reinhard Radermacher, Portable personal conditioning systems: Transient modeling and system analysis, Applied Energy, Volume 208, 2017, Pages 390-401, ISSN 0306-2619, https://doi.org/10.1016/j.apenergy.2017.10.023.

Yilin Du, Jan Muehlbauer, Jiazhen Ling, Vikrant Aute, Yunho Hwang, Reinhard Radermacher, Rechargeable Personal Air Conditioning Device, Proceedings of the ASME 2016 10th International Conference on Energy Sustainability, Charlotte, North Carolina, USA, June 26-30, 2016

Yiyuan Qiao, Yilin Du, Jan Muehlbauer, Yunho Hwang, Reinhard Radermacher, Experimental study of enhanced PCM exchangers applied in a thermal energy storage system for personal cooling, International Journal of Refrigeration, Volume 102, 2019, Pages 22-34, ISSN 0140-7007, https://doi.org/10.1016/j.ijrefrig.2019.03.006.

Yiyuan Qiao, Tao Cao, Jan Muehlbauer, Yunho Hwang, Reinhard Radermacher, Experimental study of a personal cooling system integrated with phase change material, Applied Thermal Engineering, Volume 170, 2020, 115026, ISSN 1359-4311, https://doi.org/10.1016/j.applthermaleng.2020.115026.

5 Integrated GS heat pump variants – Knoxville, US

5.1 IHP Development Background

The DOE Building Technologies Office (BTO) long-term goal is to maximize the energy efficiency of the US building stock by 2030. Maximizing building energy efficiency is an essential facilitating step to enable market uptake of nZEBs, including net-zero energy homes. To achieve this vision, the energy used by the energy service equipment (e.g., equipment that provides space heating [SH], space cooling [SC], water heating) must be significantly reduced by 50% or more compared with today's best common practice. One promising approach to achieve this is to produce one piece of equipment that provides multiple services. ORNL developed a general concept design for such an appliance, called the *Integrated Heat Pump IHP*. The IHP concept was summarized in the final report for International Energy Agency (IEA) Heat Pumping Technologies (HPT) Annex 40 (Wemhoener, 2016) with full details available in related reports (Murphy et al, 2007a), (Murphy et al, 2007b). In the following a summary and further results of field monitoring of the developed prototype embodiments are given.

5.2 Variants of the IHP Layout

There are two primary versions of the IHP: geothermal (or GS-IHP) and air-source (AS-IHP). ORNL activities have focused on developing four different embodiments of the IHP in collaboration with manufacturing partners. The first focused on an electric GS-IHP and is now a commercially available product marketed by the partner ClimateMaster, Inc. (CM). The other three are AS-IHPs (two electric-driven and one natural gas engine-driven), which were also developed collaboratively with manufacturing partners. All three AS-IHP developments have reached the prototype packaged system stage and have completed field evaluation. Details are provided in the following sections.

5.2.1 Summary of GS-IHP System Development, Analyses, and Test Results

Figure 37 shows a conceptual installation. The system uses a variable-speed (VS) compressor, a VS indoor blower (for SH/SC distribution), and VS pumps for ground heat exchanger (GHX) fluid circulation and hot water (HW) circulation. A 190–400 L (50–105 gal) water heater (WH) tank is included. Figure 3.1 depicts a horizontal GHX installed in the existing home foundation excavation, but the system can use any geothermal heat source or sink (e.g., vertical bore GHX, ground water, surface water).

5.3 GS-IHP Field Demonstration Project Summary

The material in this section is summarized from the full project report (Baxter, Munk and Gehl, 2016). In 2012, CM announced a new product, which is currently marketed as the Trilogy 45 Q-Mode.[1] It is available in two nominal SC capacity sizes: 7 kW (2 tons) and 14 kW (4 tons). Rated performance per the US Air-Conditioning, Heating, and Refrigeration Institute (AHRI) ground loop HP conditions (AHRI et al., 1998) for the larger capacity unit were heating COPs of 5.1 and 3.3 at minimum and maximum speeds, respectively, and cooling COPs of 13.2 and 6.3 at minimum and maximum speeds for the larger capacity units (Climate master, 2019). The smaller capacity unit has slightly higher efficiencies at maximum compressor speeds: 3.6 heating COP and 7.1 cooling COP. Table 8 summarizes the system rating and design performance compared with those of a conventional electric commercial rooftop HP unit (RTU) with a conventional electric storage WH.The system features a VS compressor, a VS blower for indoor air circulation, and VS pumps for GHX loop and domestic hot water (DHW) loop circulation. The system provides variable SC, space-heating, and water-heating capacity as needed by modulating over setpoint temperature ranges. Four different operating modes are available, as listed below:

[1] https://www.climatemaster.com/Homeowner/side-links/products/product-details/trilogy

- SC (factory set at 5.3–14.1 kW for the larger unit; installer adjustable to maximum 17.6 kW)
- SH (1.5–17.6 kW for larger unit)
- Combined WH plus SC (SC + WH)
- Dedicated water heating (DWH) year-round

Table 8: Summary of GS-IHP vs. conventional RTU + electric storage WH.

	Base (electric RTU/HP and WH)	**GS-IHP**
Compressor/number	**ScrolI/1-speed**	**ScrolI/VS**
Refrigerant type	R410A	R410A
Design cooling seasonal COP	3.8	N/A
Design cooling rating	14.1 kW at 35°C outdoor temperature[a]	5.3 kW at minimum speed[b] 14.1 kW at maximum speed[b]
Design heating rating	13.2 kW at 8.3°C outdoor temperature[a] 8.2 kW at −8.3°C outdoor temperature[a]	7.0 kW at minimum speed[b] 17.6 kW at maximum speed[b]
Design water heating capacity; dedicated WH	4.5 kW (conventional electric WH)	~8.2 kW, low speed ~11.7 kW, high speed (110°F entering HW temperature; 35–80°F entering water temperature (EWT) from GHX loop)[c]
Design cooling plus WH capacity; combined mode	N/A	5.3 kW cooling + 7.0 kW, low speed 14.1 kW cooling + 20.2 kW WH, high speed (43.3°C entering HW temperature)[c]
Rated cooling efficiency	3.34 energy efficiency ratio (EER) at 35°C outdoor temperature 3.8 seasonal COP[a]	13.2 COP at minimum speed[b] 6.3 COP at maximum speed[b]
Rated heating efficiency	3.05 COP at 8.3°C outdoor temperature[a] 2.26 COP at −8.3°C outdoor temperature[a]	5.1 COP at minimum speed[b] 3.3 COP at maximum speed[b]
Design water heating efficiency; dedicated WH	1.0 COP (conventional electric WH)	2.5–5.0 COP (43.3°C entering HW temperature; 35–80°F EWT from GHX loop)[c]
Design cooling plus WH efficiency; combined mode	Na	Up to 8.8 COP combined, low speed Up to 5.6 COP combined, high speed (43.3°C entering HW temp.)[c]
Unit dimension (in.)	45 L × 47 H × 76 W	25.4 L × 56 H × 30.6 W
Unit weight	590 lb, RTU	448 lb, Trilogy water source HP (WSHP)
Electrical	13.0 kW, RTU 4.5 kW, WH tank	8.5 kW, HP unit 4.5 kW, WH tank

[a]Certified per American National Standards Institute (ANSI)/AHRI Standard 210/240.
[b]Certified per ANSI/AHRI/ISO/ American Society of Heating, Refrigerating and Air-Conditioning Engineers (ASHRAE) Standard 13256-1. The Trilogy can be adjusted at installation to 17.6 kW maximum cooling capacity, as was done at the Oklahoma City site; a 17.6 kW cooling capacity conventional RTU HP was used for the baseline comparisons at that site as noted in later sections of this report.
[c]CM (Climate Master, 2019).

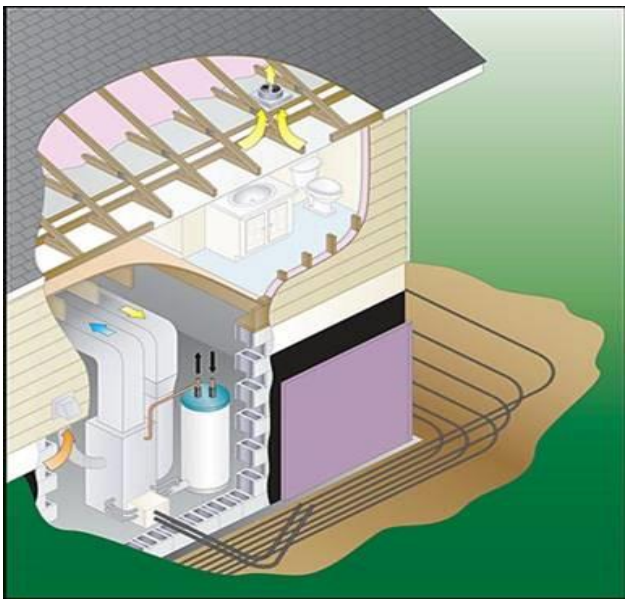

Figure 37: Conceptual installation of residential GS-IHP

The two Trilogy HW tanks are connected to a common building HW distribution system. This system includes a HW recirculation loop to minimize the wait time for HW at the fixtures in each residential unit; the recirculation pump energy use was not monitored. Only one of the tanks was instrumented to attempt to determine the HW energy delivered to the building HW distribution system. Additionally, the VS compressor and blower allow the unit to increase/decrease dehumidification (DH) (i.e., moisture removal) capacity as necessary in response to space relative humidity (RH) levels when in SC modes to maintain comfort levels in the conditioned space without sacrificing efficiency. Similarly, the air delivery temperature can be adjusted as needed in SH mode. Compact HX designs are used for the air/refrigerant SH/SC coil and the GHX loop/refrigerant and HW/refrigerant coils. This reduces the required system refrigerant charge and associated environmental risks.

5.4 Demonstration Site and Tested GS-IHP System Descriptions

CM and ORNL selected two commercial/institutional building sites for the field demonstration project. The first was a commercial kitchen attached to a day care facility located in a large church building in Knoxville, Tennessee. Knoxville is in climate Zone 4A ("mixed-humid" per Figure 38 and Table 9). The second was a homeless shelter dormitory-type building (~743 m^2 total floor space) in Oklahoma City, Oklahoma in climate Zone 3A ("warm-humid"). CM and its subcontractors (City Heat & Air Conditioning of Knoxville and Comfortworks, Inc. of Goldsby, Oklahoma) designed and installed the GS-IHP systems. Figure 38 – Figure 42 provide photos and GHX schematics for the two installations. At the Knoxville site, a single GS-IHP provided SH, SC, and DHW services for a 43 m^2 kitchen and adjoining 5.6 m^2 pantry. The occupancy schedule is 8:00 a.m. to 5:00 p.m., Monday through Friday, except for holidays. The Oklahoma City installation includes two Trilogy-based GS-IHP systems with 400 L HW tanks, each providing HVAC/WH to 10 residential units (~230 m^2 each). Because of the higher peak design cooling loads at this site, the Trilogy units were set up during installation to provide peak cooling capacity of 17.6 kW each.

Table 9: Description of US climate zones. (Source: ANSI/ASHRAE/IESNA Standard 90.1-2019.)

Nº Zone	Name	Thermal criteria
0	Extremely hot	6,000 < CDD 10 °C
1	Very hot/humid (1A), dry (1B)	5,000 < CDD 10 °C ≤ 6,000
2	Hot/humid (2A), dry (2B)	3,500 < CDD 10 °C ≤ 5,000
3A and 3B	Warn/humid (3A), dry (3B)	CDD 10 °C < 3,500 and HDD 18 °C ≤ 2,000
3C	Warm/marine	CDD 10 °C ≤ 2,500 and HDD 18 °C ≤ 2,000
4A and 4B	Mixed/humid (4A), dry (4B)	CDD 10 °C ≤ 3,500 and 2,000 < HDD 18 °C ≤ 3,000
4C	Mixed/marine	CDD 10 °C ≤ 1,500 and 2,000 < HDD 18 °C ≤ 3,000
5A, 5B, 5C	Cool/humid (5A), dry (5B)	CDD 10 °C ≤ 3,500 and 3,000 < HDD 18 °C ≤ 4,000
5C	Cool/marine	CDD 10°C ≤ 1,000 and3,000 < HDD 18 °C ≤ 4,000
6A and 6B	Cold/humid (6A), dry (6B)	4,000 < HDD 18 °C ≤ 5,000
7	Very cold	5,000 < HDD 18 °C ≤ 7,000
8	Subarctic	7,000 < HDD 18 °C

Two additional non-IHP GS HPs provide HVAC for common areas of the building. The total nominal cooling capacity for all four HP systems is 63 kW, and all are connected to a common GHX loop (Figure 42 left). Each WSHP unit uses its own internal loop circulator pump; no central system pump is used. Only one GS-IHP was instrumented and monitored in detail. The residential areas of the building are occupied continuously.

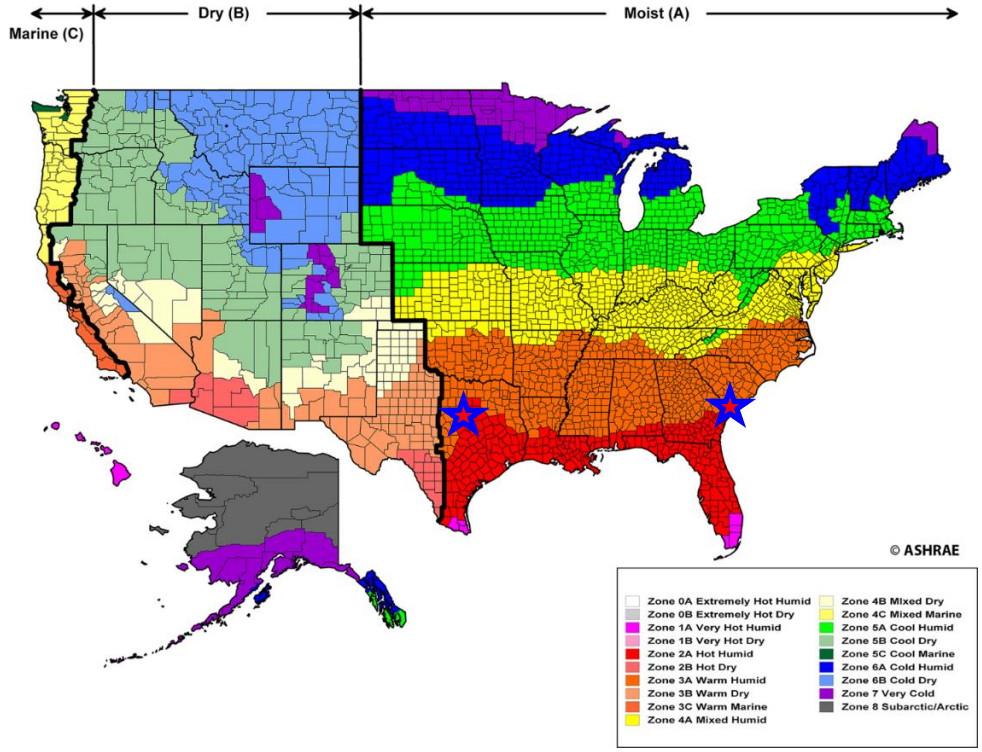

Figure 38: Map of US climate zones. Stars indicate GS-IHP demonstration site locations. (Source: ANSI/ASHRAE/IESNA Standard 90.1-2019.)

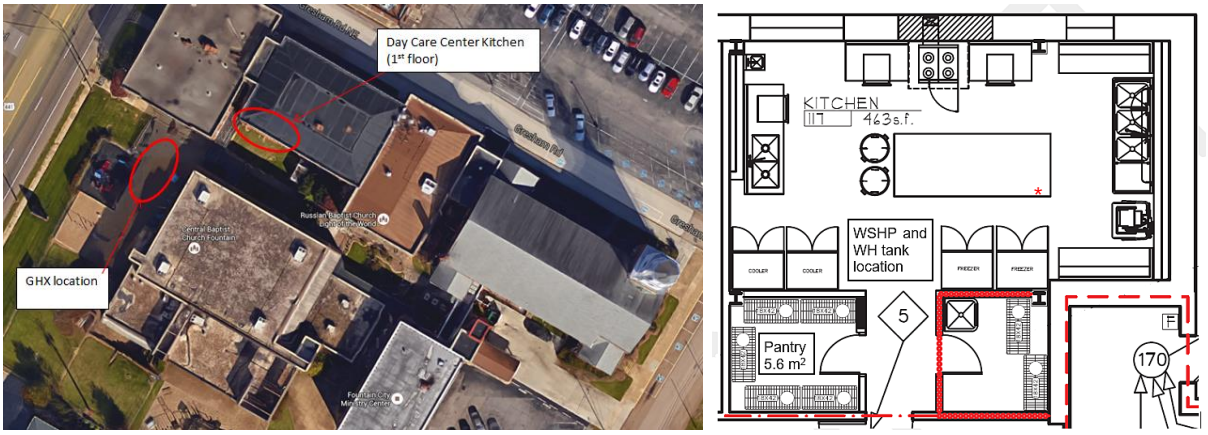

Figure 39: Aerial view of the Knoxville site. (Photo source: Google Maps) and kitchen floor plan of Knoxville site.

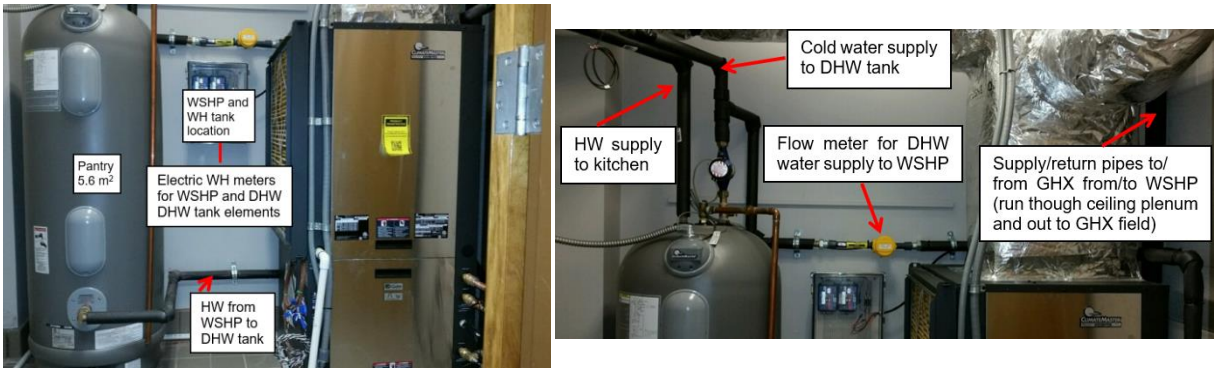

Figure 40: Trilogy WSHP system as installed (left) WH piping connections and flowmeters (right) at Knoxville site

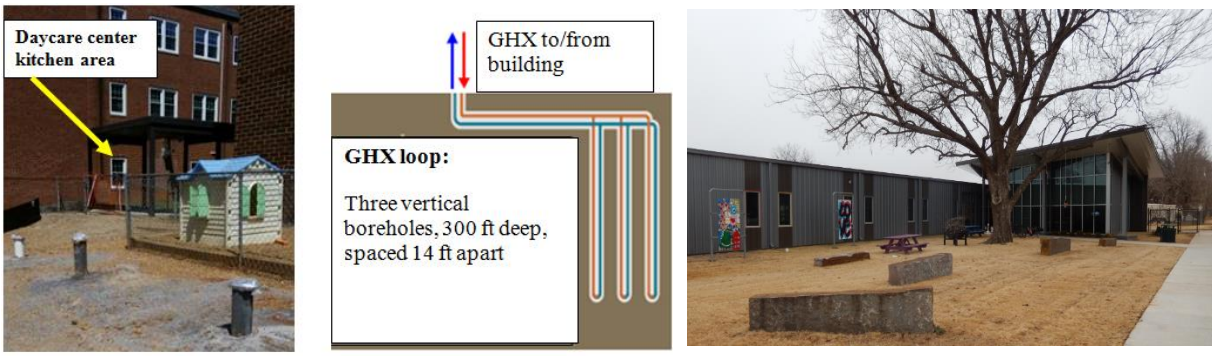

Figure 41: GHX loop location and schematic for Knoxville site (left, Graphic source: CM) and Oklahoma City site host building (right)

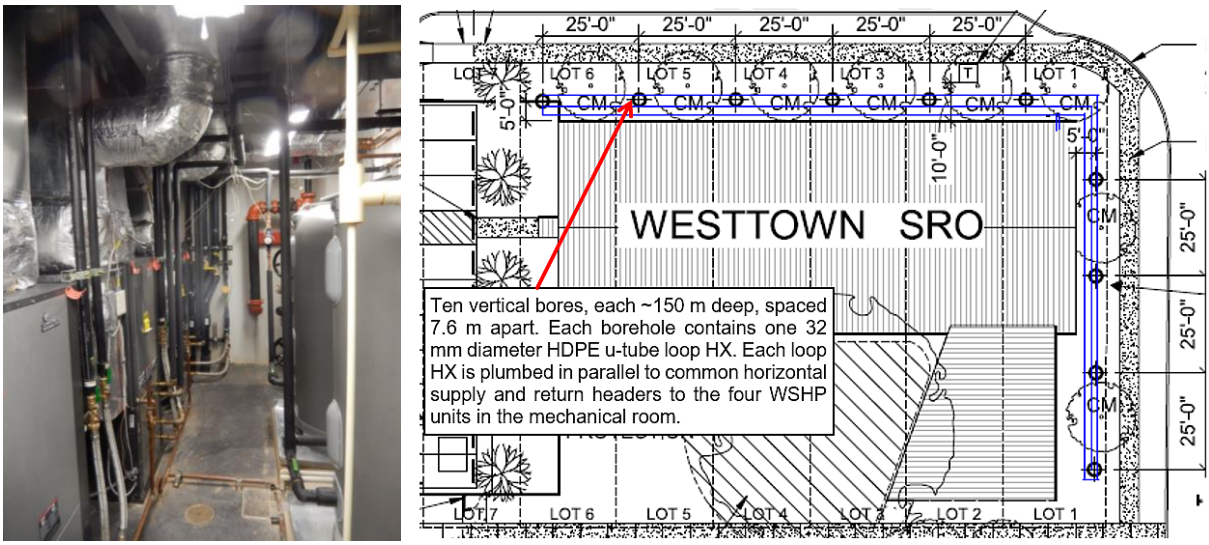

Figure 42: Oklahoma City host building mechanical room; instrumented Trilogy is on left hand side against back wall; Trilogy HW tanks are on the right. (left, Source: CM) and GHX loop location and details for Oklahoma City site (right, Source: CM.)

5.5 Instrumentation, Data Acquisition, Field Data Analysis Approach

The test systems were installed and commissioned to ensure proper operation at both sites. Data acquisition systems (DAS) were designed and installed at each site. Data monitoring at the Knoxville site began on August 18, 2015 and continued until August 18, 2016 with only one ~3 day outage. Because of construction delays at the Oklahoma City site, data acquisition installation was delayed. Partial data monitoring for SH and SC performance began on January 31, 2016. Full data collection, including WH mode operation, began May 19, 2016 and continued through September 19, 2016, but there were several outages, as noted below. Therefore, monitored data were not available to support a full year's performance summary as was the case for the Knoxville site.

The Oklahoma City site data gaps January through August 2016 include:

- April: DAS unavailable at the beginning April 28 at 3 p.m. through May 19 at 1 p.m.
- June: data missing from June 10 at 6 p.m. through June 15 at 6 p.m.
- August: DAS offline August 12–16
- September: DAS offline September 3–7

Data were collected in 15-second intervals, averaged into 1-minute intervals, and sent to a remote server at ORNL via the internet. Table 10 summarizes the DAS sensor accuracy. During data collection, the GS-IHPs were operated as normal with a wall thermostat to control SH and SC operation and a WH tank thermostat to control WH operation.

Table 10: Instrumentation used to measure GS-IHP system performance.

Monitoring point	Manufacturer	Model number	Accuracy range
Trilogy WSHP unit and WH tank element energy consumption	Continental Control Systems	WattNode models WNC-3Y-208-MB and WNB-3Y-208-P, respectively	±0.5% W reading for 5–100% rated current (±1% of reading for 1–5% rated current)
Line voltage	Continental Control Systems	WattNode model WNC-3Y-208-MB	±0.5% V reading
Supply/return temperatures, Trilogy to/from GHX loop	Omega	PM-1/10-1/8-6-1/8-P-3; platinum resistance temperature device (RTD), immersion	±(0.03 + 0.0005 |t|)°C from 0–100°C[a]
Supply/discharge temperatures, Trilogy to/from DHW tank	Omega	PM-1/10-1/8-6-1/8-P-3; platinum RTD, immersion	±(0.03 + 0.0005t)°C from 0–100°C[a]
Supply/return temperatures, DHW tank to/from building HW distribution network	Omega	PM-1/10-1/8-6-1/8-P-3; platinum RTD, immersion type	±(0.03 + 0.0005t)°C from 0–100°C[a]
Flow, GHX loop	Omega	FMG3001-PP	±0.8%, maximum (~3.8–76 l/m)[b]
Flow, DHW tank loop	Omega	FMG3001-PP	±0.8%, maximum (~3.8–38 l/m)[b]
Flow, building water supply to DHW tank	Omega	FTB8007B-PT	±1.5% (0.83–83 l/m)
ID space temperature	Trilogy onboard sensor	Thermistor included with CM thermostat	±0.56°C (±1.0°F)
ID space RH (%)	Trilogy onboard sensor	Johnson Controls model HT-6703	±3% RH
WH upper tank wall temperature	Trilogy onboard sensor	Thermistor mounted to WH tank wall	±0.56°C (±1.0°F)
Temperature in/out Trilogy air coil	Omega	Type T TC	0.75% full scale
RH% in/out Trilogy air coil	Omega	HX92AC-D	±2.5% RH from 20–80% RH; ±3.1% RH below 20% and above 80% RH at 22°C with temperature coefficient of ±0.1% RH/°F output
Ambient temperature	Local airport weather data	Ecobee website accessed via Trilogy control system	N/A

[a]All RTDs underwent five-point calibration over an expected temperature operating range of about -1-60 °C (30–140°F) against a NIST traceable thermometer; linear fit to temperature standard with R^2 of 1.000.
[b]Results of factory calibration against NIST traceable standard over expected operating flow ranges.

SH, SC, and WH energy delivered by the GS-IHP was computed for each mode using the following equations.

SC delivered (SC Mode):

$$Q_{SC} = V_{GroundLoop}\rho_{GroundLoop}c_{GroundLoop}(LWT - EWT) - W_{IHP} \quad \text{(eq. 1)}$$

SC delivered (SC + WH Mode):

$$Q_{SC} = Q_{WH,IHP} - W_{IHP} \quad \text{(eq. 2)}$$

SH delivered (SH mode):

$$Q_{SH} = V_{GroundLoop}\rho_{GroundLoop}c_{GroundLoop}(EWT - LWT) + W_{IHP} \quad \text{(eq. 3)}$$

Water heating delivered by IHP to the WH tank and connecting lines between tank and IHP (DWH mode):

$$Q_{WH,IHP} = V_{DHWLoop}\rho_{DWHLoop}c_{DWHLoop}(LDWHT - EDWHT) \quad \text{(eq. 4)}$$

Water heating delivered to building

$$Q_{WH} = V_{Hot}\rho_{Hot}c_{Hot}(T_{Hot}^{*} - T_{Cold}) \quad \text{(eq. 5)}$$

Where:
EWT is the GHX loop fluid temperature entering WSHP (RTD)
LWT is the GHX loop fluid temperature leaving WSHP (RTD)
$EDWHT$ is the domestic HW temperature entering WSHP (RTD)
$LDWHT$ is the domestic HW temperature leaving WSHP (RTD)
T_{Cold} is the cold water supply temperature to WH tank (RTD)
T_{Hot} is the HW temperature leaving WH tank (see footnote)
V is the fluid flow rate
ρ is the fluid density
c is the fluid specific heat

Energy consumption for the GS-IHP is measured directly by two watt-hour meters: one for the Trilogy unit (W_{IHP}) and one for the WH tank backup elements (W_{tank}). For the combined SC/WH mode, the energy consumption was apportioned to each output proportional to the output capacity and stored along the load data for each time step. This implicitly assumes that the efficiency, or COP, is the same for SC and WH in the combined mode.

The energy delivery and measured energy use for the GS-IHP in each mode were totalled for each month and season and compared with the estimated energy used by a baseline electric RTU/electric WH system sized to meet the same loads. Baseline RTU performance was estimated using performance curves that accounted for variations in outdoor temperature and humidity, indoor temperature and humidity, time- and temperature-controlled defrosting, cyclic losses, and supplemental resistance heating. Defrost cycles were assumed to be 5.8% of the operating time at outdoor temperatures below 40°F, and the defrost tempering heat energy was assumed to be equal to the cooling done during the reverse cycle defrost. The measured cooling load was not divided into sensible and latent parts. Since the GS-IHP varies its VS blower speed (rpm) to adjust the split of sensible and latent cooling required by the space, it is assumed to deliver the minimum total cooling energy required to maintain comfortable indoor conditions. In contrast, the baseline RTU unit does not have a VS indoor blower and therefore cannot adjust the ratio of sensible and latent cooling delivered. This results in insufficient latent cooling and discomfort or in excess latent cooling and wasted energy. As such, assuming that similar comfort levels are maintained by both systems, the SC savings calculated for the GS-IHP over the RTU system are conservative.

---

*Note 1:THot was taken to be the maximum of (1) the leaving HW temperature measured by an immersion RTD sensor in the HW exit line to the building distribution system or (2) the upper tank wall temperature measured by a thermistor located near the upper element. Many of the HW draws experienced at both sites were of such small volumes and short durations that the RTD response time was too slow to capture an accurate measure of the leaving HW temperature.

Note 2: Additionally, late in the project it was discovered that the flowmeter at the Knoxville site providing the VHot measurement was subject to some flow oscillations in the cold-water line. Because of the nature of the meter, these oscillations caused the flow measurement to be higher than the actual flow. This erroneous flow was filtered out of the data by checking the corresponding temperature of the HW leaving the tank. When oscillations caused the measured flow, the HW temperature sensor was sufficiently far from the tank, so it did not increase in temperature. Any flow data without a corresponding increase in HW temperature or that was composed of less than three pulses from the flow meter were removed from the dataset. This could have inadvertently eliminated some small flow events (<0.2 gal), so the calculation of the water heating energy delivered to the building is likely conservative.

Note 3: There was significant uncertainty at the Oklahoma City site about where to place the DHW flow meter due to the presence of a building HW recirculation system and because there were two IHP systems with water tanks. With the amount of instrumentation budgeted for the project, it was impossible to obtain a good measure of the WH energy delivered to the building HW distribution system from each individual tank with any confidence. Therefore, the tank and connecting line standby heat losses measured for the Knoxville system (~23% combined) were assumed to also apply to the Oklahoma City system. This a somewhat conservative assumption because the IHP in Oklahoma City experienced heavier and more continuous WH loads than the Knoxville system. The system in Oklahoma City spent an average of ~12% of its total test period hours in WH modes compared with <5% for the Knoxville system. With longer run times and heavier WH loads, the HW tank and connecting line standby heat losses should be a smaller fraction of the total load.

5.6 Knoxville Site System Performance Summary

Table 11 summarizes the overall GS-IHP performance monitoring results for the Knoxville site from 2 p.m. on August 18, 2015 through 12 a.m. on August 18, 2016, along with the assumptions and limitations of the comparison. Only SC and WH operation data were included in the table because no SH operation was required during the test year at the Knoxville site.

Table 11: Knoxville site GS-IHP summary performance comparison vs. baseline system.

	GS-IHP	Baseline RTU + electric WH
SC (from SC and SC + WH modes)		
Total SC delivered (kWh)	16,729	16,729
Sensible cooling delivered (kWh)	14,227	14,227
Sensible heat ratio (SHR)	0.85	0.85
SC energy use (kWh); % savings vs. baseline	2,165; 46.3%	4,032
SC COP	7.73	4.15
WH (from demand WH and SC + WH modes)		
Total HW used (gal)	19,262	19,262
Average working day HW use (gal/day)	78.3	78.3
WH output from WSHP to WH tank (kWh)	2,730	--
Water heating delivered to building (kWh)	2,106	2,106
Total WH energy use (kWh); % savings vs. baseline	646; 72.4%	2,340
GS-IHP backup tank element energy use (kWh)	1.5	--
Water heating COP	3.26	0.90[2]
Water heating COP excluding tank/line losses	4.23	1.00
Misc. energy consumption from controls, etc. (kWh)	151	151
Overall		
Energy use (kWh)	**2,962**	**6,519**
% energy savings	**54.6%**	**--**
Carbon equivalent emissions (CO_2 metric tons)[3]	**2.04**	**4.49**
CO_2 emission savings (metric tons)	**2.45**	**--**

The following assumptions were made.

1) Baseline RTU SHR—a measure of latent cooling or DH capacity—is the same as the baseline estimated for Trilogy WSHP.
2) Baseline RTU is a 48,000 Btu/h (4-ton) rated cooling capacity unit (see Table 3.1 for other ratings).
3) Baseline RTU fan power is 365 W/0.47 L/m or 365 W/1,000 cfm (AHRI, 2017)(taken from the current AHRI 210/240 ratings procedure).
4) Baseline RTU miscellaneous energy use is the same as that measured for the Trilogy WSHP.
5) Energy use for the combined SC + WH mode is divided between SC and WH proportional to the output capacities. Essentially, the COP for WH and SC in the combined mode is assumed to be the same. This slightly lowers the SC efficiency due to the higher condensing pressures required for the SC + WH mode and raising the WH efficiency relative to the SC-only and dedicated WH mode efficiencies.
6) The Trilogy sensible cooling and subsequent SHR are calculated based on the cubic feet per minute provided by the Trilogy unit, an assumption of 1.2 kg/m^3 (0.075 lbm/ft^3) air density, and measured return and supply air temperatures.
7) The baseline system uses the existing electric WH at the site; the rated energy factor (EF) is 0.9, which is the minimum EF required for electric WHs manufactured before Apr 1, 2015.

[2]Minimum energy factor rating for existing 50 gal electric storage WH manufactured before April 15, 2015 as rated per DOE test procedure.
https://www1.eere.energy.gov/buildings/appliance_standards/product.aspx/productid/27.
[3]Estimated using a kWh-to-CO_2 conversion factor of 6.89 × 10^{-4} metric tons/kWh.

The SC mode energy savings are likely somewhat conservative because the IHP and baseline RTU were assumed to maintain similar comfort sensible and latent SC loads. Since the RTU does not have a VS blower like the IHP, it would likely have to consume more energy to meet the same latent SC loads.
Figure 43 provides a graphical comparison of the monthly average overall SC COPs for the GS-IHP and baseline RTU/HP. The GS-IHP SC COPs in the plot include SC delivered in SC-only and SC + WH modes.

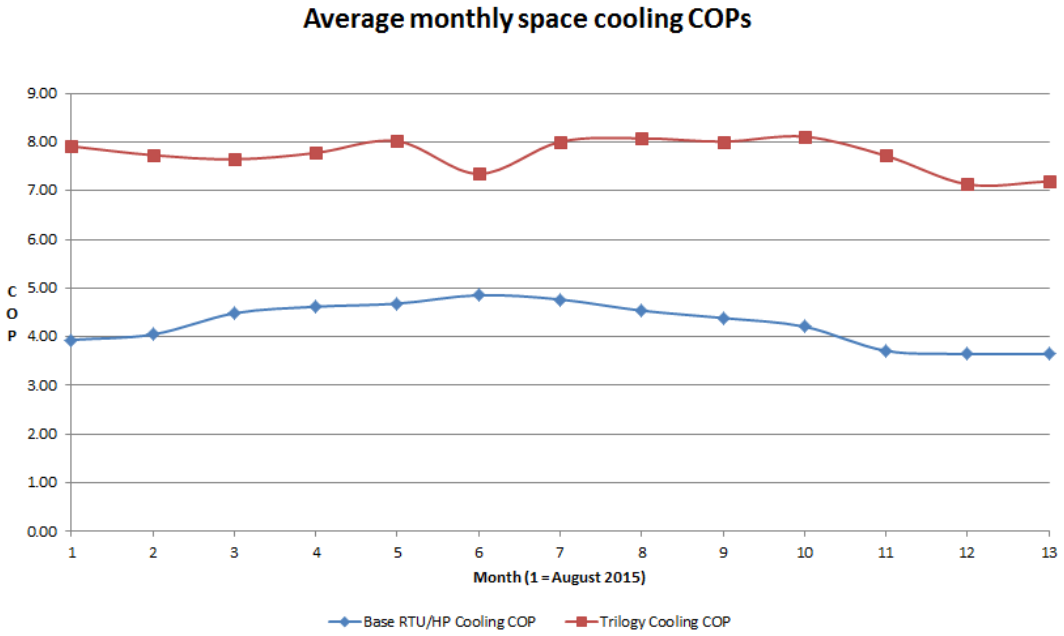

Figure 43: Knoxville site Trilogy WSHP vs. baseline RTU/HP SC monthly average COPs.

Figure 44 left compares the hourly outdoor air temperature (OAT) and EWT of the Trilogy in both modes. In the hottest parts of the summer, the EWT was consistently cooler (by >11°C [>20°F]) than the outdoor (OD) air, which minimized the condensing pressure, leading to improved SC mode efficiency. In the winter months, the EWT was much warmer than the OD air, benefitting the GS-IHP WH mode efficiency. The EWT at the end of the monitoring period was essentially the same as when the unit began operating in August 2015. This indicates that, despite the heavily SC-load dominated operation all year and the addition of the antifreeze solution in January, there was no discernable warming of the ground surrounding the GHX bores during this first year of operation. The GHX loop could have been somewhat shorter, reducing system cost but sacrificing some energy-saving potential due to reduced efficiency.

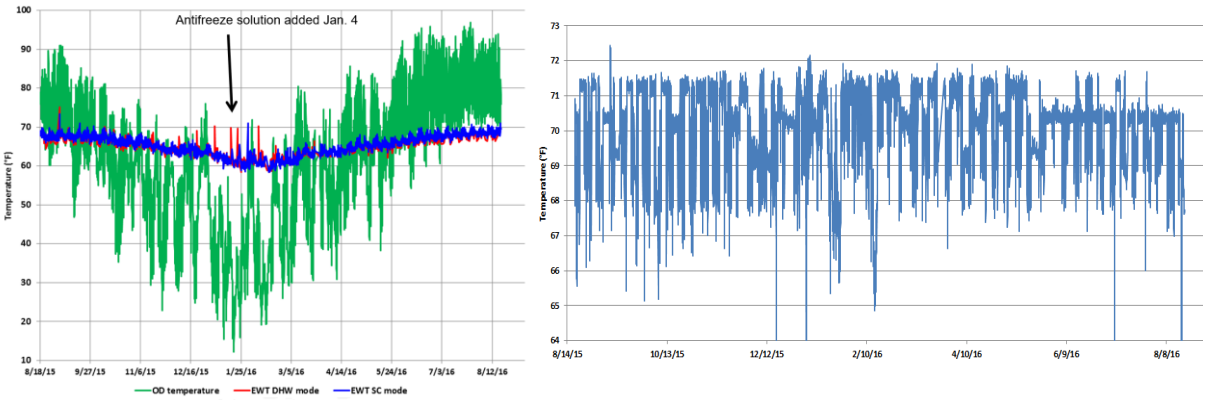

Figure 44: Knoxville site Trilogy WSHP EWT vs. OAT (left) and Knoxville site kitchen space temperature measured at thermostat during test year (right)

Also, the kitchen staff kept the SC setpoint low, as evidenced by the space temperature history during the test period shown in Figure 44 right. During the occupied periods (i.e., weekdays), the air temperature in the kitchen ranged as low as ~18°C (~64°F).

In addition to the energy savings, the GS-IHP system significantly reduced the hourly average kilowatt demand at the Knoxville site. The monthly peak hour kilowatt demand is shown in Table 12 for the GS-IHP and baseline systems. The maximum average hourly demand each month for the GS-IHP was 54–78% lower than that of the baseline system.

Table 12: Knoxville site peak hourly kilowatt demand by month, GS-IHP vs. baseline.

Month	GS-IHP demand (kW)	Date	Baseline demand (kW)	Date
Aug. 18–31, 2015	1.705	--	4.545	--
September 2015	2.923	9/2/15, 12–1 p.m.	4.349	9/2/15, 1–2 p.m.
October 2015	1.642	--	5.290	--
November 2015	1.888	11/6/15, 12–1 p.m.	5.444	11/10/15, 1–2 p.m.
December 2015	1.603	--	7.110	--
January 2016	1.593	--	5.508	--
February 2016	1.538	--	5.407	--
March 2016	1.664	--	5.969	--
April 2016	1.510	--	5.647	--
May 2016	1.778	--	5.676	5/20/16, 2–3 p.m.
June 2016	2.301	6/14/16, 12–1 p.m.	10.425	6/16/16, 12–1 p.m.
July 2016	1.682	--	5.557	--
August 1–18, 2016	1.331	--	5.280	--
Total period	2.923	9/2/15, 12–1 p.m.	10.425	6/16/16, 12–1 p.m.

The kitchen staff behavior was perhaps the most significant factor influencing the IHP system peak demand at this specific location. Figure 45 illustrates the hourly IHP system, tank element power, and baseline RTU system power, along with outdoor temperature, HW tank temperature (at the top element location), thermostat cooling setpoint temperature, and HW consumption for the week beginning August 30, 2015.

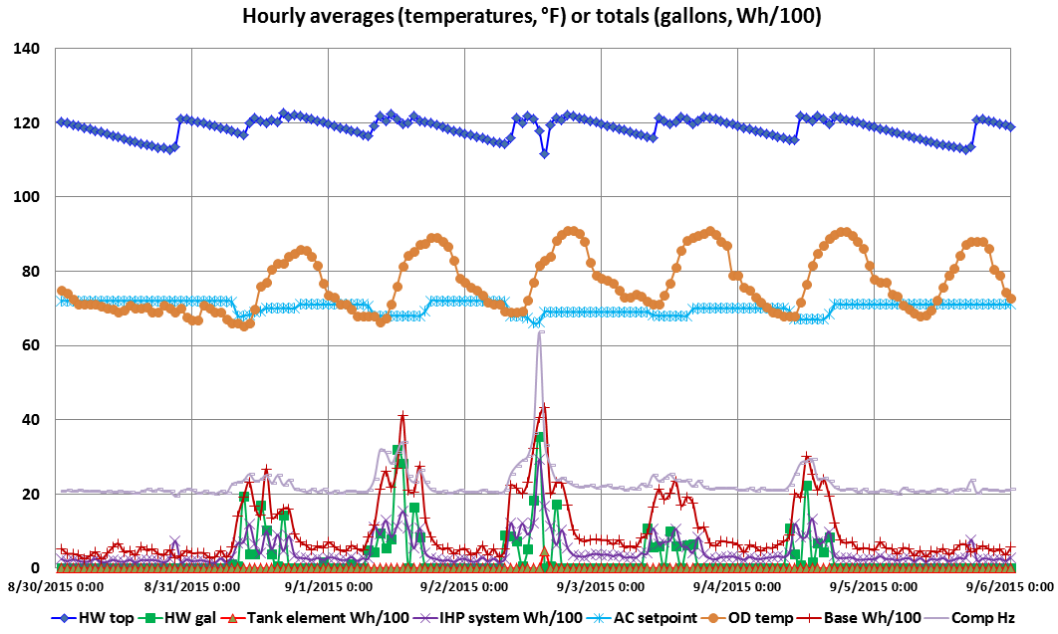

Figure 45: Knoxville site maximum IHP hourly peak demand week. (Note: the IHP and tank element power values are divided by 100 to make all the parameters fit on the chart.)

The IHP (purple line) and baseline system (red line) September peak demands occurred on Wednesday of that week. The IHP peak demand is not coincident with the outdoor temperature (orange line).

Instead, it coincides with the point where the kitchen staff abruptly lowered the thermostat set temperature (light blue line), causing the system to increase to almost maximum compressor

speed (light purple line) for about an hour to meet the sudden increase in SC demand. On the previous day—with similar OD temperatures and slightly lower peak HW usage (green line) but no sudden setpoint reduction—the IHP peak was only about half (1.52 kW vs. 2.92 kW). In contrast, the baseline system—which does not have variable capacity capability to improve efficiency—peak demand (red line) was estimated to be only about 0.2 kW lower (4.11 vs. 4.32 kW). Similar thermostat adjustments were also largely responsible for the IHP system peaks in November and June. The average hourly compressor speed absent abrupt thermostat adjustments was generally ~50–70% of maximum.

Energy cost savings for the Knoxville site were computed based on the energy and demand savings and the July 2016 commercial rate data from the local electric utility.[4] During June, July, August, and September, energy and demand charges were $0.12171/kWh and $13.92/kW. For all other months, the rates were $0.12130/kWh and $13.13/kW. Costs and savings for the GS-IHP vs. the baseline are given in Table 13. Total estimated energy cost savings were ~64%. Almost two thirds of the savings were due to the lower demand charges.

Table 13: Knoxville site GS-IHP HVAC/WH energy cost savings (August 18, 2015–August 18, 2016).

	Baseline RTU/HP and electric WH	GS-IHP
Electricity consumption	$792	$360
Electricity demand	$1,052	$312
Total costs	$1,844	$672
Energy cost savings vs. Baseline	--	$1,172
% cost savings vs. Baseline	--	63.6%

5.7 Oklahoma City Site GS-IHP System Performance Summary

The assumptions listed for Table 11 for the Knoxville site data analyses (reiterated with two differences as noted) also apply to the Oklahoma City site data analyses. The following assumptions were made.

1) Baseline RTU SHR is the same as that estimated for Trilogy WSHP.
2) Baseline RTU is a 17.6 kW rated cooling capacity unit (vs. 14.1 kW for the Knoxville site due to lower design load).
3) Baseline RTU fan power is 365 W/0.47 m^3/s, or 365 W/1,000 cfm (AHRI, 2017).
4) Baseline RTU miscellaneous energy use is the same as that measured for the Trilogy WSHP.
5) Energy use for the combined SC + WH mode is divided between SC and WH proportional to the output capacities. Essentially, the COP for WH and SC in the combined mode is assumed to be the same. This slightly lowers the SC efficiency due to the higher condensing pressures required for the SC + WH mode and raising the WH efficiency relative to the SC-only and dedicated WH mode efficiencies.
6) The Trilogy sensible cooling and subsequent SHR are calculated based on the cubic feet per minute provided by the Trilogy unit, an assumption of 1.2 kg/m^3 (0.075 lbm/ft^3) air density, and measured return and supply air temperatures.
7) The baseline system requires a new electric WH. The rated EF is 0.94, which is the minimum EF required for electric WHs manufactured after April 1, 2015. For the Knoxville site, the original electric WH, which was installed before April 2015, was used with an EF of 0.9.

Table 14–Table 16 summarize the Oklahoma City GS-IHP performance for SH, SC, and WH operation, respectively.

As shown in Table 14, the IHP system demonstrated an overall SH COP of almost 5.0 and energy and cost savings of ~52% over the 61.7 days for which data were available

[4]Knoxville Utilities Board, *General Power Rate—Schedule GSA*, July 2016. http://www.kub.org/wps/wcm/connect/3bfe2f80424c71338027b1d8d4cab33c/GSAJuly.pdf?MOD=AJPERES&CACHEID=3bfe2f80424c71338027b1d8d4cab33c.

Table 14: Oklahoma City site SH performance comparison, IHP vs. baseline RTU/HP.

Month	IHP (COP)	SH delivered (kWh)	IHP SH energy use (kWh)	Baseline RTU energy use (kWh)	IHP energy savings (%)	IHP SH energy cost ($)	Baseline RTU energy cost ($)	IHP energy cost savings (%)
January 31	4.86	26.93	5.54	10.37	46.6	0.32	0.59	46.6
February	4.85	2,101.82	433.43	915.40	52.7	24.84	52.45	52.7
March	5.04	1,062.94	211.02	426.51	50.5	12.09	24.44	50.5
April 1–28	5.27	263.43	49.94	99.99	50.0	2.86	5.73	50.0
Total	4.94	3,455.12	699.94	1,452.57	51.8	40.11	83.21	51.8

Table 15: Oklahoma City site SC cooling performance comparison, IHP vs. baseline RTU/HP

Month	IHP (COP)	Total SC delivered (kWh)	Total IHP SC energy use (kWh)	Baseline RTU energy use (kWh)	IHP energy savings (%)	IHP SC energy cost ($)	Baseline RTU energy cost ($)	IHP energy cost savings (%)
April 1–28	7.17	98.48	13.73	25.92	47.0	0.79	1.49	47.0
May 19–31	8.39	950.14	113.19	247.30	54.2	6.49	14.17	54.2
June[a]	7.08	3697.49	522.51	1,045.08	50.0	29.94	59.88	50.0
July	6.60	4,594.56	695.99	1,356.30	48.7	39.88	77.72	48.7
August[b]	6.80	3,229.54	475.22	939.58	49.4	27.23	53.84	49.4
September[c]	8.05	366.95	45.56	98.87	53.9	2.61	5.67	53.9
Total	6.93	12,937.16	1,866.19	3,713.05	49.7	104.32	212.76	49.7

[a]gap in data from June 10–15
[b]gap in data from August 12–16
[c]gap in data from September 3–7

Table 16: Oklahoma City site WH performance comparison, IHP vs. baseline RTU/HP. (Note: performance at this site is estimated assuming the ratio of WH delivered to the building is the same as measured at the Knoxville site.)

Month	Daily HW use (gal/d)	IHP (COP)	Total WH delivered to bldg. (kWh)	Total IHP WH energy use (kWh) (tank element kWh)	Baseline WH energy use (kWh)	IHP WHenergy cost ($)	Baseline WHenergy cost ($)
May 19–31	161	4.12	127.17	30.84 (0.21)	133.19	1.77	7.63
June[a]	167	4.27	286.64	67.09 (3.68)	302.64	3.84	17.34
July	182	4.72	1,008.41	213.81 (4.99)	1062.5	12.25	60.88
August[b]	181	4.45	808.35	181.59 (9.77)	853.48	10.41	48.909
September[c]	280	4.12	530.84	128.94 (0.68)	564.25	7.39	32.33
Total	189	4.44	2,761.42	622.28 (19.11)	2,916.05	35.66	167.09
% savings				78.7%			78.7%

[a]gap in data from June 10–15
[b]gap in data from August 12–16
[c]gap in data from September 3–7

Energy cost savings were computed using the standard residential service rates from the Oklahoma Gas and Electric Company (OGE).[5] OGE charges a standard rate of $0.0573/kWh year-round with a slightly higher rate ($0.068) in June through September for consumption in excess of 1,400 kWh/month and a lower rate ($0.0173) in November through May for consumption under 600 kWh/month.

[5]OGE, *Standard Pricing Schedule: R-1 Residential Service*, August 2012. https://oge.com/wps/wcm/connect/de21b39f-2d52-402f-82e6-a6826999d724/3.00+R-1.pdf?MOD=AJPERES&CACHEID=de21b39f-2d52-402f-82e6-a6826999d724.

For analysis purposes, the standard rate was assumed to be applied all year. The total electric cost savings for the monitored unit were ~$43. Assuming the average SH daily load and efficiency for the entire heating season would be the same as that of the monitored period, total SH energy and cost savings are estimated to be ~2,060 kWh and $118.

For SC operation, data were available for 1,17.6 days, over which the IHP demonstrated a COP of ~6.9 with almost 50% energy and electric cost savings compared with the estimated performance of the baseline RTU (Table 15). The delivered SC energy to the building is a combination of the SC delivered in two modes: SC only and SC + WH. Approximately 87% of the total SC load was delivered in SC-only mode operation. Total electricity cost savings for the monitored unit were ~$105. OGE also offers residential customers a time-of-use (TOU) rate option for June–October. From 2–7 p.m., the electricity use rate is $0.14/kWh, and for all other hours the rate is $0.027/kWh.

With the TOU rate, both the IHP and SC energy cost savings for the period would drop slightly to ~$100.

Assuming the average SC daily load and efficiency for the entire cooling season would be the same as that of the monitored period, the total SC energy and cost savings are estimated to be ~2,760 kWh and ~$158.

Estimated WH performance at the Oklahoma City site is given in Table 16. Operation data were available for 109.6 days. For that period, the IHP's estimated WH mode COP was ~4.45 with ~79% energy and electricity cost savings compared with the baseline electric WH, while delivering almost 715 L/d of HW to the residential units in the building (~71.5 L/day/unit). The WH energy delivered to the building is a combination of the WH delivered to the building in two modes: dedicated WH and SC + WH with over 80% coming during the SC + WH operating mode. Total electricity cost savings for the monitored unit were ~$131. With the TOU rate assumption, IHP WH energy cost savings for the period would drop slightly to ~$125.

Assuming the average WH daily load and efficiency for the entire year would be the same as that of the monitored period, total WH energy and cost savings are estimated to be ~12,460 kWh and ~$714.

Figure 46 left compares the hourly OAT and EWT of the Trilogy for SH, SC, and WH operating modes (combined SC + WH mode does not use the GHX). In the hottest parts of the summer, the EWT was consistently cooler than the OD air, which minimized the condensing pressure and improved SC mode efficiency. In the winter months, the EWT was warmer than the OD air on average, benefitting the GS-IHP SH and WH mode efficiency.

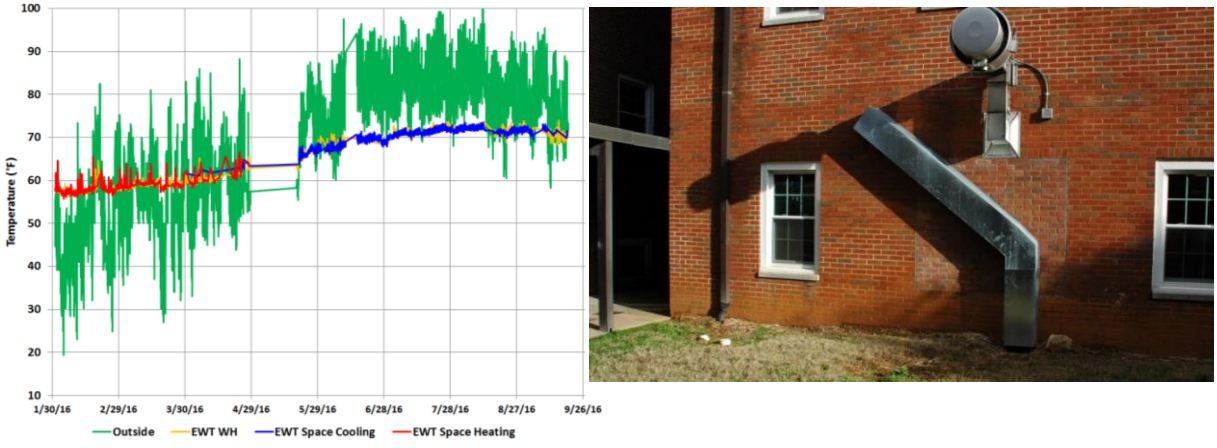

Figure 46: Oklahoma City site Trilogy WSHP EWT vs. OAT Knoxville site GHX loop headers attached to a wall outside the kitchen facility.

The monthly hourly average peak kilowatt demand at the Oklahoma City site is shown in Table 17 for the GS-IHP and baseline systems. Comparing Table 17 with Table 12 shows that the Trilogy system peak demand was generally higher at the Oklahoma City site than at the Knoxville site. Several factors contributed to this difference. First, the Trilogy WSHPs at the homeless shelter were configured to deliver a maximum cooling capacity of 17.6 kW due to the higher design loads at the shelter vs. those at the commercial kitchen at the Knoxville site.

Table 17: Oklahoma City site peak hourly kilowatt demand by month, GS-IHP vs. baseline.

Month	GS-IHP demand (kW)	Date	Baseline demand (kW)	Date
January	0.937	--	2.869	--
February	3.388	2/27/16, 4–5 a.m.	10.283	2/26/16, 4–5 a.m.
March	3.139	3/19/16, 1–2 a.m.	10.574	3/19/16, 2–3 a.m.
April	4.437	4/13/16, 6–7 p.m.	7.302	4/2/16, 4–5 a.m.
May	2.289	5/25/16, 6–7 p.m.	6.605	5/28/16, 4–5 p.m.
June	6.367	6/14/16, 5–6 p.m.	7.960	6/14/16, 5–6 p.m.
July	5.671	7/27/16, 5–6 p.m.	9.869	7/25/16, 6–7 p.m.
August	7.024	8/3/16, 5–6 p.m.	9.144	8/3/16, 4–5 p.m.
September	4.315	--	8.070	--
Total period	7.024	8/3/16, 5–6 p.m.	7.201	2/26/16, 4–5 a.m.

The higher SC loads at the shelter required the Trilogy to run at generally higher compressor drive frequencies (hertz) and, thus, higher compressor speeds, sometimes reaching peaks of almost 70 Hz (~4,200 compressor rpm). In contrast, the Trilogy unit at the Knoxville site seldom experienced compressor drive frequencies higher than ~40 Hz. Therefore, hourly SH or SC energy use (i.e., hourly power demands) for the IHPs at the Oklahoma City site was higher.
Additionally WH demands at the shelter were larger and more constant than at the Knoxville kitchen facility. As a result, the backup electric elements in the WH tanks were used more frequently than those at the Knoxville site. Although the total elements usage at the shelter was modest (~19 kWh from May–September and only ~1 kWh for January–April), sometimes element operation coincided with peak air-conditioning demand periods. This resulted in the IHP system experiencing occasional sharp, short-term peaks during summer months.

5.7.1 Installation Costs at Each Site

Actual system installation cost data were compiled for each site and are listed below. In addition to the actual cost for the Knoxville site, an assumed “mature market” installation cost estimate was made for use in the payback analysis discussed in this report. Payback estimates (high and low) were made for a GS-IHP system of the Knoxville site design vs. the baseline RTU/HP and electric WH using the range of GS-IHP installation cost estimates.
The primary variable affecting GS-IHP system installation cost is the external geothermal heat source/sink. As noted, this usually involves drilling/excavating and installing a GHX loop—usually of the vertical bore field type. For the Knoxville site, three “out of normal” installation issues were experienced that negatively affected the actual system costs.

- First and most important were the drilling issues related to the urban location. The primary complication was that provisions had to be made to recover all the drilling cuttings and fluids to avoid overloading city storm sewers. A vacuum pump truck had to accompany the drill rig to the site to accomplish this recovery, which significantly increased drilling costs.
- Secondly, the space available for the GHX field at the site was limited, so a horizontal boring machine was used to run the GHX header pipes from the GHX field to the building. In most cases, a much less expensive trenching machine is used to dig a trench for the headers. The space issue also limited the maximum distance between the boreholes to 4.3 m instead of CM’s normally recommended 6–8 m spacing.
- Finally, the GHX header piping needed to be partly exposed to ambient air because it was impossible to run the headers under the building to the WSHP location next to the kitchen facility due to existing underground infrastructure. The header piping had to be run up the outside wall and through a ceiling plenum above the WSHP (Figure 46 right and Figure 40 right), which added ~1 day to the installation time. This situation occurs only rarely in the experience of the installing contractors. It also required an antifreeze solution to be added to the water in the GHX loop in early January 2016 to avoid any potential loop freeze problems. This added an estimated $700 to the system cost (the cost of the antifreeze plus an additional site visit) and slightly reduced the system performance relative to a water-only loop.

The installation contractor estimated that for a more rural location without all these complicating factors, the GHX install costs would be reduced by a factor of 2–3.[6]
No "out of normal" GHX installation issues occurred at the Oklahoma City site.
The Knoxville site GS-IHP installation cost estimate is as follows:

GHX actual (per installer billing): $38,000 (~$138/m bore)
GHX mid (without issues): $15,000 (~$56/m bore) (compared with US average costs of $49/m bore in the South and $42.62 in the Midwest (Battocletti et al., 2013))
GHX low (mature market estimate): $9,600[7] (~$10.70/bore ft)
Trilogy unit: $9,800[8] (compared with ~$5,100 typical cost for nonpremium WSHP (Battocletti et al., 2013))
Indoor installation: $1,600[9]
Totals

high:	$49,400
low:	$26,400
mature market:	$21,000

Knoxville site baseline RTU/HP + electric WH system install cost estimate:
New RTU unit: $4,100 for 14 kW (4-ton) unit per (Ingram, 2016)
Roof curb: $1,500
Structural: $1,700
Plans/permits: $2,000
Crane: $1,000
Connection to existing ductwork: $1,000
Total: $11,300
Excepting the RTU, baseline installation cost estimates were based on costs given in the Gas Engine Heat Pump field demonstration report by Vineyard et al. (2015). Before the IHP was installed, heating and cooling for the site kitchen facility were supplied by a central system that served the entire building. Because there are heavy internal loads in the kitchen due to refrigerator/freezer units, cooking equipment, dishwasher, and other tools, the existing system had inadequate cooling capacity during workdays. Thus, for the baseline system used in this comparison, it is assumed that a new RTU/HP dedicated to the kitchen area will be installed, which would require some structural roof modifications to accommodate the unit weight and new ductwork from the RTU to the existing kitchen ductwork. For the baseline water heating, it was assumed that the existing electric WH would be used, so no install costs related to WH were included.
The Oklahoma City site installation (new building) cost estimate is as follows:[10]
Total system estimate:
GHX actual (per installer billing): $51,200 (~$10.2/bore ft)
Equipment (four WSHP units plus ERV): $39,100
Indoor GHX loop and DHW tank connections: $6,500
Totals: $141,200
Subtotal estimate for one Trilogy IHP (assumes GHX loop with 1,250 bore ft total):
GHX: $12,800 (~$10.2/bore ft.)
Equipment: $9,800
Indoor GHX loop and DHW tank connections: $2,025

[6]Personal communication, M. Davis (City Heat and Air) to Van Baxter, August 26, 2016.
[7]Personal communication, D. Ellis (Comfortworks, Inc.) to Van Baxter, August 29, 2016. Estimated mature market GHX installation cost including drilling, u-tube pipe loop insertion, backfill/grouting boreholes, trenching and header pipe to building, and filling/flushing the GHX pipe loop.
[8]Personal communication, D. Ellis (Comfortworks, Inc.) to Van Baxter, August 29, 2016. Estimated mature market selling price for Trilogy unit including DHW tank, installation, and commissioning.
[9]Includes removing existing WH tank, connecting WSHP to GHX headers, installing water piping connections between WSHP and DHW tank, and connecting to existing building air ducts and water pipes.
[10]Personal communication, D. Ellis (Comfortworks, Inc.) to Van Baxter, August 28, 2016. Total system equipment cost includes two Trilogy (IHP) WSHPs with 400 L DHW tanks and two non-IHP WSHPs with thermostats and miscellaneous materials along with one energy recovery ventilator (ERV) at $6,800. Ductwork cost was $50,700 for the entire building and was assumed to be the same for IHP and baseline installations.

Totals: $24,625

Oklahoma City site baseline RTU/HP + electric WH system install cost estimate:

New RTU unit: $4,300 for 17.6 kW (5-ton) unit (Ingram, 2016)

Roof curb: $1,500

Structural: $1,700

Plans/permits: $2,000

Crane: $1,000

Connection to existing ductwork: $1,000

New 105 gal electric WH $1,900[11]

Total: $13,400

5.8 Summary Cost and Payback Assessment

A payback analysis is provided in Table 18 based on the Knoxville site system design and the three GS-IHP cost assumptions given above. The "high" cost assumption uses the GHX cost as billed by the contractor for the Knoxville site. The "low" cost assumption is given based on the contractors' estimate that GHX cost could have been up to one third of the actual cost if not for the "out of normal" conditions noted previously. The mature market cost assumption is based on experience with many installations in Oklahoma. Finally, an alternative GHX financing approach was considered. For this case, the utility was assumed to install and own the GHX (Cunningham, 2016). A GHX cost recovery charge of 2% of the GHX installation cost is added to the electric bill, reducing the total annual energy cost savings to the building owner(Battocletti et al., 2013). Using the energy cost savings from Table 13, the payback for the GS-IHP ranges from ~8.5 to >30 years for the low- to high-GHX cost ranges, assuming the building owner pays the cost of the GHX installation up front. Assuming the utility installs and owns the GHX (i.e., building owner pays only for the Trilogy and associated indoor installation), the payback period could drop to <1 year.

Table 18: Knoxville site payback analysis.

	Equipment costs ($)		GHX installed cost ($)	Total cost($)	Cost difference ($)	Energy cost savings($)	Payback (yrs)
	Price	Installation					
Conventional RTU/HP and electric WH	4,100	7,200	N/A	11,300	N/A	N/A	N/A
GS-IHP; high GHX cost assumption	9,800	1,600	38,000	49,400	38,100	1,172	**32.5**
GS-IHP; low GHX cost assumption	9,800	1,600	15,000	26,400	15,100	1,172	**12.9**
GS-IHP; mature market cost	9,800	1,600	9,600	21,000	9,700	1,172	**8.3**
GS-IHP; mature market GHX cost; utility owns GHX assumption	9,800	1,600	N/A	11,400	100	980[a]	**0.1**

[a]Utility adds cost recovery surcharge totaling 2% of GHX installation cost per year to bill ($192).

[11]Price quote from Home Depot in September 2016 for 105 gal electric WH ~$1,500; assumed $400 for installation.

5.9 GS-IHP Field Demonstration Conclusions and Observations

These demonstrations were performed in Knoxville and Oklahoma City. The Knoxville site was a small commercial kitchen that experienced a year-round SC load and heavy HW demands during the work week (Monday–Friday).The Oklahoma City site was a homeless shelter (dormitory-like facility) that featured relatively balanced SH and SC and WH loads with SC being the largest. Both sites allowed the GS-IHP to take advantage of its combined SC + WH mode that featured extensive recovery of the normally wasted system condenser heat for water heating. During August 2015–August 2016, the Knoxville site GS-IHP provided 53.7% total source energy savings compared with a baseline electric RTU/HP and electric WH. Peak demand savings were 54–78% per month. Energy savings of 54.6% and energy cost savings of 55.9% were achieved (almost evenly split between reduced demand charges and electricity consumption savings). The GS-IHP also saved a significant amount of carbon emissions, which were ~2.45 metric tons for the August 2015–August 2016 test year. If trading for carbon credits ever become a reality, then additional cost savings would be realized. These savings significantly exceeded the project technical performance goal of ≥45% energy and carbon emission reductions. No SH loads were experienced for this site; only SC and WH operation was required for the entire test year.

For the Oklahoma City site, DAS installation delays prevented the collection of a full year of performance data. However, enough data were obtained to allow a reasonable estimate of SH, SC, and WH energy savings and efficiency vs. the baseline system.

SH: from Table 3.7, total energy savings of ~753 kWh (~52%) and average COP of ~4.9

SC: from Table 3.8, total energy savings of ~1,847 kWh (~50%) and average COP of ~6.9

WH: from Table 3.9, total energy savings of ~2,293 kWh (~78%) and average COP of ~4.4

Over the actual monitoring period, the GS-IHP at the site demonstrated total site electricity savings of ~4,890 kWh (~60%) and carbon-emission savings of ~3.4 metric tons, greatly exceeding the project's technical goal. Assuming that the daily average loads and COPs above are the same for the balance of the year for each mode, the total annual energy savings are estimated to be ~12,460 kWh with carbon-emission savings of ~8.6 metric tons. The WH savings indicated above are estimated assuming that the system at the Oklahoma City site experienced the same HW tank and connecting line standby heat losses (as a percentage of the total load) that were measured at the Knoxville site. This field study successfully demonstrated the energy savings, environmental savings, and operational benefits of GS-IHP technology for small commercial building applications. Both demonstration systems significantly exceeded the project technical objectives of >45% energy and carbon-emission savings (>50% at both sites). The best applications of the GS-IHP system are buildings or specific small zones of buildings that have high HW loads coincident with high SC loads. Payback analyses were conducted for the Knoxville site system based on the annual energy savings demonstrated. The specific site conditions (e.g., limited area, local regulations) caused drilling costs to be about three times higher than what is typical for the area. For the actual GHX cost, simple payback vs. the baseline RTU/HP/electric WH system were >30 years (Table 3.11). With more typical GHX costs for the area, the payback is approximately 13 years. For a mature market cost assumption based on experience at the Oklahoma City site, the payback drops to ~8 years for many installations, which is still likely higher than what is acceptable for most commercial building owners. Assuming an alternative GHX financing option were available in which the local utility (or another entity) installed and owned the GHX loop and amortized the cost via a surcharge on the electric bill, system payback could be reduced to ~0.1 year.

The economics of GS-IHPs will vary from site to site for several reasons, including the following.

- Regional differences in drilling costs, local site conditions and requirements, and financing options can cause the GHX loop installation costs to vary widely, even within a given region. Where local site conditions are unfavorable (e.g., restricted area, local permitting/regulation restrictions, as experienced at the Knoxville site), GHX installation costs can be prohibitive.
- Local electricity rate structures could limit the operating cost savings achievable, leading to higher payback periods.

6 Integrated AS heat pump variants – Knoxville, US

6.1 Electric AS-IHP System Development, Analyses, and Test Results

Full details of the AS-IHP concept development can be found in Murphy et al. (2007b) with a shorter summary in the Annex 40 final reports (Wemhoener, 2016, Baxter et al. 2015). Most of the material in this section is summarized from the two prototype system development reports (Baxter et al., 2015, Baxter et al., 2017). Figure 47 show conceptual installations for the two different AS-IHP prototype systems developed. Each system uses a VS compressor, VS indoor blower (for SH/SC distribution), and VS outdoor fan. One system (Figure 3.17) also includes an integral HW circulation pump that might be single-, multi-, or VS. One electric AS-IHP prototype and the gas engine-driven AS-IHP prototype are of this general configuration. The second electric prototype system (Figure 3.18) has a separate dedicated HP water heater/DH unit that can provide DWH and dedicated year-round DH. A 190 L (50 gal) WH tank is included. Both prototype electric AS-IHP systems have 10.5 kW (3-ton) nominal cooling capacities, and the prototype gas engine AS-IHP was a nominal 17.6 kW (5-ton) size.

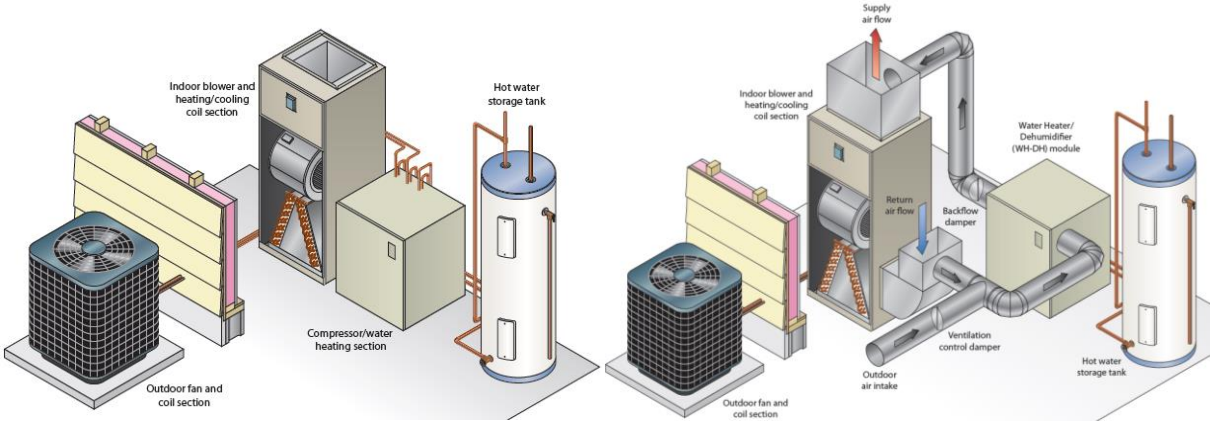

Figure 47: Conceptual installation of AS-IHP system concept 1 (left) and system concept 2 (right)

6.2 Electric AS-IHP 1—Single-Compressor or Combined System

ORNL and an ASHP manufacturing partner, Nortek Global HVAC, collaborated to design and develop a prototype of an AS-IHP based on the concept in Figure 3.17 suitable for existing residential applications using R-410A refrigerant. A nominal 10.6 kW (3-ton) design cooling size was selected for development. ORNL and manufacturer team members engaged in an iterative process of prototype analysis/design, lab testing, and redesign based on lab results. Three generations of prototypes were developed, which led to field testing. The design uses a VS compressor, blower, and fan. Dual electronic expansion valves are used to provide a wide range of refrigerant flow control. The final prototype design used compact HX designs for all three system HXs (indoor and outdoor air coils and refrigerant-to-water HX).

6.2.1 Field performance observations

Figure 48: Field test site in Yarnell Station neighborhood, Knoxville, Tennessee (left), Prototype installation: indoor sections (HW storage tank, compressor and water heating module, and indoor fan coil) (middle) outdoor fan coil section (right)

Figure 49: Field data monitoring system (left) and HW use control valves.

A 1-year field test was initiated in a 223 m^2 (2,400 ft^2) test house (Figure 48 left) in Knoxville, Tennessee in May 2014. Pictures of the field test system are included in Figure 48, and the DAS is shown in Figure 49. Before the field testing started, the test house occupancy simulation was set up. The water draw schedule used at the site was based on the latest Building America water draw generator (DOE, 2013). Latent, sensible, and other building internal loads were based on the Building America House Simulation Protocols (Hedron and Engelbrecht, 2010). Occupancy simulation devices followed a schedule input via a database that is read by a programmed controller for operating space heaters to simulate sensible heat and humidifiers to simulate latent heat. HW loads (e.g., dishwasher, clothes washer, showers, sinks) were simulated by operating solenoid-controlled water valves according to the programmed schedule with an average HW use of 213 L/day. Figure 3.22 shows the HW valves and controller setup. Temperature control setpoints of 49.0°C (120°F) for WH, 24.4°C (76°F) for SC, and 21.7°C (71°F) for SH were implemented in the system controls before starting data monitoring. The primary operating modes experienced during this period were:

- SC only (Dedicated SC)
- SC + desuperheater (DS) WH (SC + DS)
- SC + FC WH (SC + WH)
- SH only

6.3 Prototype Field Performance Summary and Observations

Both the SC and SH seasonal COPs were lower than those estimated using the AHRI 210/240 (1998) procedures with the rated values for the prototype, as seen in Table 19. The AHRI estimates were computed using the minimum (i.e., more efficient thermal envelope) and maximum (i.e., less efficient thermal envelope) house load line assumptions (DHRmin and DHRmax) and using the actual demonstrated test house load lines.

Table 19: Site-measured seasonal SH/SC COPs vs. estimated AHRI 210/240 (1998) ratings for prototype system.

Mode	Field measured	AHRI 210/240	% deviation field vs. rated
SH $SCOP_h$	2.05	For DHRmin load: 2.98 For DHRmax load: 2.44 For house loads: 2.64	31 16 22
SC $SCOP_c$	5.14	For default load and 0.2 Cd: 5.49 For house loads: 5.60	6 8

Field measurements on two single-speed (SS) ASHPs were taken in the Knoxville area in 2011–2012. Both were tested in one two-story house; SS unit 1 conditioned the downstairs, and unit 2 conditioned the upstairs. Heating season measurements showed a $SCOP_h$ of 1.52 and 1.76 for units 1 and 2, respectively (Munk et al., 2013). These are 32% lower and 22% lower than the $SCOP_h$ rating for the units of 2.26 (per AHRI 210/240 based on DHRmin load line). This is like the 31% deviation in Table 3.12 from the estimated AHRI rating for the field prototype based on the DHRmin load line. However, for cooling operations, the two SS ASHPs had field-measured $SCOP_c$s of 2.08 and 2.46 (a 45% and 35% deviation from rated), whereas the field AS-IHP prototype field-measured $SCOP_c$ was 5.14 (only a 6% deviation from estimated rating). There are several reasons why the AS-IHP field prototype's measured SH COP is lower than expected.

- Blower energy use is higher at the field site than was measured in the lab test phases of the project due to higher duct system external static pressure losses. This is somewhat peculiar for the changes made in the test house ducting system to accommodate the AS-IHP. However, residential duct systems generally have higher pressure losses than implicitly assumed in AHRI 210/240. (This also negatively affects the SC seasonal COP.)
- The $SCOP_h$ procedure does not account for defrost tempering heat usage which accounted for >10% of the total field system energy use in February alone.
- The indoor temperature during the heating season averaged close to 72°F, whereas lab testing and the HSPF procedure assume 70°F.
- The standard house load line used in the HSPF procedure is lower than that experienced at the test house during the 2014/2015 winter test season.
- Many of the issues related to the SH control for the field-test prototype could also be an unintended consequence of using a generic, low-cost, two-stage thermostat to control a VS system. Setting up optimal sequence timing to control the compressor speed based only on a high- or low-stage thermostat input is a significant challenge. This approach is unlikely to provide good results in all homes due to differences in equipment sizing relative to the actual heating load and the thermal mass of the home.

Table 20 compares the average heating and cooling degree days for Knoxville with those experienced during the 2011–2012 and 2014–2015 test years. The 2014–2015 test year weather for Knoxville was somewhat cooler than the long-term averages per ASHRAE (2013) for the heating (~12% colder) and cooling seasons (~8% cooler). The 2011–2012 actual weather (when the two SS ASHPs were tested) was a bit warmer than normal—22% warmer during the heating season and 14% warmer during the cooling season.

Table 20: Average vs. 2014–2015 test site heating and cooling degree days.

Location	Annual °F-days heating(18.3°C base)	Annual °F-days cooling(18.3°C base)
Knoxville		
Average[1]	1997	841
2011–2012[2]	1553	958
2014–2015[2]	2136	825
2014–2015[3]	2233	778

[1]1986–2010 averages, ASHRAE (2013).
[2]Test year actuals from National Oceanic and Atmospheric Administration for Knoxville McGhee-Tyson airport weather station (NOAA, 2015)
[3]For test year May 3, 2014–May 2, 2015; site-measured actual.

It is not unusual for actual measured HP HSPFs to be degraded by 30% or more compared with the HSPF rating (based on the DHRmin load line) due to the reasons cited previously and other miscellaneous effects, such colder-than-normal winters. The higher house load effect alone likely accounts for more than half the degradation.

Estimated field prototype AS-IHP energy savings vs. baseline minimum efficiency system at test site

The annual energy use of a baseline system (3.8 $SCOP_c$ and 2.26 $SCOP_h$ [Region IV] SS ASHP and electric WH) that meets the field test site loads was estimated. The HSPF and SEER ratings for the baseline unit were adjusted downward by 27 and 40%, respectively, based the average field-measured deviations from rated efficiencies experienced by the SS ASHPs previously field tested in a similar size nearby house in the Knoxville area (Munk et al., 2013). The results for this comparison are shown in Table 21. Since the tank and HW distribution line losses from the HW storage tank were unaccounted for in the AS-IHP field performance, they were also omitted from the baseline equipment efficiency (e.g., baseline WH COP = 1.0). The table shows that the largest percentage and absolute savings come from water heating at 61% and 1,905 kWh, respectively.
SC and SH energy savings are estimated at 1,800 kWh (55%) and 1,461 kWh (20%), respectively. The estimated total annual savings for the AS-IHP vs. estimated baseline energy use at the Knoxville site are about 38%. Heavy reliance on backup electric elements for SH and defrost tempering and higher indoor blower energy usage (vs. lab-measured performance)

were significant contributing factors, causing the lower-than-expected SH performance of the AS-IHP field prototype system. A smaller rated capacity IHP combined with a better insulated house (closer to the DHRmin load assumption used by the AHRI 210/240 procedure) would be a much closer match to the preferred application and would possibly have yielded total energy savings of ~45% or more at the test site.

Table 21: AS-IHP 2014–2015 measured performance vs. estimated baseline performance at the test site.

Mode		AS-IHP	Baseline system estimated performance	Percent savings over baseline
SC	COP (SEER)	5.14 (17.52)	2.29 (7.80)	
	Delivered (kWh)	7,416	7,416	
	Consumed (kWh)	1,444	3244	55%
SH	COP (HSPF)	2.06 (7.01)	1.65 (5.62)	
	Delivered (kWh)	12,125	12,125	
	Consumed (kWh)	5,899	7,360	20%
WH	COP	2.68	1	
	Delivered (kWh)	3,104	3,104	
	Consumed (kWh)	1,199	3,104	61%
Total	**Consumed (kWh)**	**8,542**	**13,708**	**38%**

Applying the AS-IHP system to commercial buildings for which the annual loads are dominated by WH and SC needs would also be expected to yield much higher annual energy savings than were demonstrated during this residential field test.

6.4 Electric AS-IHP 2

ORNL has been engaged with another manufacturing partner (Lennox Industries) to develop a field-test prototype of the second AS-IHP concept system, as shown in Figure 50 left.

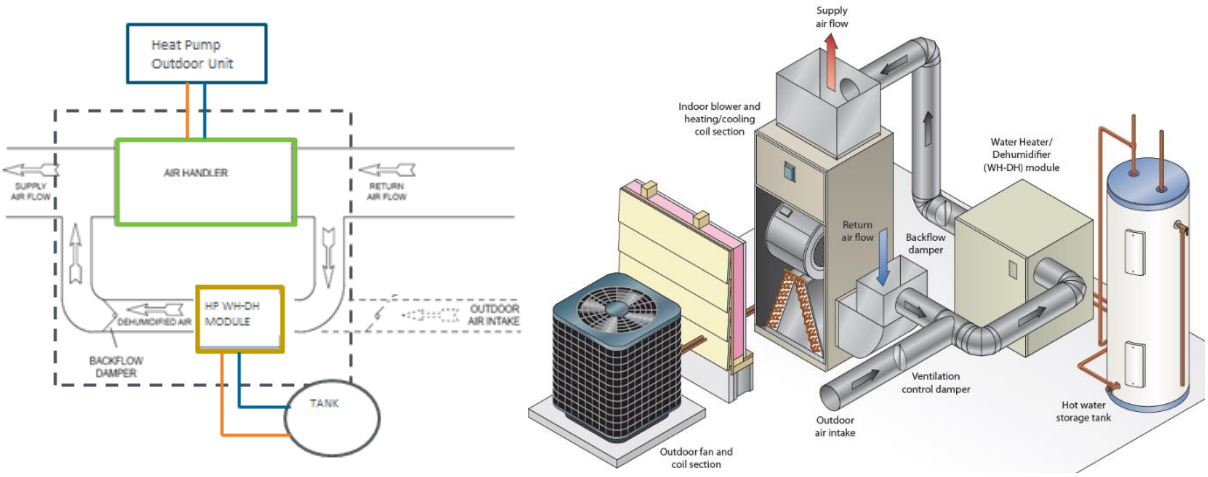

Figure 50: Two-box AS-IHP concept schematic (left) and Two-unit AS-IHP field-test system arrangement (right)

6.4.1.1 WH-DH module and AS-IHP system field-test prototype design summary

The WH-DH module design is based on US Patent 8,689,574 B2 (Uselton, 2014). Figure 51 left is a photograph of the field-test WH/DH unit with its side panels removed to show the control board. Figure 51 right provides a CAD drawing of the general layout of the field-test prototype WH/DH design. A drawing of the AS-IHP field-test system arrangement is provided in Figure 50 right. The system design intent was to pair the WH/DH field-test prototype with a Lennox high-efficiency, VS XP-25 ASHP. The XP-25 family of ASHP products has rated $SCOP_c$s of 5.9–7.0 and $SCOP_h$s of 2.8–3.0 (Lennox, 2016). The model selected for the field-test AS-IHP was rated at 10.1 kW of cooling with a $SCOP_c$ of 6.3 and DOE Climate Region IV $SCOP_h$ of 2.9. Significant components of the WH/DH are a SS compressor, SS water pump, VS fan, fin-and-tube refrigerant-to-air evaporator, brazed plate refrigerant-to-water condenser, and fin-and-tube refrigerant-to-air condenser, as depicted in Figure 3.30.

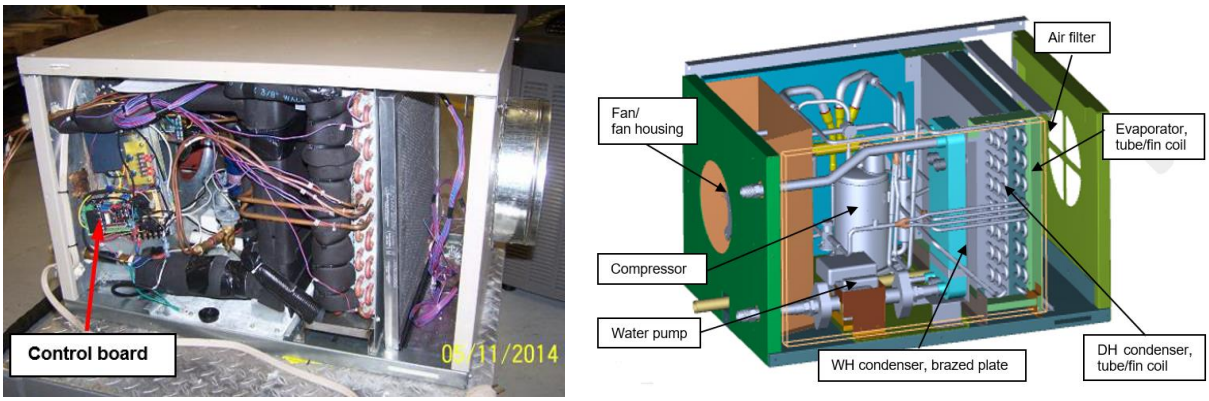

Figure 51: Field-test WH/DH prototype (left) and CAD drawing of field-test prototype WH/DH module (right)

A solid-state microcontroller manages the competing requests for service with WH having priority over DH. The VS blower initially used the same speed for WH, DH, and fresh-air ventilation (V) modes.
Early in Summer 2016, a control change was implemented to slow the WH/DH fan during V mode (details are provided in the DH performance discussion below).

6.5 Field Test Setup

The XP-25 ASHP and WH/DH prototype were shipped to ORNL in early 2015 and installed in June–July 2015 at the Knoxville test house (Figure 48 left) for a 1-year field test. A photo of the field-test system is included in Figure 52, and the field DAS is shown in Figure 49 left. Full data monitoring of the AS-IHP system began in August 2015 and continued through September 2016. Monitoring the WH/DH module continued through May 2017 to evaluate the effect of some design and control modifications implemented due to the initial test-year results.

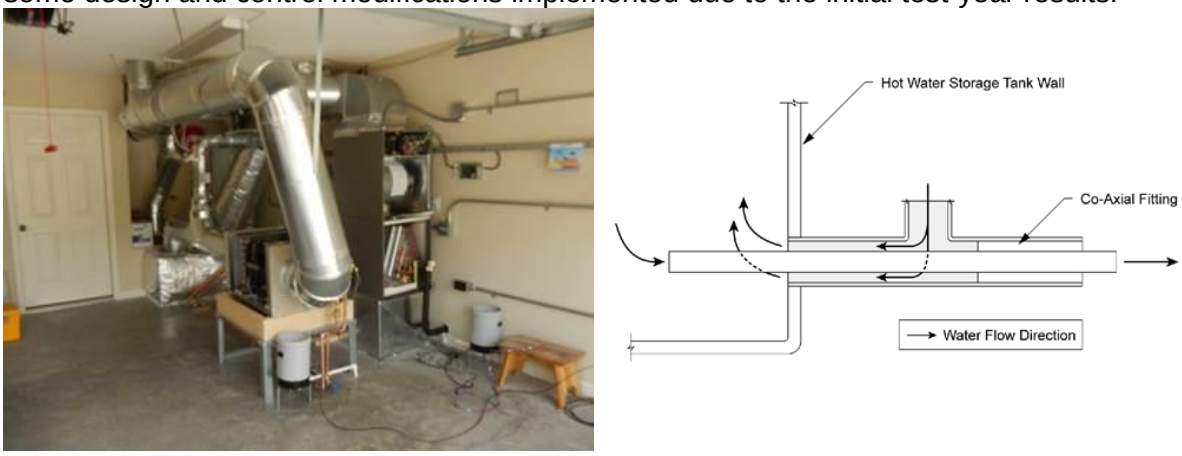

Figure 52: Field-test prototype during installation. ASHP indoor air handler and WH/DH prototype shown with rain gauges for condensate collection to monitor DH and latent cooling loads (left) and schematic of coaxial tank water fitting

The same house occupancy simulation protocol used for the AS-IHP 1 field test was also used for the test of AS-IHP 2 prototype system. The field DAS was set up to collect data at 15 second intervals with 1 minute, 15 minute, 1 hour, and daily averages. Data were stored on servers located at ORNL. A dedicated internet connection was set up to allow the Lennox project team to monitor data collection in real time.

6.5.1 Equipment setup

The space-conditioning system included zone controls and dampers that allowed the upstairs and downstairs zone temperatures to be controlled independently. The zoning system also controlled the ASHP airflow based on fixed airflow values that were assigned to each zone during system commissioning. The thermostat setpoints were 71.0°F (21.7°C) for the heating seasons and 76.0°F (24.4°C) for the cooling seasons. The ASHP operating mode was switched manually between heating only and cooling only as needed.

The WH/DH was connected to a standard electric storage WH with copper pipe and a concentric fitting that was inserted in place of the typical drain at the bottom of the WH (Figure 3.33). The power to the lower thermostat/element was disconnected and rewired to provide a low-voltage signal to the WH/DH when WH was required.
The return air for the WH/DH was ducted from the return plenum of the HP. The supply air was ducted separately from the WH/DH with one duct terminating on the second floor of the house and the other on the first floor. Controlled fresh-air intake is one difference between the field-test system and the baseline equipment. A constant 45 cfm (21 L/s) of outdoor air was provided to the house. Homes with tightly sealed envelopes need mechanical fresh air V to maintain acceptable indoor air quality.

6.5.2 Instrumentation

The ASHP was instrumented for air-side heating and cooling capacity measurements, as well as additional measurements of refrigerant-side pressures and temperatures. The condensate drained from the evaporator coil was also measured to provide a check on the air-side latent capacity measurement. The WH/DH was instrumented for water-side WH capacity measurements and air-side capacity measurements for DH and the cooling by-product from the WH mode. Like the ASHP, the condensate drained from the WH/DH was also measured to provide a check on the air-side latent capacity. Solid-state transducers were used to measure the total and component energy use of the ASHP and WH/DH.

6.6 WH/DH Module DH Mode Performance

During AS-IHP system test year (October 2015–September 2016)

The WH/DH was called to dehumidify when a low-voltage alternating current (AC) signal was supplied. In a typical installation, this would be provided by a humidistat. However, since the home was already instrumented with humidity sensors, the data logger was used to provide the contact closure functionality of a humidistat. The call for DH mode was supplied to the WH/DH when the Level 1 or Level 2 humidity sensors read over 55% RH, and it was removed when both sensors read below 51% RH. The WH/DH maintained the humidity in the house excellently with the highest hourly average humidity measurement during the study being 54.8%.
One issue observed during WH/DH operation involved the evaporation of condensate remaining on the evaporator coil during V mode (i.e., essentially, all the hours when neither the DH nor WH mode operation occurred). The DH and WH modes condense moisture from the air on the evaporator coil, as shown in the top plot of Figure 3.34. The blue highlighted sections indicate that the unit is operating in DH mode. In this mode, the unit provides positive latent cooling and negative sensible cooling (i.e., heating). The house humidity is reduced as moisture is removed from the air. The pink highlighted sections indicate operation in the V mode. In this mode, the unit provides negative latent cooling (i.e., evaporates moisture into the air) and sensible cooling due to the evaporative cooling effect.
This increases the house humidity and negates part of the work done during the DH mode. Based on a comparison of the air-side latent capacity during the DH mode and the latent capacity calculated based on the measured condensate leaving the unit, approximately 33% of the condensed moisture was being evaporated during the V mode. This results in an effective DH efficiency that is one-third lower than its steady-state efficiency. The first step taken to mitigate this effect involved reducing the airflow through the unit during the V mode. The initial equipment setup required the V airflow to be like that of the WH and DH (~300 cfm) to ensure the proper outdoor air V rate of 45 cfm. This was due to the small size of the fresh-air intake duct relative to the WH/DH return duct. In June 2016, a damper was added to the WH/DH return duct upstream of the fresh-air intake. This damper was closed during the V mode, reducing the airflow to the required V rate since the unit was now pulling in 100% fresh air instead of a mixture of fresh air and indoor air. This also significantly reduced the V mode fan power to ~13 vs. ~53 W before installing the damper. The bottom plot in Figure 3.34 shows DH and V cycles of the WH/DH after the damper was installed, as well as reduced airflow composed of 100% fresh air for V. During the V mode, the condensate evaporation was significantly reduced, as indicated by the latent capacity being only slightly negative.

The DH cycle frequency was also reduced, and the humidity in the home increased at a much slower rate, although the outdoor conditions were slightly drier for the data shown in the bottom plot of Figure 3.34.
Once again, a comparison between the air-side latent capacity measured during the DH mode and the condensate collected from the WH/DH indicated that only 5% of the condensed moisture was evaporated back into the air during the V mode. This is a significant reduction compared with the 33% evaporation rate seen before the return air damper was installed.

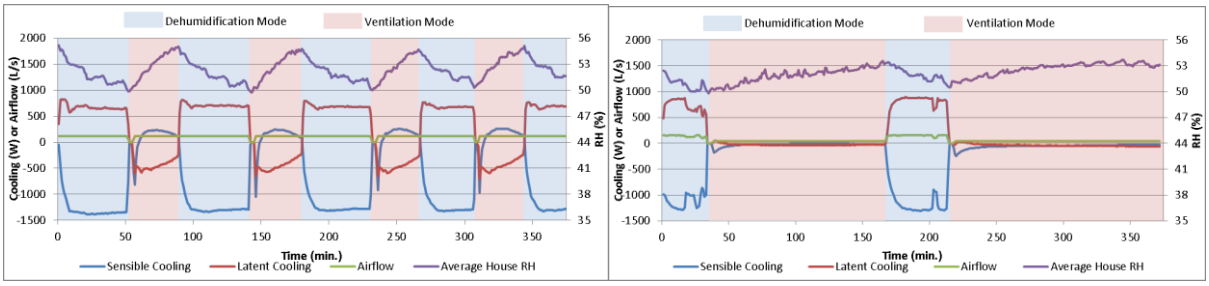

Figure 53: WH/DH cycling between DH mode and V mode with condensate evaporation during V for equal V and DH airflow rates (top plot) and with reduced airflow during V mode (bottom plot) (Munk et al., 2017).

The monthly run time and average efficiency based on the measured air-side latent capacity are shown in Figure 3.35. As noted, condensate evaporation in the V mode likely resulted in increased DH run time for all months before and including June 2016. July and August 2016 showed significant (i.e., >100 hours per month) DH run time due to high outdoor humidity. September 2016 had a higher average outdoor humidity than October–December 2015 but had significantly less DH run time, illustrating the reduction in the re-evaporation of condensate during V mode. For the months with significant run time, the efficiency for DH was ~1.5–2.1 L/kWh. There were measurement issues related to the air-side capacity of the WH/DH for August–October 2015, so this period was excluded from the calculation of the average DH efficiency of 1.7 L/kWh.

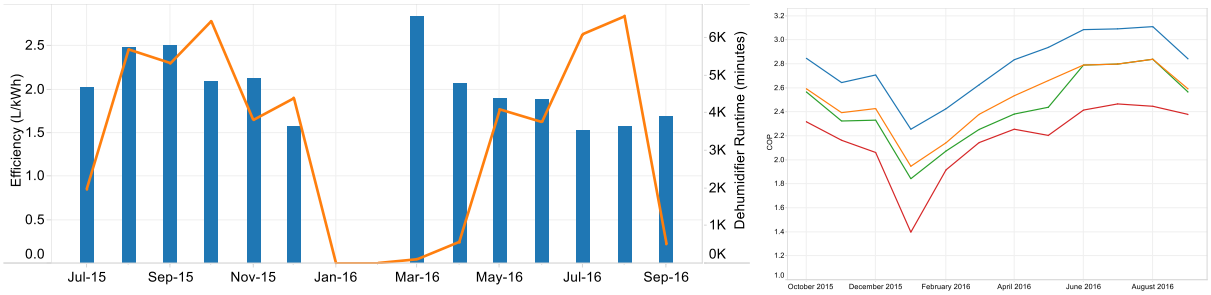

Figure 54: Monthly DH efficiency and run time (left, (Lennox Inc., 2014) and monthly average WH mode COPs of the WH/DH HP with and without backup resistance heat use and heat losses from the storage tank and water lines connecting the WH/DH to the storage tank (Lennox Inc., 2014) (right)

6.6.1 WH/DH Module WH Mode Performance

The monthly WH efficiencies for the WH/DH are shown in Figure 3.36. The different lines indicate system performance at various points as heat is generated by the WH/DH unit (HP), transferred to the storage tank, and leaves the storage tank to be used in the house. The blue line shows the COP of the HP only, which does not account for backup resistance heat use and losses associated with the interconnecting lines and storage tank. These COPs range from a low of 2.3 in January to a high of 3.1 in August. As mentioned earlier, there were no HW draws for 20 days in January. Without the flow of cold makeup water into the tank, the EWTs seen by the WH/DH will be at least as high as the lower thermostat “make” temperature of approximately 112°F (44.4°C). The higher EWTs seen by the WH/DH when recovering from standby losses compared with recovering from HW use resulted in lower-than-average COPs for January.
The orange line in Figure 3.36 shows the COP of the WH/DH when accounting for heat loss in the water lines that connect the WH/DH to the storage tank. Immersion temperature sensors located on both ends of the interconnecting water lines allowed the heat loss to be measured.

Despite the water lines being insulated, the measured heat loss from these lines averaged 9.8% of the heat provided by the WH/DH HP.
Examining a 1-week snapshot of data indicated that, on average, the water lines lost 76% of their heat relative to the garage temperature between WH cycles. The copper water lines were 35.8 ft (10.9 m) long and0.75 in. (1.9 cm) diameter. Over the test year there were 2007 WH cycles. The heat loss from the water in the lines during periods when the WH/DH was off is estimated to be 738 kBtu (216 kWh) or 6.2% of the WH delivered by the WH/DH. Using the average garage temperature, average water temperature in the lines, and insulation thickness, the heat loss from the lines when the WH/DH was operating in WH mode was calculated to be 453 kBtu (133 kWh) or 3.8% of the WH provided by the WH/DH. Combining the calculated off-cycle and WH cycle line losses yields a calculated value of 10.0% heat loss, which agrees well with the measured line losses of 9.8%.
The green line in Figure 3.36 shows the system COP when including backup resistance heat use but excluding tank losses. After filtering the data for periods when the WH/DH was shut down for sensor maintenance or other issues, the backup resistance energy use for the yearlong period was just 60.2 kWh or 5.4% of the total energy used for WH.
Finally, the red line in Figure 3.36 shows the COP of the entire system. This was calculated by dividing the measured WH energy being delivered to the house at the outlet of the storage tank by the total energy use of the WH/DH and backup resistance elements. Based on the measured data, the tank losses are 9.9% of the WH energy delivered to the tank (omitting data from 20 days in January of no HW use). This value is aligns with the performance expectations of a typical electric storage WH tank having a rated EF of 0.9, which is the minimum allowable EF for electric storage WHs manufactured before April 2015 in the United States.
The annual WH mode COPs for the WH/DH were 2.75, 2.48, 2.39, and 2.19 for the HP only, HP with line losses, HP with line losses and backup resistance use, and entire WH/DH system, including tank/line losses and backup resistance heat use, respectively. To achieve the highest overall system WH efficiencies, it is important to limit the length and diameter of the water lines connecting the WH/DH to the storage tank as much as possible, insulate these lines, and use a well-insulated storage tank.

6.6.2 AS-IHP System SC Performance

The monthly and seasonal SC performance of the ASHP and the effect of the WH/DH operation on SC are summarized in Table 22. The average monthly cooling COPs of the ASHP were between 4.32 and 5.59 with a seasonal average of 4.44. The WH mode of the WH/DH provides SC as a by-product of its operation. The DH mode also generates sensible heating in addition to latent cooling with a net SH effect, as indicated by negative values in the table.

Table 22: SC data for ASHP and AS-IHP system, including cooling and heating byproducts of the WH/DH (Lennox Inc., 2016).

Month	April 2016	May 2016	June 2016	July 2016	Aug. 2016	Sept. 2016	Oct. 2016	Totals
System SC delivered (kWh)	191	674	1,819	2,317	2,304	1,812	271	9,189[a]
ASHP	122	526	1,697	2,242	2,233	1,680	141	8,641
WH/DH mode	-4[b]	-30	-23	-56	-50	-5	-23[b]	191
WH/DH WH mode	73[b]	178	144	132	121	137	153[b]	938
ASHP SC energy use (kWh)	22	99	385	517	517	383	25	1948
ASHP average COP	5.57	5.34	4.41	4.34	4.32	4.39	5.59	4.44
System average COP	8.68	6.84	4.72	4.48	4.46	4.77	10.84	4.72[a]
Average OD temperature (°C)	15.7	18.9	25.1	26.4	26.3	23.7	15.1	21.6
While ASHP cooling	25.0	25.3	28.1	28.4	28.0	26.9	23.4	27.6
ASHP run hours	22.5	95.0	300.5	400.3	409.7	329.3	31.4	1,588.7

[a]Total system SC delivered and average system COP do not include WH/DH cooling/heating effects for April and October because the cooling demand was very low for these months; therefore, the WH/DH operation likely did not significantly affect the cooling load experienced by the ASHP.
[b]Only includes days of the month when the ASHP was in the cooling mode.

The “free cooling” effect that the WH operation has on the overall AS-IHP system (i.e., ASHP and WH/DH combined) SC efficiency results in monthly cooling COPs for the system between 4.46 and 10.84.The very high system COPs during April and October indicate a larger ratio of “free cooling” from the WH/DH to cooling supplied by the ASHP. However, much of the SC delivered by the WH/DH in these months was likely not satisfying a real demand for SC, and the house was being overcooled. Therefore, the WH/DH cooling effect for these 2 months was not included in the seasonal average SC COP for the system. With this consideration, the system’s seasonal average SC COP was 4.72, which was 6.3% higher than the COP of the ASHP alone. For the cooling season, this 6.3% efficiency increase results in estimated SC energy savings due to the operation of the WH/DH of 122 kWh.

6.6.3 AS-IHP System SH Performance

The monthly and seasonal SH performance of the ASHP and the effects of the WH/DH operation on SH are summarized in Table 23. As noted, when the WH/DH operates in WH mode, it provides SC as a by-product. However, for the heating season, the latent cooling provides no energy benefit or penalty, so the data shows only the sensible cooling. Similarly, for the limited run time in the DH mode, Table 23 only accounts for the sensible heating. The monthly SH COPs for the ASHP only are 2.00–3.43. The lowest COPs correspond to months with high backup resistance heat use. For January 2016, backup resistance heat use accounted for approximately one third of the total SH energy use. The average ASHP SH COP during the evaluation period was 2.38. When the cooling and heating by-products of the WH and DH modes of the system are accounted for, the overall AS-IHP system SH COP is reduced to 2.23—a 6.3% reduction.

Table 23: SH data for ASHP and AS-IHP system, including cooling and heating byproducts of the WH/DH (Munk et al., 2017).

Month	Oct. 2015	Nov. 2015	Dec. 2015	Jan. 2016	Feb. 2016	Mar. 2016	April 2016	Totals
Total sensible heating delivered (kWh)	172	1,344	1,687	4,029	2,723	1,192	384	11,651[a]
ASHP	171	1,431	1,764	4,158	2,974	1,408	505	12,411
WH/DH mode	43[b]	77	77	0	0	1	1[b]	199
WH/DH WH mode	-42[b]	-164	-154	-129	-251	-216	-122[b]	-1078
SH energy use (kWh)								
Total	50	502	677	2,076	1,289	478	153	5,225
Backup	0	0	120	684	299	32	1	1,136
Defrost	0	0	19	54	24	8	0	105
Av. ASHP COP	3.43	2.85	2.61	2.00	2.31	2.94	3.29	2.38
Av. system COP	3.44	2.68	2.49	1.94	2.11	2.49	2.51	2.23[a]
Av. OD Temp (°C)	15.1	11.5	10.6	1.5	5.4	12.5	15.7	10.3
While ASHP heating	10.2	5.9	5.3	0.2	2.1	5.8	7.6	3.3
Run hours	27.0	260.2	289.2	592.0	449.0	241.3	87.9	1,946.6
Defrost hours	0.0	0.0	4.0	10.7	5.1	2.1	0.2	22.1

[a]Total system SH delivered and average system COP do not include WH/DH cooling/heating effects for April and October because the heating demand was very low for these months; therefore, the WH/DH operation likely did not significantly affect the heating load experienced by the ASHP.
[b]Only includes days of the month when the ASHP was in the heating mode.

Table 24: Site-measured seasonal SH and SC COPs vs. estimated AHRI 210/240 ratings for ASHP unit used in AS-IHP system.

Mode	Site-measured SCOPs	AHRI 210/240 ratings	% deviation, field vs. rated
SH $SCOP_h$	2.38	Region IV HSPF: For DHRmin load: 2.93[a] For DHRmax load: 2.22 For house loads: 2.34	 −18.8 +7.0 +1.8
SC $SCOP_c$	4.44	SEER: For default load and Cd: 6.30 For house loads: 6.90	 −29.5 −35.7

[a]From AHRI (2016).

For the heating season, this 6.3% reduction in overall efficiency results in an estimated SH penalty due to operation of the WH/DH of 330 kWh.The SC and SH average measured seasonal efficiencies (COP or SEER in Btu/Wh) for the ASHP unit deviated significantly from AHRI 210/240 (AHRI 2008) rated values, as seen in Table 24. The AHRI estimates were computed using the minimum and maximum house load line or design heating requirement (DHRmin and DHRmax) assumptions and for the actual measured test house load lines during the 2015–2016 field-test period. Figure 55 compares these heating and cooling loads with the AHRI 210/240 heating and cooling load lines based on the rated heating capacity Q(47) at 8.3°C ambient and the rated cooling capacity Q(95) at 35°C.

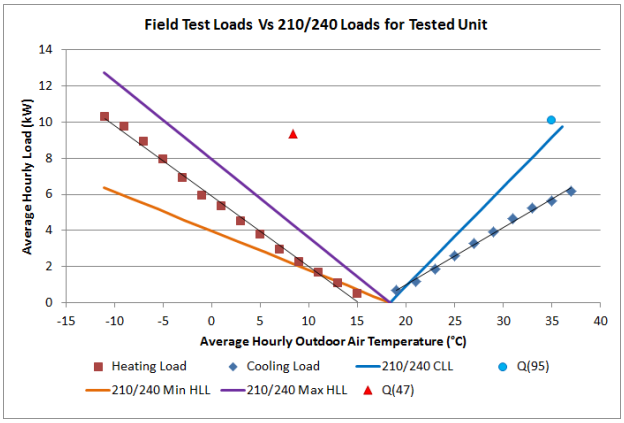

Figure 55: Field-test house 2015–2016 heating and cooling load lines vs. AHRI 210/240 load lines (maximum and minimum).

The ASHP of the AS-IHP field-test prototype might show these deviations compared with its rating values for several reasons.

- Blower energy use is higher at the field site due to higher duct system ESP losses than those assumed for the rating calculations. This is somewhat peculiar to the zoned distribution system used at the test house and to other changes made in the ducting system to accommodate the AS-IHP. However, residential duct systems generally have higher ESPs than the ~37 Pa (0.15 in. water gauge) implicitly assumed in AHRI 210/240.
- The two-zone duct system in the test house caused the ASHP to operate at higher speeds than the space loads would warrant during times when both zones simultaneously called for SC or SH (Munk et al., 2017). This reduced the energy savings that could have accrued from lower speed operation during mild weather periods in SH and SC seasons. (The effect was greater in the SC season.) Additionally, the data indicate that the compressor speed was allowed to vary even though the supply airflow was dictated by the zone(s) calling for conditioning. This results in the system running at suboptimal combinations of compressor speed and airflow, which also reduces efficiency.
- The $SCOP_h$ procedure does not account for defrost tempering heat usage. This accounted for ~2% of the total field system SH energy use during the test year.
- The indoor temperature during the heating season averaged 21.9°C, whereas the $SCOP_h$ calculation procedure assumes 21.1°C.
- The indoor dry bulb temperature during the cooling season averaged 24.4°C, whereas the $SCOP_c$ procedure assumes 26.7°C.
- The standard minimum house-heating load line used in the $SCOP_h$ procedure has a lower slope than that experienced at the test house (Figure 55). This results in a lower design-heating load than that experienced by the test house. This is primarily why ~22% of the total SH seasonal energy use for the field-test system was from backup resistance heat (Table 3.16) even though the 2015–2016 SH heating season in Knoxville was warmer than average, having ~18% fewer heating degree days based on the local airport weather station (Table 3.18).
- The test year cooling season in Knoxville was significantly warmer than average, having ~39% more cooling degree days as measured at the local airport weather station (Table 3.19). This resulted in many more hours of high-speed operation during SC than is normally expected, adding to the impacts from the zoned duct system.

Table 25 compares average heating and cooling degree days for Knoxville with those experienced during the 2011–2012 and 2015–2016 test years.

Table 25: Average vs. 2015–2016 test site heating and cooling degree days.

Location	Annual °F days heating(18.3°C base)	Annual °F days cooling(18.3°C base)
Knoxville Average[a]	1,997	841
2011–2012[b]	1,553	958
2015–2016[b]	1,642	1,170
2015–2016[c]	1,864	1,070

[a]1986–2010 averages from ASHRAE (2013).
[b]Test year actual values from National Oceanic and Atmospheric Administration (2015) and (2016) for McGhee Tyson Airport weather station.
[c]For test year October 2015–September 2016; site-measured actual.

6.6.4 Estimated AS-IHP Savings vs. Baseline

The annual energy use of a baseline system (3.8 $SCOP_c$ and 2.26 $SCOP_h$ [Region IV] SS ASHP and electric WH) meeting the field-test site loads was estimated. The HSPF and SEER ratings for the baseline unit were adjusted downward by 27 and 40%, respectively, based on the average field-measured deviations from rated efficiencies experienced by SS ASHPs previously field tested in the Knoxville area (Hedron and Engelbrecht, 2010). The results for this comparison are shown in Table 26. Since the HW tank heat losses were unaccounted for in the AS-IHP field test, they were also omitted from the baseline equipment efficiency (e.g., baseline WH COP of 1.0). This comparison assumes that the baseline ASHP meets the same total DH load as the prototype AS-IHP system. The largest percentage of savings come from WH at 58% (1,593 kWh). The WH energy savings estimate includes the effect of the 20-day period in January when the HW load was zero, so this savings estimate is likely somewhat conservative. SC + DH are estimated at 1,812 kWh (45%), and SH energy savings are estimated at 1,836 kWh (26%). The estimated total annual savings for the AS-IHP vs. the estimated baseline energy use at the Knoxville field-test site are ~38%. Heavy reliance on backup electric elements for SH and defrost tempering coupled with higher indoor blower energy usage vs. manufacturer's data were likely the primary causes of the lower-than-expected AS-IHP field-test prototype system SH performance.

Table 26: AS-IHP system 2015–2016 energy savings vs. estimated baseline system performance at the test site (based on 13 SEER ASHP field tests in 2011–2012).

Mode		AS-IHP	Baseline system estimated performance[a]	Percent savings over baseline
SC + DH	Delivered (kWh)	9,189	9,189	
	Consumed (kWh)	2,201	4,013	45%
SH	Delivered (kWh)	11,651	11,651	
	Consumed (kWh)	5,225	7,061	26%
Water heating	COP	2.39	1	
	Delivered (kWh)	2739	2,739	
	Consumed (kWh)	1,146	2,739	58%
Total	**Consumed (kWh)**	**8,572**	**13,813**	**38%**

[a]Estimated per average measured performance of two 13 SEER ASHPs tested in the Knoxville area in 2011–2012 (Munk, Halford and Jackson, 2013).

6.7 Gas Engine-Driven AS-IHP System Development Summary

Gas engine-driven heat pumps (GHP) can be an attractive economic choice in parts of the United States where typical engine fuels—such as natural gas, propane, or liquefied petroleum gas—can be less expensive than electricity. Compared with conventional fuel-fired furnace heating systems, GHPs are projected to reduce SH fuel consumption by 35% and water heating fuel consumption by 80%. GHPs can also significantly reduce summer cooling electric peak demand by over 80% compared with electric air-conditioning systems (Zaltash et al, 2008).

ORNL and its partners—Southwest Gas Corp (SWG), a gas utility company, and Intellichoice Energy, engineering consultancy company—have been collaborating to develop a multifunction (or IHP type) GHP for commercial and residential building applications. The system design was based on the needs of the SWG market located in the Southwestern United States (Figure 56). This area is a part of the US warm-dry climate zone (figure 3.2) and is characterized by very long, very hot summers but also very cold winters in some areas due to elevation.

Figure 56: SWG utility service area.

6.8 Commercial Gas Engine-Driven AS-IHP Summary

Commercial system development was completed first, and NextAire Inc., a manufacturing partner, introduced a system to the US market in 2012 (Figure 57). Its design cooling capacity was ~39 kW (~11 tons) at 35°C outdoor temperature with a COP of 1.1; the design heating capacity was ~42 kW (~142,000 Btu/h) at 8.3°C with a COP of 1.5 (Nextaire). The system also provides ~18 kW of water heating via engine heat recovery at maximum engine speed (2,400 rpm).

Figure 57: Commercial gas engine AS-IHP installed on the roof at the field demonstration site and final version of the prototype residential gas engine AS-IHP.

Most of the material in this section is summarized from the final report on a field demonstration project conducted during 2014–2015 in Las Vegas, Nevada (Vineyard et al., 2015). A commercial building with approximately 4,150 m^2 that consisted of retail space, offices, kitchen space, and warehouse storage hosted the demonstration (Figure 58). Approximately 325 m^2 of space was conditioned by the GHP-RTU.

The remainder of the building was conditioned by conventional electric RTUs. The space conditioned by the GHP-RTU included a training room, two machine rooms, and warehouse storage. The energy cost savings and a payback analysis are summarized in Table 3.20. Equipment costs for the base electric RTU HP were obtained from the manufacturer. The gas AS-IHP RTU cost was obtained from the manufacturer and is based on a cost for selling a quantity of 1,000 units per year. The installation cost for the gas AS-IHP was $3,000 higher than that of the base electric RTU due to the cost of reinforcing the roof to support the additional weight of the gas unit.

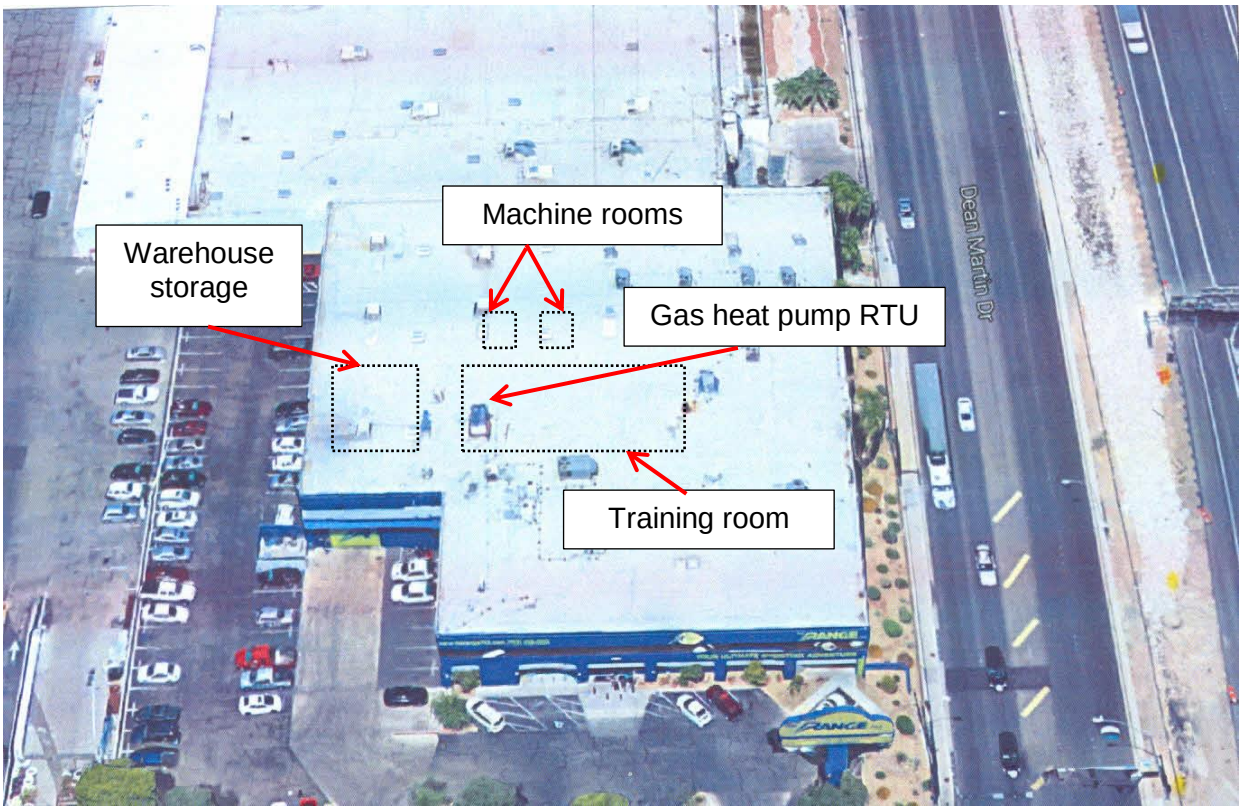

Figure 58: Aerial view of the demonstration site. (Source: Google Maps)

The total cost difference between the gas AS-IHP and the baseline system is $6,000, giving a payback for the gas AS-IHP ranging from 3.5 to 3.7 years, depending on the type of WH used in the base system.

Table 27: Commercial gas engine AS-IHP energy cost savings and payback vs. baseline electric RTU with electric and gas WHs.

	Equipment cost ($)	Installed cost($)	Total cost ($)	Cost difference ($)	Energy cost savings ($)	Payback (years)
Conventional RTU	10,000	6,250	16,250			
Gas AS-IHP vs. base RTU with gas WH	13,000	9,250	22,250	6,000	1,619	**3.7**
Gas AS-IHP vs. base RTU with electric WH	13,000	9,250	22,250	6,000	1,706	**3.5**

6.9 Residential Gas Engine-Driven AS-IHP Development Summary

A prototype residential scale version of a GHP was developed and lab and field tested. Full details of the residential system development are found in Momen et al. (2015), and a summary can be found in the HPT Annex 40 final report (Wemhoener, 2016).

Lab test results confirmed a cooling capacity of ~17 kW at 35°C outdoor temperature with a COP of 1.1; a heating capacity of ~20 kW at 8.3°C with a COP of 1.5; and a water heating capacity of ~9 kW of water heating via engine heat recovery. Eight prototype systems were field tested in the Las Vegas area.

The energy cost savings results vs. an electric baseline system are summarized in Table 28. Figure 3.36 provides a photograph of the prototype design final configuration. The prototype design was optimized to have the smallest possible footprint, the lowest possible electric consumption, and the best possible efficiency. Unfortunately, its production cost was estimated to be about $15,000 (Momen, Abu-Heiba and Vineyard, 2015). SWG estimates that a unit cost target should be $8,000 for the gas HP to penetrate the market.

Table 28: Prototype demonstrated energy costs vs. baseline system at Las Vegas test sites

Site #	Baseline energy costs ($)	Gas AS-IHP prototype energy costs ($)	Savings (%)
1	3,083	2,877	6.7
2	3,061	2,660	13.1
3	2,356	2,068	12.2
4	1,569	1,442	8.0
5	3,163	2,760	12.7
6	3,237	2,819	12.9
7	3,379	2,798	17.2
8	3,680	3,375	8.3

This cost is too high for the system to be commercially viable. Therefore, ORNL and its partners undertook a project under a DOE technology commercialization fund (TCF) support (Doe, 2019) to reduce the manufacturing cost and improve the residential gas AS-IHPs commercial viability. To achieve this goal, the following objectives were identified:

- Identify and implement a different engine that meets the capacity, efficiency, and reliability targets
- Value engineer the unit to reduce the cost of the components and manufacturing
- Complete a commercialization study to identify entry points to the market

To date, the results of this project indicate that a cost reduction of at least 43.5% is achievable (Figure 3.37). Although this is positive, the unit cost remains too high to penetrate the bulk of the US residential market. However, it is at a level that early adopters (e.g., homeowners and home builders focused on sustainability and maximum energy efficiency) might be willing to install systems.

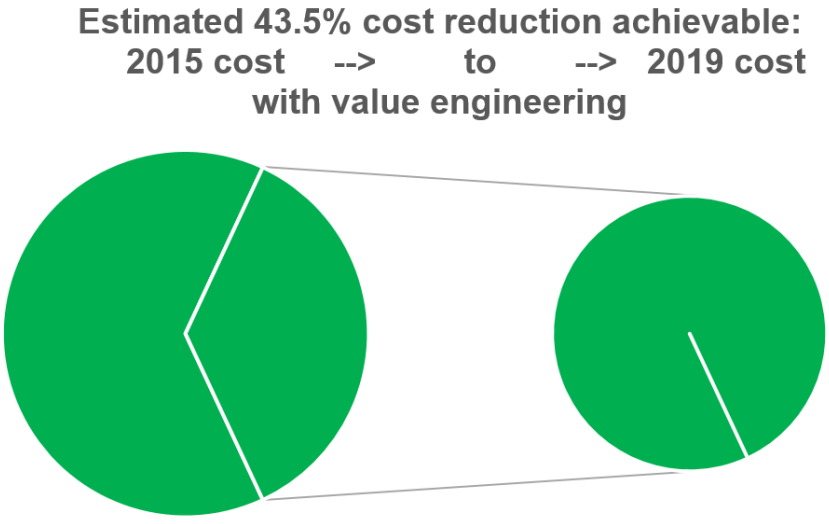

Figure 59: The TCF project shows potential to reduce the cost of prototype residential gas engine AS-IHP by ~43.5%.

An in-depth market study was conducted as part of the TCF project. One principle recommendation from the study is to add additional high-value features or amenities to the system where feasible. One such feature could be to enable the system to include electric generation capability to allow the system to continue operation during loss of electric grid events and possibly run some essential electric appliances as a side benefit. Some investigation into this possibility was already undertaken (Momen, Abu-Heiba and Vineyard, 2015). One possible implementation approach during grid outage situations is to increase the engine speed to maximum and engage a 5 kW AC generator component. The generator would produce approximately 1.6 kW AC power for fans and other electricity needs of the HP system, along with ~1–2 kW of additional electric power for emergency external needs, such as lighting and refrigerators. With an average electricity demand of 2–3 kW (40–60% of rated output), the 5-kW generator efficiency is high (~70%). Cost reduction and value-added efforts are ongoing.

6.10 IHP Systems

6.10.1 Key Observations and Future Potential

- Electric-driven GS-IHP.
  - This commercial product was introduced to the US market in late 2012 by CM, its Trilogy Q-Mode system.[12] The product remains on the market as of this report's preparation date.
  - Field demonstration results for two systems in commercial/institutional applications showed annual energy and energy cost savings of ~60% vs. a baseline AS HP with electric resistance WH.
  - Payback vs. the baseline system.
    - Estimated at ~8 years under favourable ground-loop HX installation conditions
    - Can exceed 20 years if loop install costs are high
    - Payback can be almost immediate with third-party ground loop installation and cost recovery on monthly electric bills
- AS-IHP: Prototypes of two different AS-IHP system arrangements were field tested in Knoxville, Tennessee.
  - System 1: Single compressor or combined system.
    - Features a VS compressor and fans, as well as a multispeed pump for DHW circulation.
    - Field test results showed 38% energy savings vs. baseline ASHP for HVAC and electric WH system.
  - System 2: Two-compressor system.
    - The system consists of a high-efficiency ASHP for SH/SC coupled with a separate HP WH/DH unit. The two systems can be coupled via the air-circulation duct system or can be separate.
    - Field-test results showed 38% energy savings vs. baseline ASHP for HVAC and electric WH system.
    - The separate WH-DH unit includes a demand DH mode for indoor-space air and V air, which is especially useful during spring and fall months when SH and SC loads are small.
    - This IHP concept is also the most adaptable for retrofit applications.
  - Both systems showed much better cooling and water-heating performance than SH, which suffered from reliance on electric resistance backup heating requirements.
  - Small commercial applications with annual loads dominated by SC and water-heating demand are deemed to be most ideal applications for these systems.
- Gas engine-driven AS-IHP.
  - This IHP concept features a natural gas-driven VS engine and scroll compressor and VS fans.
  - Commercial-size system (~40 kW cooling capacity) on the US market since 2012.

[12] https://www.climatemaster.com/Homeowner/side-links/products/product-details/trilogy.

- Field demonstration in Las Vegas, Nevada showed simple payback vs. electric ASHP + WH of under 4 years.

- Residential size prototype (~17.6 kW cooling capacity) developed.
  - Production cost of prototype ~$15,000; too high for market.
  - Value engineering project demonstrated that a potential cost reduction of ~44% is achievable; this could attract energy or “green” conscious buyers but is still too high for most of market.
  - Market study recommended including an electric generation capability to enable the unit to start and run during grid outages and run critical appliances (e.g., refrigerator); key value-added benefit.

7 Air source heat pump testing – Gaithersburg, US

7.1 Background: NZERTF, Gaithersburg, Maryland

The residential-style net-zero home on the NIST main campus offers a unique test bed for residential air-conditioning technologies. Several air-conditioning systems can be installed in the home in parallel so that the selected system can be operated at nearly the same weather conditions and load profile. With this in mind, a small duct high-velocity (SDHV) HP was installed in parallel with a conventionally ducted air-source HP to answer the following question: Can an SDHV HP system whose ductwork is much easier to install than a conventional duct system provide comparable energy-use efficiency? The two systems were installed side by side in the house with one system operating for a week and the other system operating for a week in an alternating fashion for a whole cooling and heating season. The main parameters that could answer the question were measured on both systems—namely, electrical energy use and cooling/heating thermal energy. Human comfort performance of the two systems is described in a complementary publication by Kim et al. (2019).
A more complete description of the net-zero home is found in Fanney et al. (2015). The net-zero house (Figure 60) includes a detached two-car garage. It is a two-story, three- to four-bedroom house with three full bathrooms and is separated from the garage by a breezeway. The first floor includes a utility closet for the clothes washer and dryer and a future multisplit HP indoor unit, a kitchen and dining area, a family room, an office (optional bedroom), a full bathroom, and a foyer open to the second floor. The second floor comprises a master bedroom with an adjoining bathroom, two additional bedrooms, a second bathroom, and a hallway. The house includes a full 135 m^2 (1,435 ft^2) basement. The detached garage contains the data acquisition/control equipment associated with the facility. The front of the house faces true south and accommodates two solar systems: a 10.2 kW photovoltaic system located on the main roof and four 2.2 m^2 (24 ft^2) solar thermal collectors on the roof of the front porch.

Figure 60: NZERTF: left front at ground level (left) and right front elevated view (right).

Because of the home's air tightness, it is mechanically ventilated according to ASHRAE Standard 62.2 (2010). NZERTF uses a heat recovery ventilator to provide outdoor air to all bedrooms. The ventilator operates to deliver 136 m^3h^{-1} (80 cfm) for 45 minutes of every hour. This system operates independently of the HVAC systems and has a separate duct system.
Many investigations have been performed to examine the performance of various HVAC systems in low-load homes. The largest body of work has been performed by the national laboratories funded by DOE's Building America Program (2019).
Poerschke and Rudd (2016)studied the efficacy of using small duct airflow distribution systems in several different home-run configurations. Their goal was to optimize air distribution and minimize temperature differences in the test homes. They showed that this could be done with their central manifold systems while maintaining air-distribution energy efficiencies between 0.16 and 0.22 W cfm^{-1}. They attempted to design air-distribution manifolds and small duct (i.e., PVC pipe) combinations that allowed for better balance when changes were made to a run. This work could provide good data for a training dataset in many multifactor optimization algorithms. Duct design methods should change to reflect the operating regimes of multispeed and variable-speed equipment. The ducting should be designed to optimize the lifetime performance of the system, meaning the ducting should give the best performance for the most likely static pressures (i.e., airflow rates) that will occur. Duct design tools should incorporate more detailed load information along with weather data files and operational models to produce a ducting system optimized for the lowest lifetime air-moving cost to the consumer.

This is a complicated, multi-objective optimization problem that has been examined by many researchers, such as Besant and Asiedu (2000), Tsal et al. (1988), Caldas and Norford (2003), and Jorens et al. (2018). Residential duct designers need a product that can be used by nonexpert practitioners to design residential duct systems for the lowest lifetime cost.
Martin et al. (2018) performed testing on the same SDHV system as was installed in NZERTF. They examined the energy use and dehumidification performance of the SDHV in a hot-humid climate (zone 2a). Their design-cooling load was only 13% greater than that of NZERTF. The 14 SEER, variable-speed, SDHV system used 8.2% less energy in the cooling season than a 13 SEER single-speed system and 16.7% more energy than a 22 SEER, variable-capacity system, but the SDHV system maintained lower humidity levels overall than the other systems.

7.2 Test Setup

7.2.1 Test House

The first and second floors have a combined living area of 252 m^2 (2,713 ft^2). Including the basement (actively conditioned) and attic (passively conditioned), the total floor space is 425 m^2 (4,578 ft^2). The building has a total conditioned volume of 1,268 m^3 (44,773 ft^3), which includes the attic and basement spaces. The window-to-wall area ratio for the first floor's north, south, east, and west sides are 0.167, 0.201, 0.143, and 0.048, respectively. In the same order, the second floor is 0.123, 0.285, 0.050, and 0.050. The outside perimeter length of the basement and first floor is 47.155 m (154 ft, 8.5 in.), and the second floor is 42.418 m (139 ft, 2 in.). The building envelope was constructed by using a continuous air-barrier system to minimize infiltration with building ventilation provided by a heat recovery ventilation system. Five blower door tests were conducted at various stages of construction, and the final test, conducted after the house was complete, yielded an air exchange rate of 802 m^3h^{-1} (1,200 cfm) at 50 Pa (0.2 in wg) corresponding to 0.63 air changes per hour. Details can be found in Fanney et al. (2015). A detailed TRNSYS model of the house was developed by Balke et al. (2018).
The house is in DOE climate zone 4A. This climate zone is defined as mixed humid with IP units CDD 50°F ≤ 6,300 and 3,600 < HDD 65°F ≤ 5,400 and SI units CDD 10°C ≤ 3,500 and 2,000 < HDD 18°C ≤ 3,000 (Table 3.1). The house design cooling and heating thermal loads are 4,722 W (16,114 $Btuh^{-1}$) and 5,667 W (19,336 $Btuh^{-1}$). This is equivalent to 11.11 Wm^{-2} and 13.33 Wm^{-2} at design day cooling and heating temperatures of 32.8°C (91°F) and -8.9°C (16°F).
The HPs were controlled by wall-mounted thermostats that measured temperature in the living room and dining room area, as shown in Figure 61. These were the only thermostats used, so all operations were as if the house were a single zone. The cooling season setpoint temperature was 23.8°C (75°F), and the heating season setpoint was 21.1°C (70 F).

Figure 61: Thermostat locations: (a) wide view and (b) detailed view.

7.2.2 Air-Duct Systems for the HPs

NZERTF has four separate air-duct systems: (1) a conventional duct system used with air-to-air or ground-source HPs, (2) an SDHV air-distribution system used in conjunction with an air-to-air SDHV HP, (3) a dedicated duct system associated with the heat recovery ventilator, and (4) a short-run supply air-duct system on the first and second floors for two ceiling-mounted cassette-type mini air handlers used with multisplit, variable-speed, air-source HPs.
All four duct systems are within conditioned spaces. Further discussions will focus on the conventional and high-velocity duct systems.

The conventional duct system was designed for less than a 124.5 Pa (0.5 in wg) static pressure drop at supply and return duct airflow rates of 2,039 m^3h^{-1} (1,200 cfm) with all air supplies fully open. The insulated main trunk lines are located with the air handler in the basement. Multiple supply registers are in each room of the house. Return ducts are in central locations on the first and second floors. The SDHV air-distribution system begins in the basement with an insulated main trunk line that outlines the basement perimeter, allowing take-offs for individual room air-supply registers that supply the first floor. A large, insulated, supply riser feeds a similar ring in the attic. The trunk lines are 22.9 cm (9 in.) in diameter and are designed for an airflow rate of 2,039 m^3h^{-1} (1,200 cfm). The take-off ducts that supply the individual registers are 6.35 cm (2.5 in.) in diameter.

7.2.3 Tested HPs and Measurement Uncertainty

The rated cooling and heating performance of the two HP systems at AHRI Standard 210/240 (2017) conditions is shown in Table 29.

Table 29: Rated performance of the two HP systems.

System	SEER (Btu $[Wh]^{-1}$)	EER cooling (Btu $[Wh]^{-1}$)	HSPF region IV (Btu $[Wh]^{-1}$)	Cooling capacity, W (Btu h^{-1})	Heating capacity, W (Btu h^{-1})
Conventional (two-stage)	15.80	13.05	9.05	7,620 (26,000)	7,796 (26,600)
SDHV (variable-speed)	14.00	7.45	8.35	8,558 (29,200)	10,317 (35,200)
Calculated LOADS				4,723 (16,114)	5,667 (19,336)

The calculated loads and duct layout were determined by the original architectural firm by using a computer program that used ACCA Manual J (2012a) and ACCA Manual D (2012b). Oversizing the variable speed equipment allows the equipment to operate at partial load for most of its run time and thus operate at a higher efficiency. A thorough discussion of selecting variable speed equipment based on efficiency and the implications for human comfort can be found in Cummings and Withers (2014) and Shirey et al. (2006).

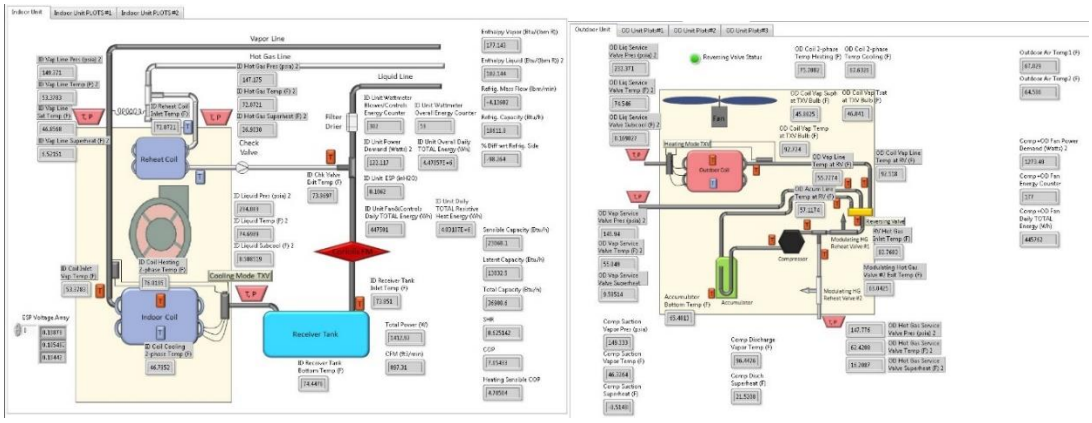

Figure 62: Measurement points for (a) two-stage CDHP and (b) SDHV, variable-speed HP.

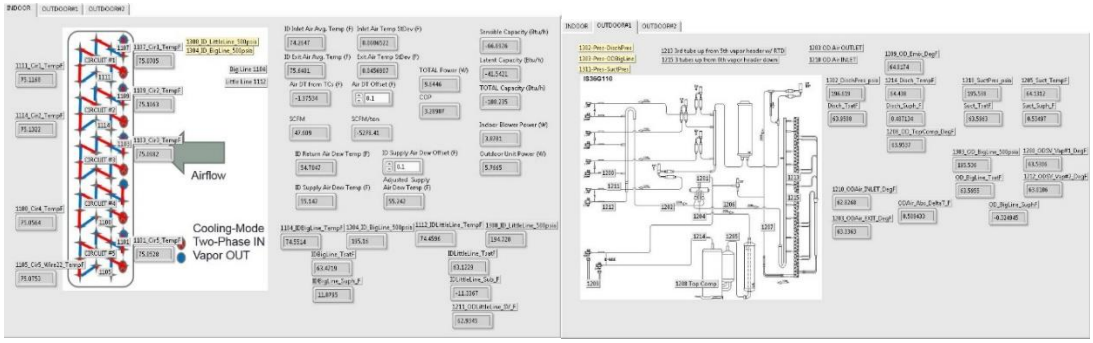

Figure 63: Measurement points for (a) two-stage CDHP and (b) SDHV, variable-speed HP.

Both systems were fully instrumented and connected to data acquisition devices that monitored them continuously with 10 second scans during the off-period and 3 second scans during the on-period. The data were saved and aggregated for each testing day.
Figure 62 and Figure 63bshows the measured points for each system. Figure 64 shows the conventionally ducted HP (CDHP) system, and the SDHV system at the installed locations in NZERTF.

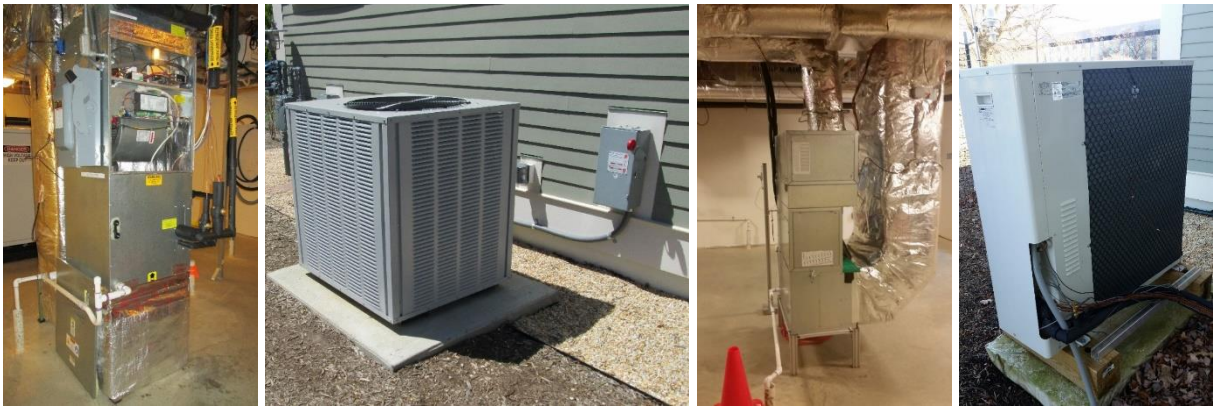

Figure 64: CDHP system indoor and outdoor units at NZERTF: indoor air handler (left) and outdoor unit (mid left) and SDHV system indoor and outdoor units at NZERTF: indoor air handler (mid right) and outdoor unit (right).

Table 30 lists the measurement uncertainties for both systems at a 95% confidence level. A detailed uncertainty analysis was performed in Davis et al. (2014). The plus or minus uncertainties included with measured quantities are calculated as two standard deviations of multiple measurements. The uncertainty of values calculated from a least squares fit is listed as twice the fit standard error (k = 2 coverage factor) unless stated otherwise.

Table 30: Measurement uncertainties.

Instrument	Range	Total uncertainty at a 95% confidence level
T-type thermocouples	-10–55°C (16–131°F)	±0.6°C (1.0°F)
High-pressure transducer	6,895 kPa (1,000 psig)	±0.25% of reading
Low-pressure transducer	3,447 kPa (500 psig)	±0.25% of reading
Air pressure differential (ESP[1])	0–187 Pa (0–0.75 in. H_2O)	±0.8% of reading
Indoor blower and controls power meter	0–300 VAC, 5 Amps, 1,000 W	±5 W
Indoor total power meter	0–300 VAC, 100 Amps, 20,000 W	±100 W
Outdoor unit power meter	0–300 VAC, 20 Amps, 4,000 W	±20 W
Supply air dewpoint temperature sensor	-28.8–49°C (-20–120 °F)	±1.0°C (1.8°F)
Coriolis refrigerant mass flow meter on CDHP	0–2,180 kg h^{-1} (0–80 lb min^{-1})	±0.15% of reading
Volumetric airflow rate	85–2,039 m^3h^{-1} (50–1,200 cfm)	5.5% of value
Sensible capacity	1,465–11,137 W (5,000–38,000 Btu h^{-1})	4–7%
Latent capacity	293–2,931 W (1,000–10,000 Btu h^{-1})	25–40%
Total capacity	2,931–11,137 W (10,000–38,000 Btu h^{-1})	7–10%
COP	0–6	8–12%

7.2.4 Results

The two systems operated side by side with one unit operating for 1 week followed by the other unit operating for 1 week. This weekly flip-flop, instead of a daily flip-flop, was necessary due to the large thermal inertia of the net-zero house. A net-zero house can go for weeks with no space conditioning given its low losses to the environment, so a weekly flip-flop was judged to

be a better way to compare and remove the performance overlap of the two systems. CDDs and HDDs are used to normalize the results and provide a better comparison of the heating and cooling performance of the two systems. Even though the two systems operated side by side in a weekly alternating pattern, weather variability prevented the two systems from having an equal number of CDDs and HDDs.

7.2.5 Cooling Season

The cooling season weather conditions seen by the two systems are characterized in Figure 65 left by using CDDs with respect to a base of 50°F (10°C). The conventionally ducted system experienced almost 31% more CDDs, even though the two systems were alternating operations weekly.

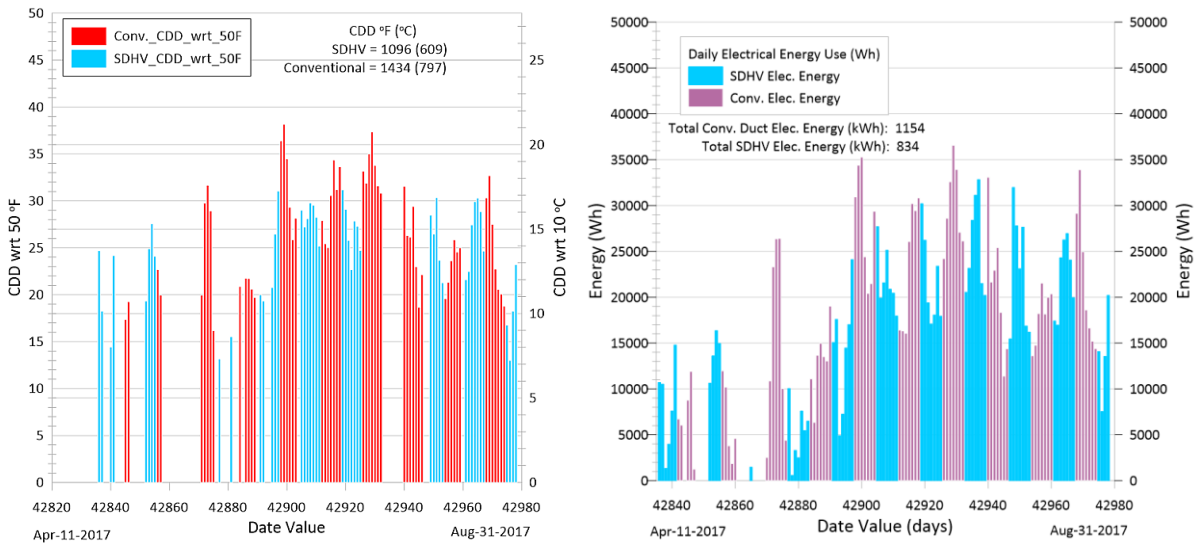

Figure 65: CDDs seen by both systems (left) Cooling electrical energy use for the entire cooling season (right).

7.2.6 Cooling Energy

Figure 65 right shows the average daily energy usage for the two systems along with the totals for the entire cooling season. Because of the higher number of CDDs seen by the conventional system, its energy usage was 38% greater. Figure 66 left shows the daily total electrical energy usage with respect to the CDDs of the two systems.

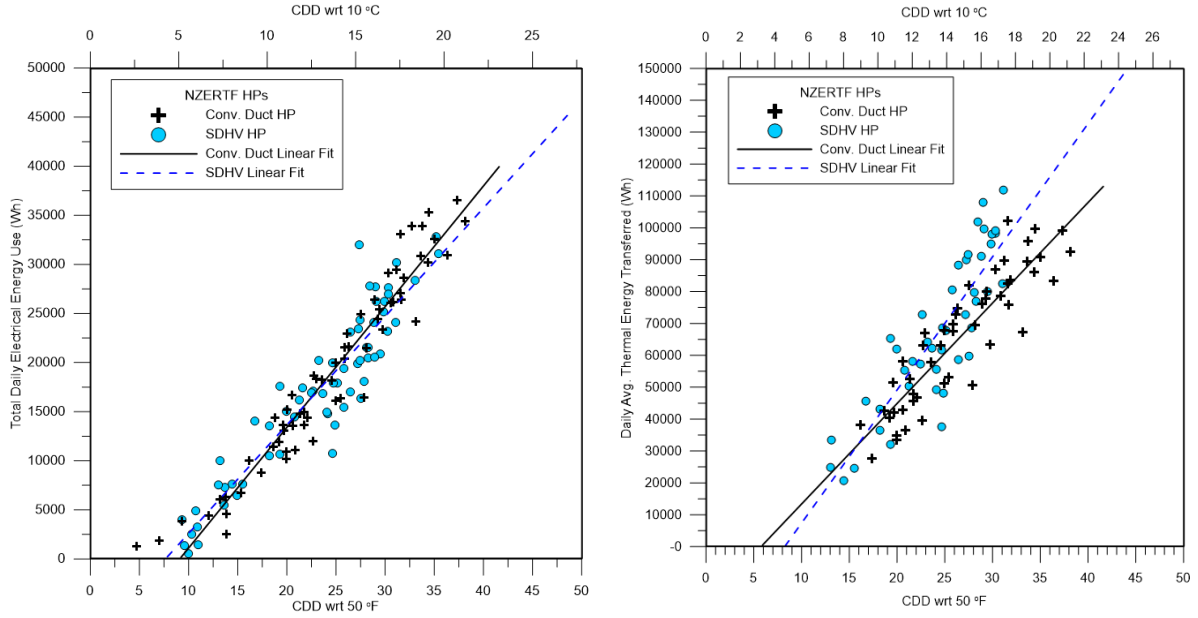

Figure 66: Cooling season electrical energy usage (left) and cooling season thermal energy (right)

There is no statistical difference in their normalized average daily energy use for the cooling season at a 95% confidence level. The daily electrical energy usage per CDD for the CDHP

and SDHV were (2.327 ± 0.209) kWh°C^{-1} ([1.293±0.116] kWh°F^{-1}) and (1.916 ± 0.302) kWh°C^{-1} ([1.069±0.168] kWh°F^{-1}), respectively. The difference in the cooling season electrical energy usage per CDD was statistically insignificant; on average, the SDHV system used (282 ± 1,126) Wh less electrical energy per CDD. The daily thermal energy removed per CDD for the CDHP and the SDHV were (1,738 ± 233) Wh°C^{-1} ([3,123 ± 420] Wh°F^{-1}) and (2,282 ± 359) Wh°C^{-1} ([4,107 ± 647] Wh°F^{-1}), respectively (Figure 66 right). The difference in the cooling season thermal energy removed per CDD was statistically insignificant. Figure 67 left examines the daily average airflow rates of the two systems. The SDHV system operated at (177 ± 20) cfm lower daily average airflow rates. Figure 67 right shows the fan efficacy of the two systems as a function of their daily percent run times. The SDHV system clearly operates at a lower Watt-per-unit airflow rate due to its lower flow rate. Both systems used comparable electronically commutated motors (ECMs).

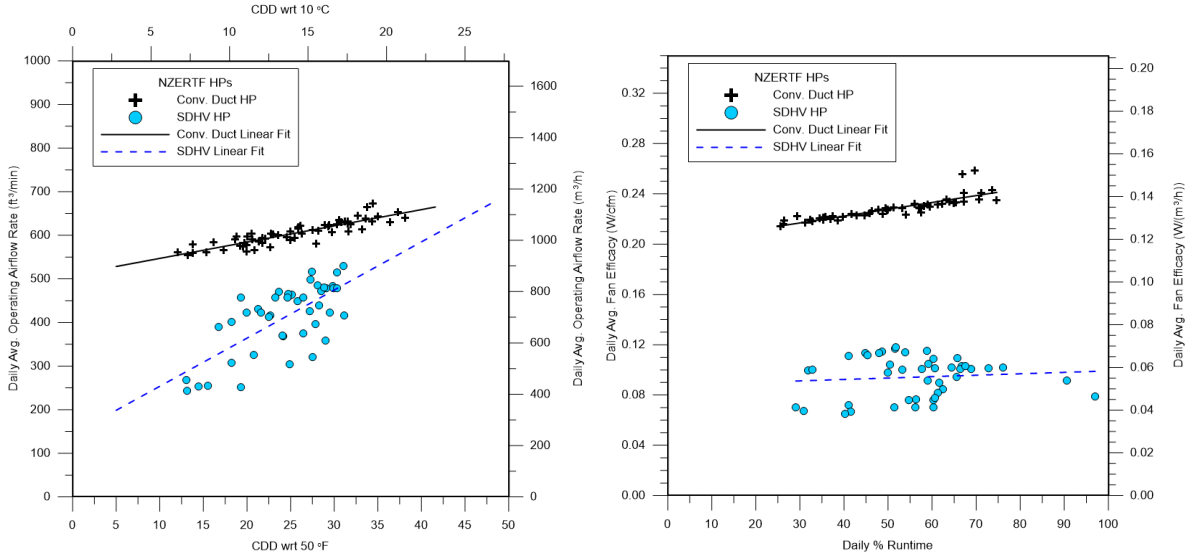

Figure 67: Cooling daily average operating airflow rates as a function of CDD (left) and Cooling daily average indoor blower efficacy (W/[unit volume flow])

Although the two systems usually operated at different airflow rates, they still circulated the same total volume of air in the house, as shown in Figure 68 left. This figure shows that the total number of house air changes as a function of CDD was statistically equivalent for the two systems.

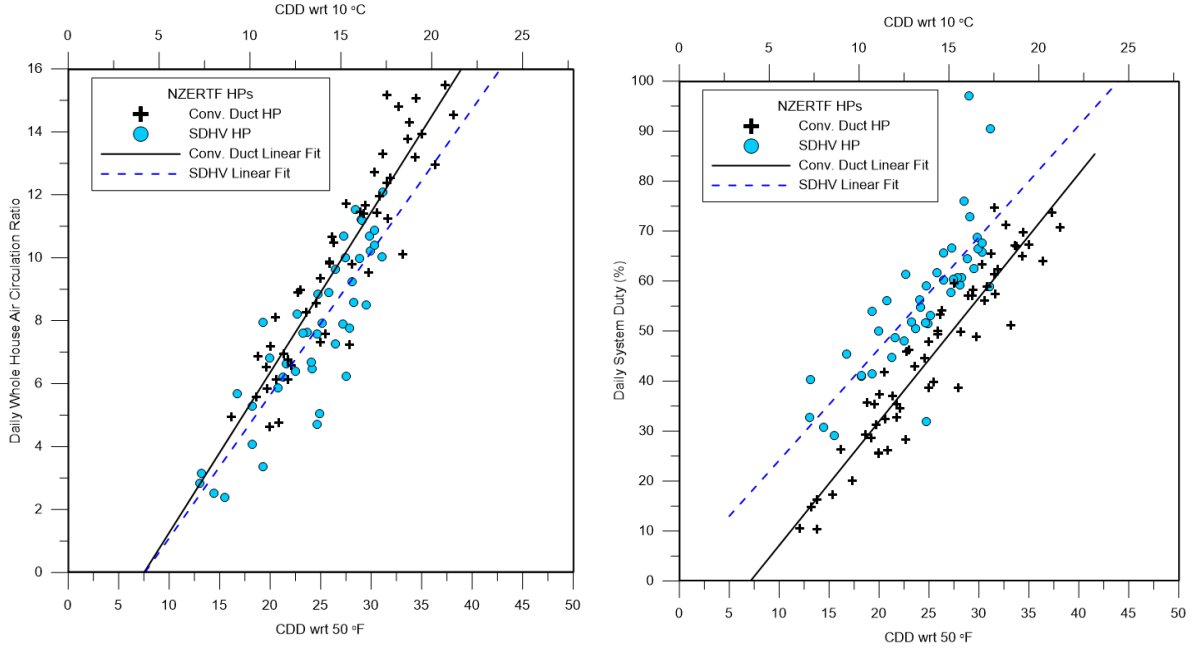

Figure 68: Daily cooling air circulation ratio (i.e., number of whole house air volume air changes through the air handler) (left) and cooling daily system percent duty (right)

Although the SDHV system operated at lower total airflow rates, it operated for longer periods of time to produce equivalent total air changes. The operating times are shown more clearly in Figure 68 right.
Figure 66 left showed that the two systems used the same average daily electrical energy per CDD; however, the SDHV system operated at a (4.0 ± 0.2)°C ([7.27 ± 0.44]°F) lower supply air temperature (Figure 69 left) than the CDHP and a 3.70 ± 0.22°C (6.66 ± 0.42°F) greater delta temperature (Figure 69 right) across the air handler than the CDHP. Figure 70 shows that the two systems had comparable average return air temperatures with the SDHV averaging slightly lower than the CDHP (-0.33 ± 0.10)°C ([-0.60 ± 0.18°F]).

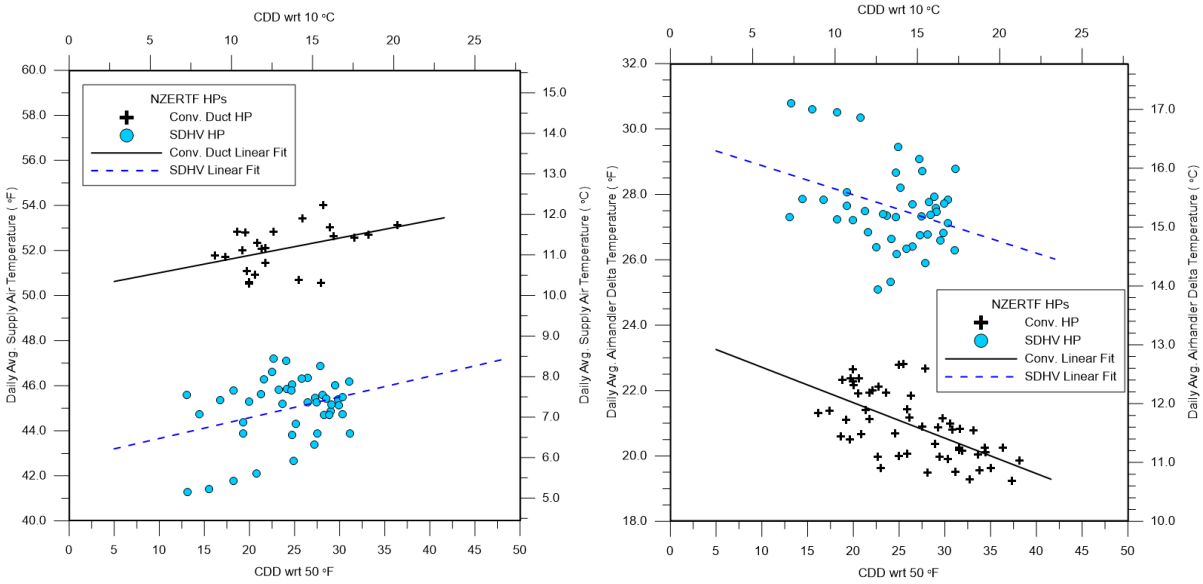

Figure 69: Cooling average operating supply air temperatures (left) and Cooling average operating indoor unit air temperature change (right)

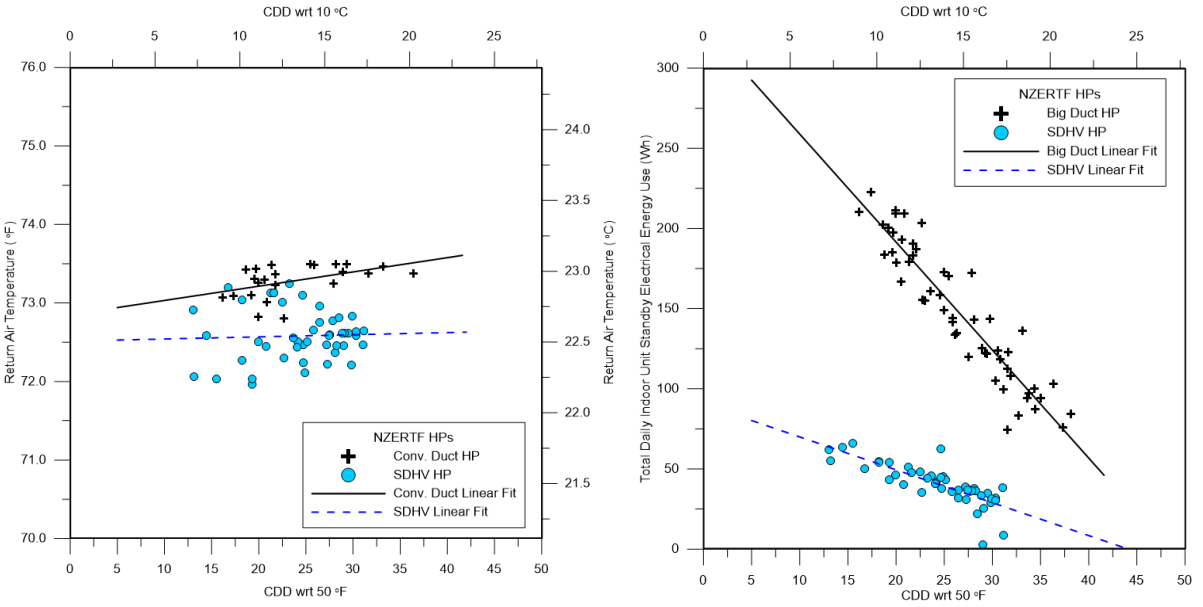

Figure 70: Cooling daily average operating return air temperatures and Cooling indoor unit daily standby energy use (right)

7.2.7 Cooling Standby Energy Use

Table 31 shows the average power demand during standby for the two systems. During standby, the system is not performing any cooling, heating, or ventilation functions. Any electrical energy that is consumed is not being used to condition the space, and it is a waste of energy that reduces overall space-conditioning efficiency. The system is still powered up, and the indoor and outdoor unit controls are consuming energy.

The large difference between the power demands is due to the difference in the type of low-voltage transformer used by the two systems; the SDHV uses a toroidal transformer, whereas the CDHP uses an E-core, laminated steel-plate type transformer.

Table 31: Cooling standby power demand.

System	Indoor standby (W)	Outdoor standby (W)
CDHP	11.9	23.4
SDHV	3.9	7.7
% difference with regard to CDHP	-67%	-67%

Figure 71 shows the two different types of transformers installed in the systems.

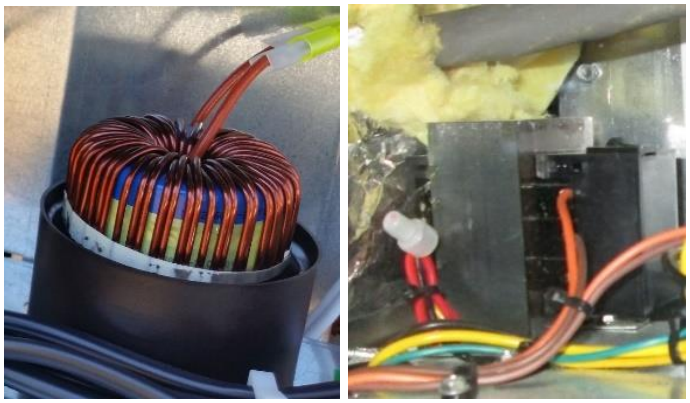

Figure 71: Low voltage transformers in the two systems: CDHP E-core laminated plate (left) and SDHV toroidal (right)

The indoor standby energy use of the SDHV system averaged (113.5 ± 7.0) Wh per day less than the CDHP (Figure 70 right), whereas the outdoor standby averaged (222.3 ± 14.3) Wh less (Figure 72 left). These results combined for the SDHV system to produce a total daily standby energy use that was (335.8 ± 21.3) Wh less than the CDHP (Figure 72 right).

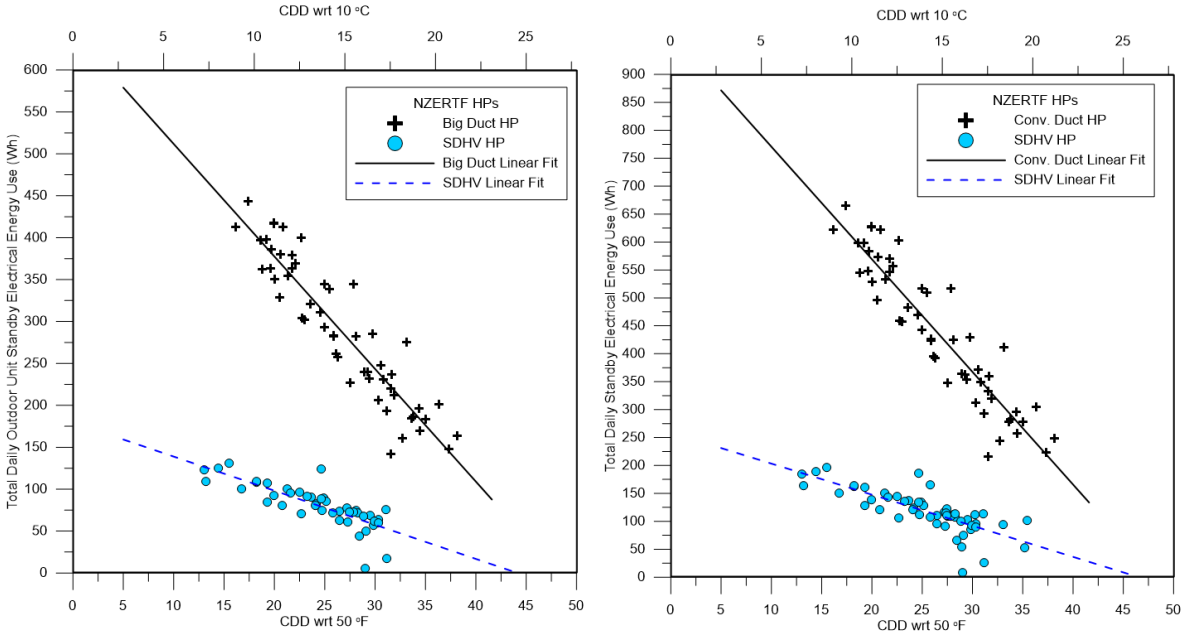

Figure 72: Cooling outdoor unit daily standby energy use (left) and Cooling system daily total standby energy use (right)

7.2.8 Cooling Efficiency

Figure 73 shows the cooling COP as a function of CDDs. There is more scatter in the variable speed COP data than for the two-stage HP. The SDHV system averaged a slightly higher COP for the cooling season being (0.396 ± 0.113) higher than the CDHP.

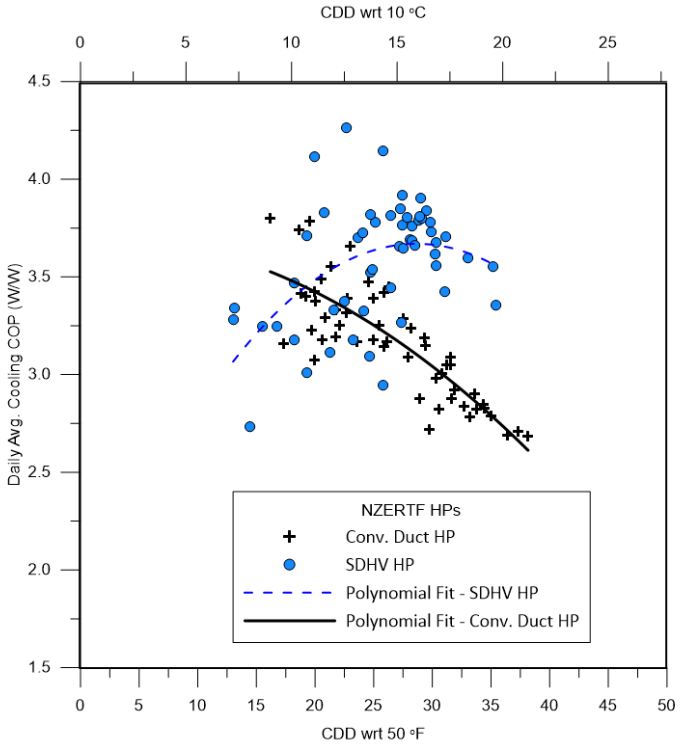

Figure 73: Cooling season COP

Figure 74 left and Figure 74 right show the compressor suction and discharge refrigerant saturation temperatures, respectively, for a comparable day for the two systems. In Figure 74 left the CDHP has an on cycle from approximately 700–2,400 seconds, whereas the SDHV system runs continuously over that same time. Figure 74 right shows that the evaporator saturation temperature of the CDHP is 5°C (9°F) higher than the SDHV, whereas the discharge saturation temperatures are within 2°C (3.6°F) of each other.

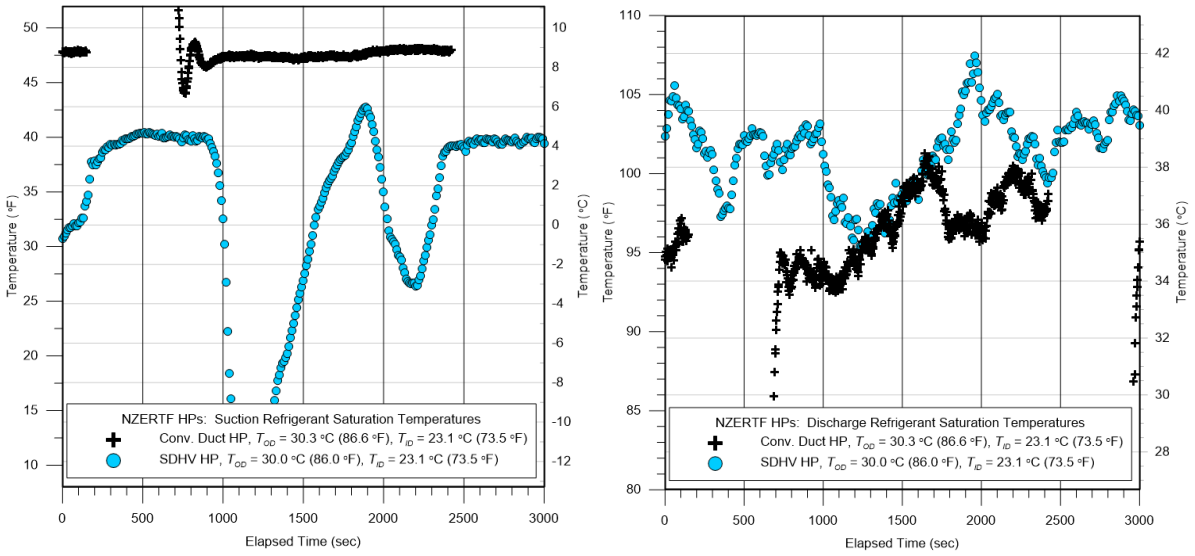

Figure 74: Cooling suction refrigerant saturation temperature example (left) and Cooling discharge refrigerant saturation temperature example (right)

This means that the SDHV system was operating at a higher temperature lift than the CDHP. The temperature lift for the two systems is shown in Figure 75 left. If the SDHV system hunting behavior between 1,000 and 2,000 seconds is neglected, then the SDHV operated with approximately 35°C (63°F) lift, and the CDHP operated with 27°C (49°F) lift. If everything else were equal, then the CDHP should have a higher COP because it was operating at a lower lift; however, Figure 75 right shows that the instantaneous COP was better for the SDHV system.

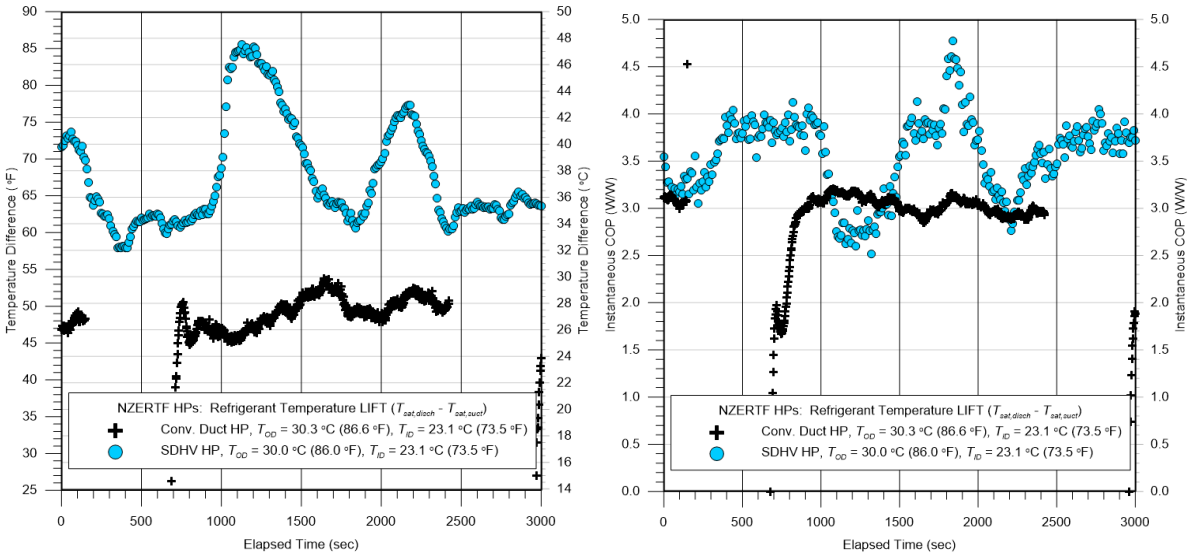

Figure 75: Cooling temperature lift example (left) and cooling instantaneous COP example (right)

The reasons are shown in Figure 76 left and Figure 76 right, which show the instantaneous power and capacity, respectively. The capacity is equivalent, but the power demand of the SDHV system is less. The SDHV system showed this behavior consistently, producing higher COP even though it was operating at a higher lift (condenser refrigerant saturation temperature and evaporator saturation temperature difference). This behavior could have been modified in the control system to raise the evaporator saturation temperature when there was less need for dehumidification, thus increasing COP during more of the operating time.

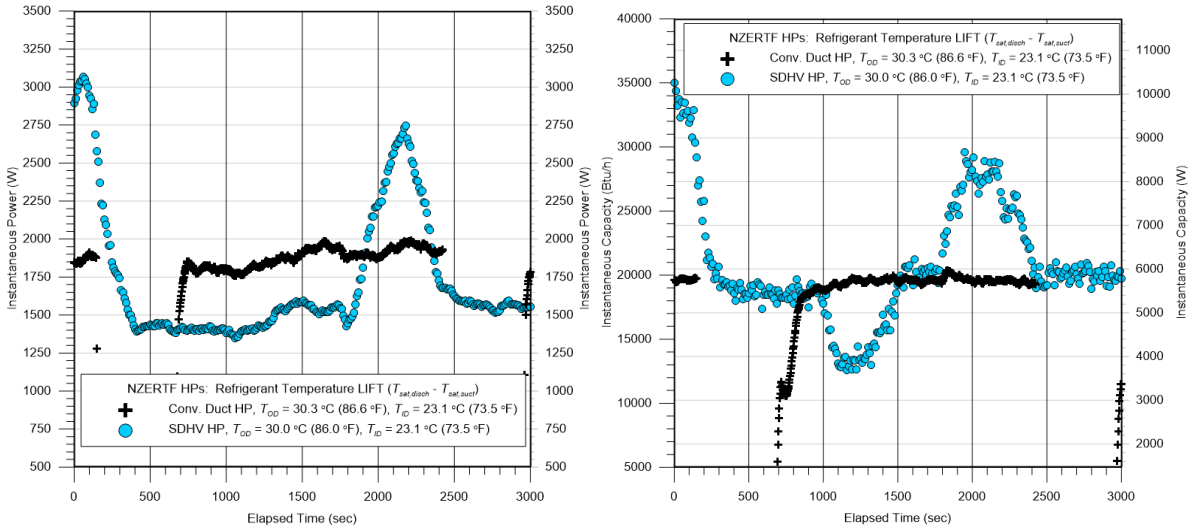

Figure 76: Cooling instantaneous power example (left) and Cooling instantaneous capacity example (right)

Figure 77 shows a comparison of the daily average COP as a function of the daily average outdoor dry-bulb temperature. The SDHV, variable-speed system tended to operate at higher COPs for most of the outdoor conditions shown. The CDHP experienced higher temperature degree days but maintained good COP running at its lowest stage. Even on the highest temperature days, the CDHP operated at its low-stage capacity. The higher temperatures experienced by the CDHP lowered its average COP compared with the SDHV.

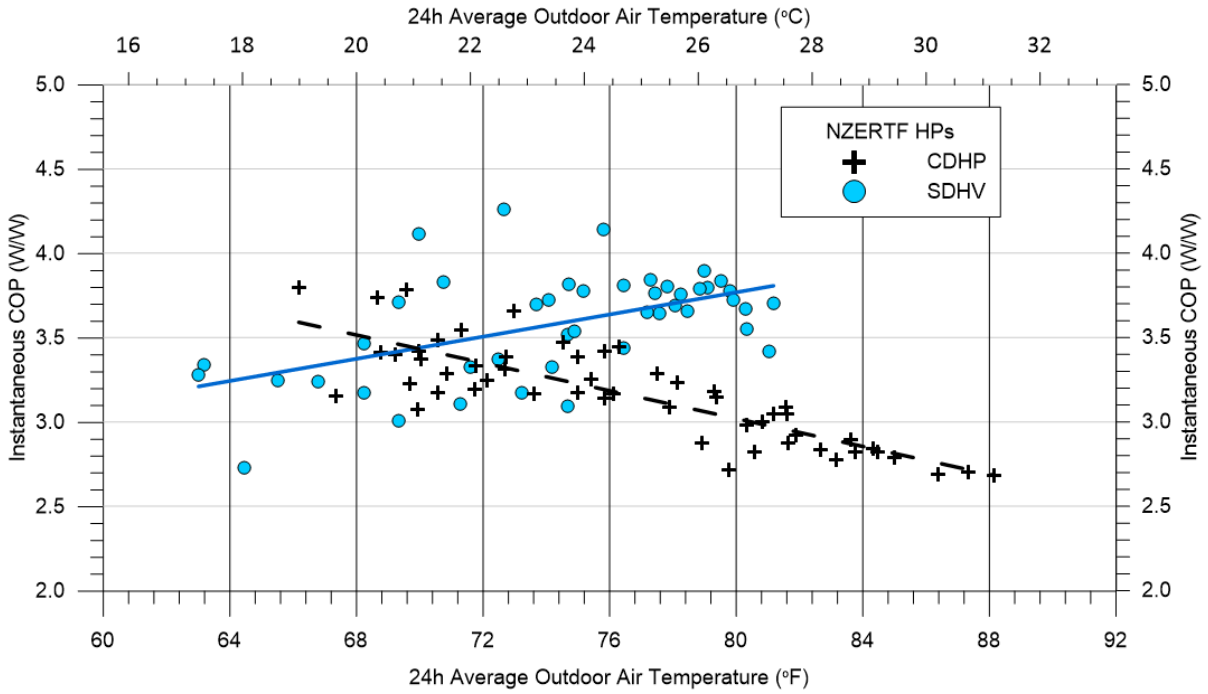

Figure 77: Cooling COP as a function of daily average outdoor temperature.

7.2.9 Heating Season

Figure 78 left compares the HDDs with an 18.3°C (65°F) reference for the two HP systems. The heating season was from November 16, 2016 to April 2, 2017. The SDHV system had 22.4% more HDDs than the CDHP, even though they were operating on a weekly alternating schedule. For the heating season, as in the cooling season, degree days are used in the plots to normalize the results.

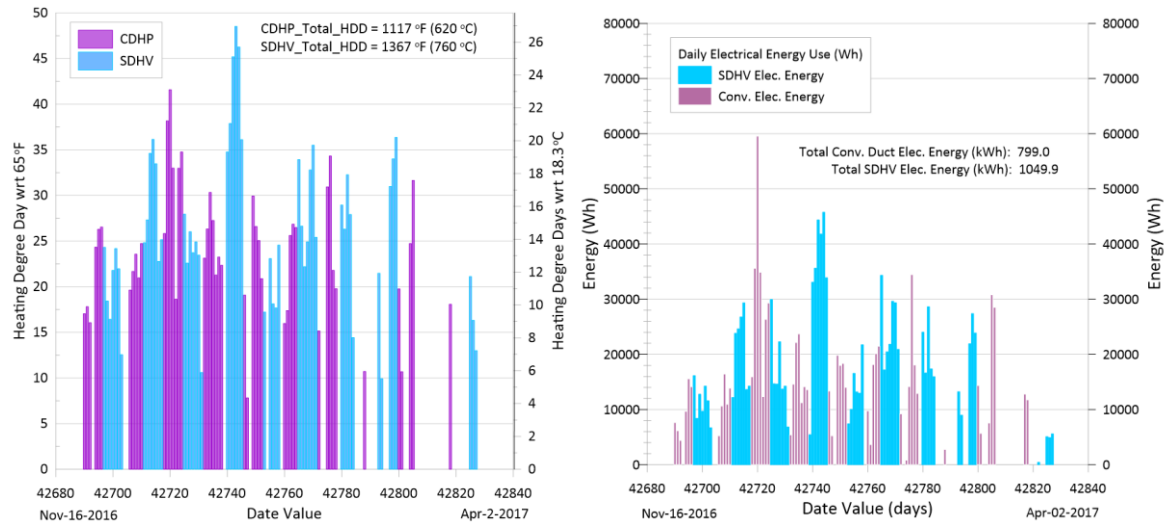

Figure 78: HDDs for the CDHP and SDHV (left) and Heating season daily and total electrical energy use (right)

7.2.10 Heating Energy

Figure 78 right shows the daily average electrical energy consumed by the systems as a function of HDD. Because of the higher number of HDDs, the SDHV consumed 31.4% more electrical energy over the heating season. The daily electrical energy usages per HDD for the CDHP and SDHV (Figure 79 left) were (1,975 ± 355) $Wh°C^{-1}$ ([1,09 7± 197] $Wh°F^{-1}$) and (1,931 ± 243) $Wh°C^{-1}$ ([1,073 ± 135] $Wh°F^{-1}$), respectively. The difference in heating season electrical energy usage per HDD was statistically insignificant. The daily thermal energy transferred per HDD (Figure 79 right) for the CDHP and the SDHV were (860 ± 208) $Wh°C^{-1}$ ([1,548 ± 374) $Wh°F^{-1}$) and (939 ± 173) $Wh°C^{-1}$ ([1,690 ± 311] $Wh°F^{-1}$), respectively. The difference in the cooling season thermal energy removed per HDD was statistically insignificant.

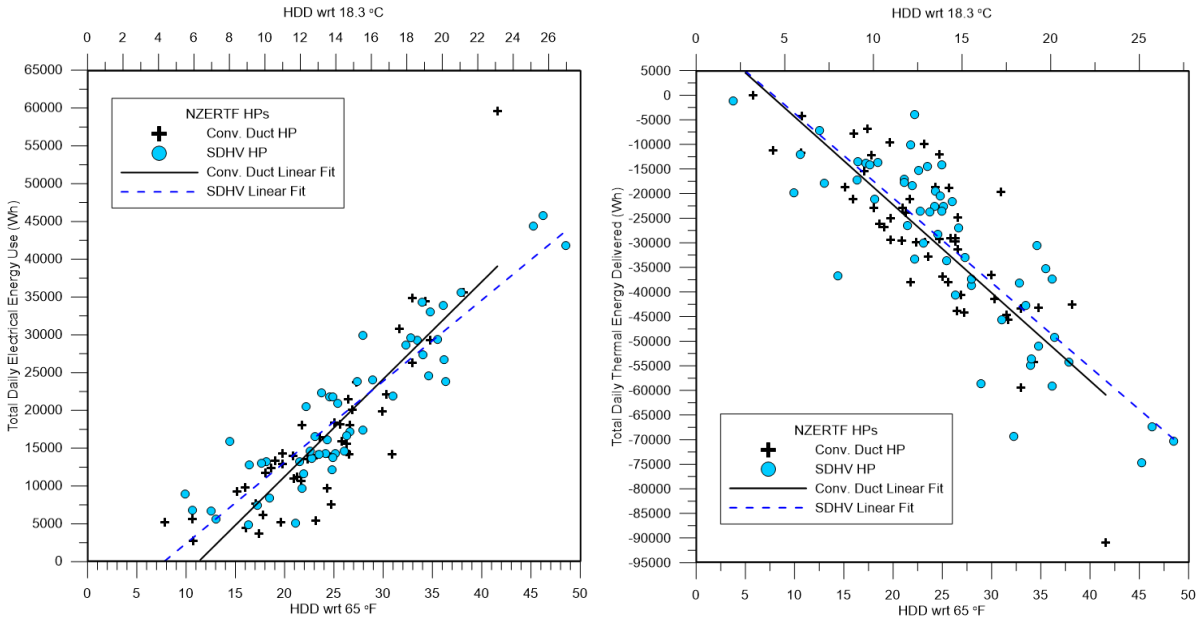

Figure 79: Heating season electrical energy use as a function of HDDs. (left) and Heating season thermal energy delivered (right)

Figure 80 left shows that the SDHV system operated at a lower average daily airflow rate than the CDHP. The SDHV operated at (625 ± 53.2) m^3h^{-1} ([368 ± 31.3] cfm) lower average airflow than the CDHP. Similar to the cooling mode, the SDHV indoor blower operated in a more efficient range (Figure 80 right).

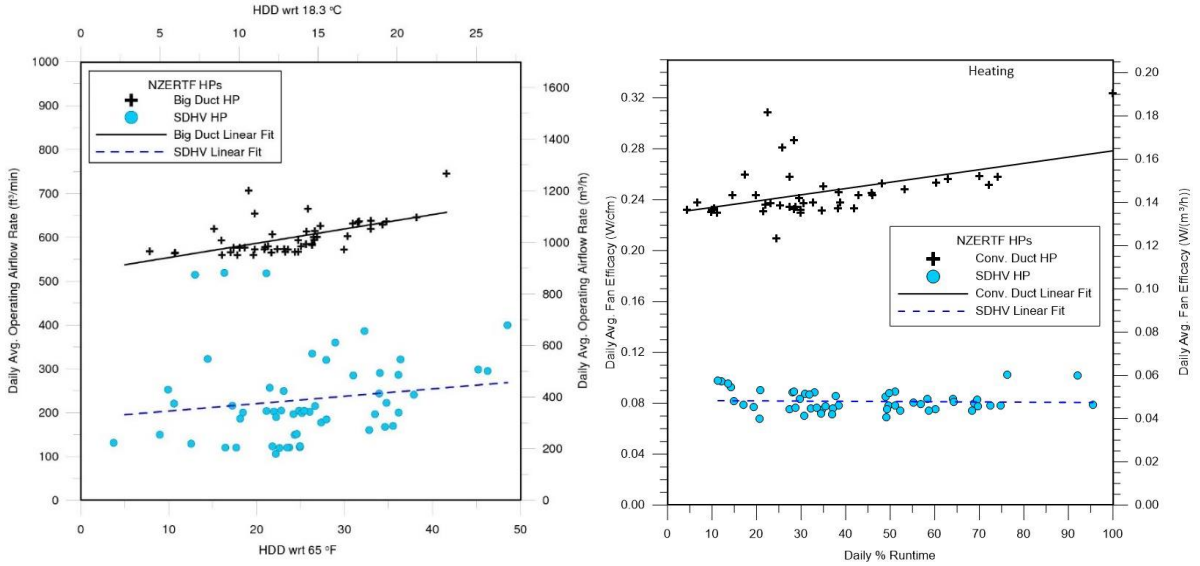

Figure 80: Heating daily average operating airflow rates.(left) and Heating average indoor blower efficacy (W/[unit volume flow]) (right).

Unlike the cooling mode, the SDHV circulated an average of (3.6 ± 0.8) fewer air changes (Figure 81 left) while operating for about the same number of hours per day (Figure 81 right). The SDHV had a higher supply of air delivery temperature (Figure 82 left) and a higher average temperature change across the air handler ([13.9 ± 1.6]°C [(25 ± 2.8)°F] higher, Figure 82 right). House average return air temperatures were equivalent (Figure 83). The SDHV system was delivering higher energy supply air to meet the load at a lower airflow rate.

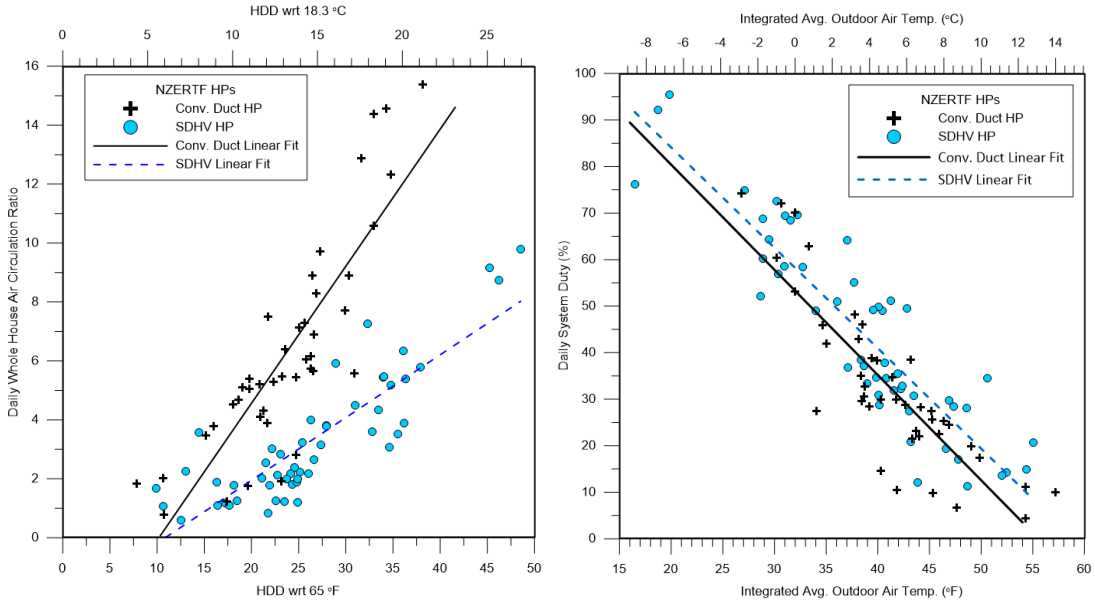

Figure 81: Daily heating air circulation ratio (left) and Heating daily system percent duty (right)

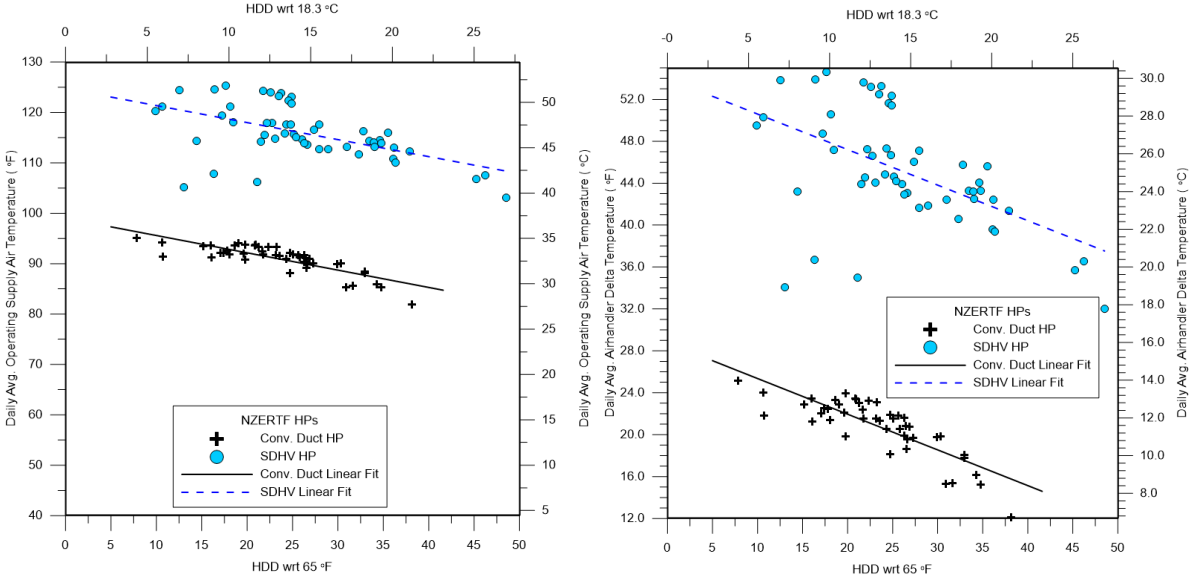

Figure 82: Heating average operating supply air temperatures (left) and Heating average operating indoor unit air temperature change (right)

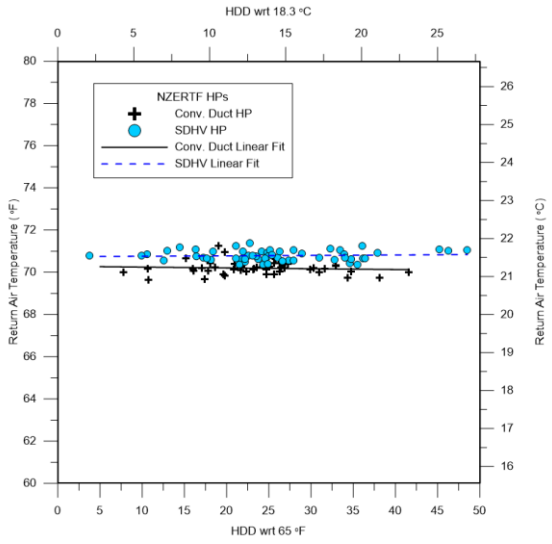

Figure 83: Heating daily average operating return air temperature.

7.3 Heating Standby Energy Use

Heating standby energy use for the indoor unit is shown in Figure 84 left. The SDHV indoor air handler averaged (123.0 ± 9.4) Wh less daily standby energy than the CDHP with an almost constant demand of 4 and 11 W for the SDHV and CDHP, respectively (Figure 84 right).

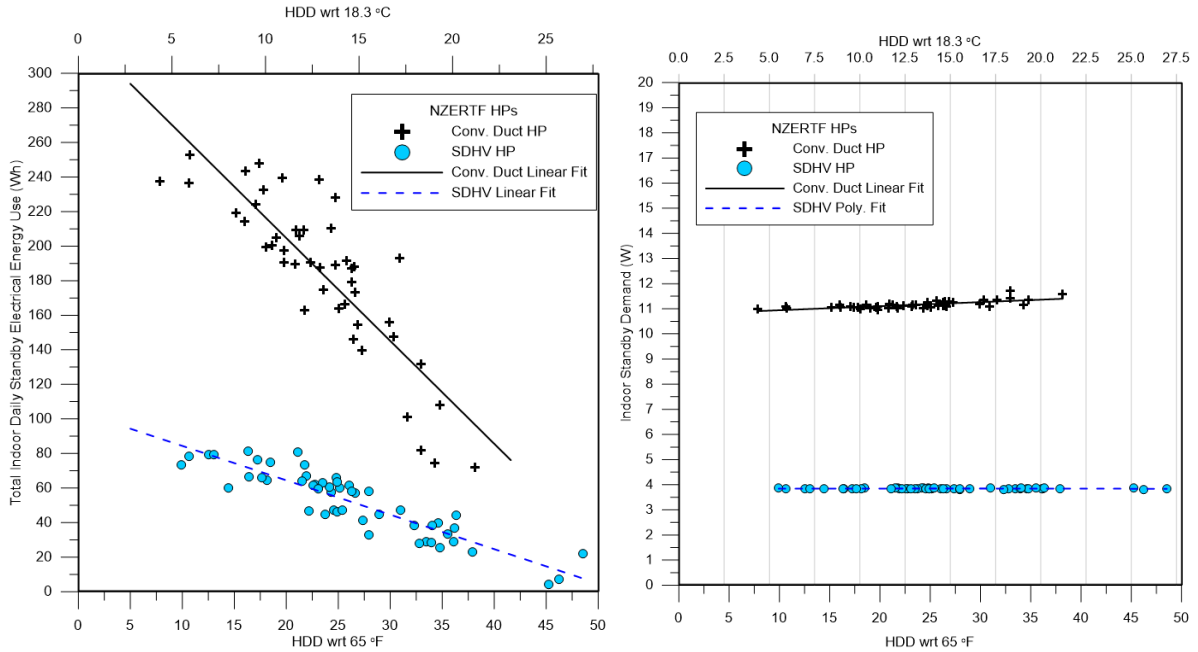

Figure 84: Heating ID unit standby energy use (left) and heating ID unit standby power demand (right)

The SDHV outdoor unit standby energy use (Figure 85 left) did not have a constant demand with HDD but increased at the colder outdoor temperatures (Figure 85 right) due to electric resistance compressor sump heating. The decrease in CDHP energy use at high HDD was due to less standby time. The CDHP has an external electric resistance sump heater, but it was never energized during the heating season.

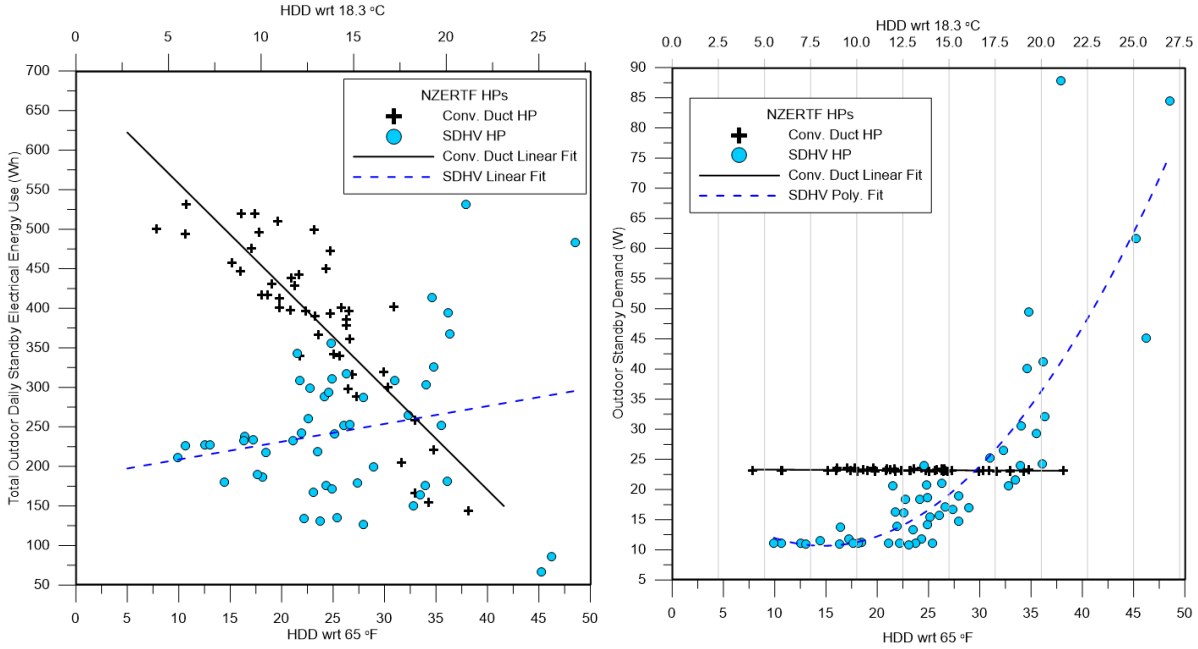

Figure 85: Heating OD unit standby energy use (left) and heating OD unit standby power demand (right)

The overall result for total standby energy use is shown in Figure 86. The SDHV system consumed an average of (255.5 ± 46.0) Wh less standby energy daily than the CDHP.

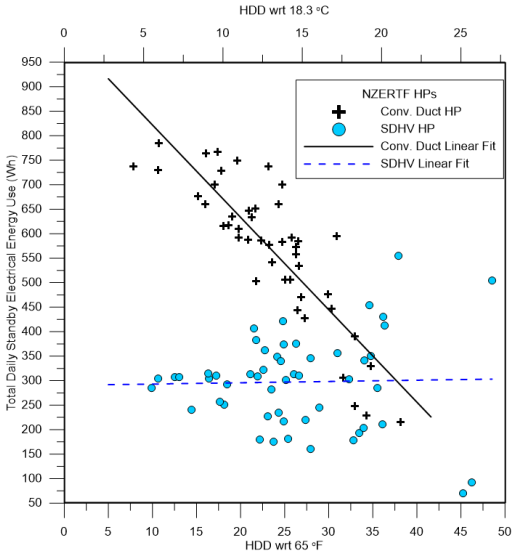

Figure 86: Heating system standby total energy use.

7.4 Heating Efficiency

Figure 87 left shows the daily average heating COP as a function of the HDD. High-supply air temperatures were produced by the SDHV system, which reduce the "cold blow" effect that many people complain about when a new HP is retrofitted to a hot air furnace system (Bouchelle et al, 2000). These high temperatures were meant to reduce the cold blow effect, but instead they directly affected the heating COP. As a remedy to the excessively high supply air temperatures, new firmware was uploaded to the SDHV system controller, which produced significant changes in heating efficiency and supply air temperature (Figure 87 right). The CDHP had an average daily heating COP of (1.9 ± 0.4) compared with (1.8 ± 0.9) for the SDHV with original firmware. The CDHP average heating COP was statistically equal to that of the SDHV that runs the original firmware. The SDHV system with the new firmware averaged a heating COP of (2.5 ± 1.1). The heating COP of the new firmware SDHV was (0.6 ± 0.18) higher than the CDHP over comparable temperature conditions. Further testing of the new firmware is needed to reduce its standard error and improve the comparison with the CDHP.

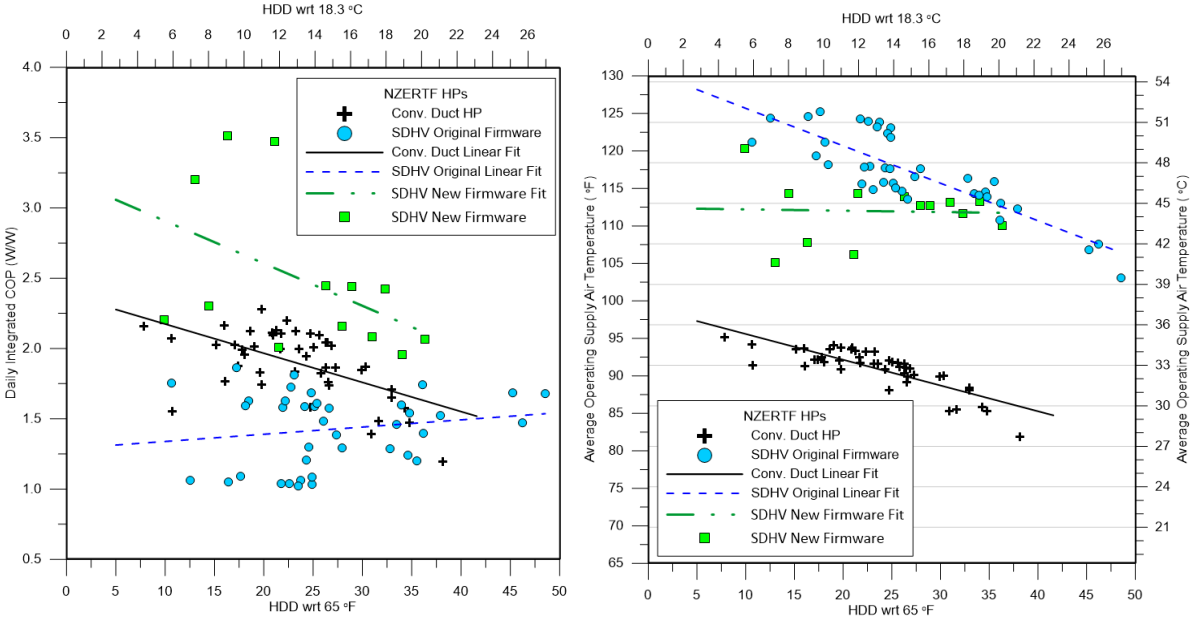

Figure 87: Heating COP vs. HDD with original and new firmware (left) and heating supply air temperatures with original and new firmware (right)

Figure 88 shows the daily average heating COP of the two systems as a function of outdoor air dry-bulb temperature.

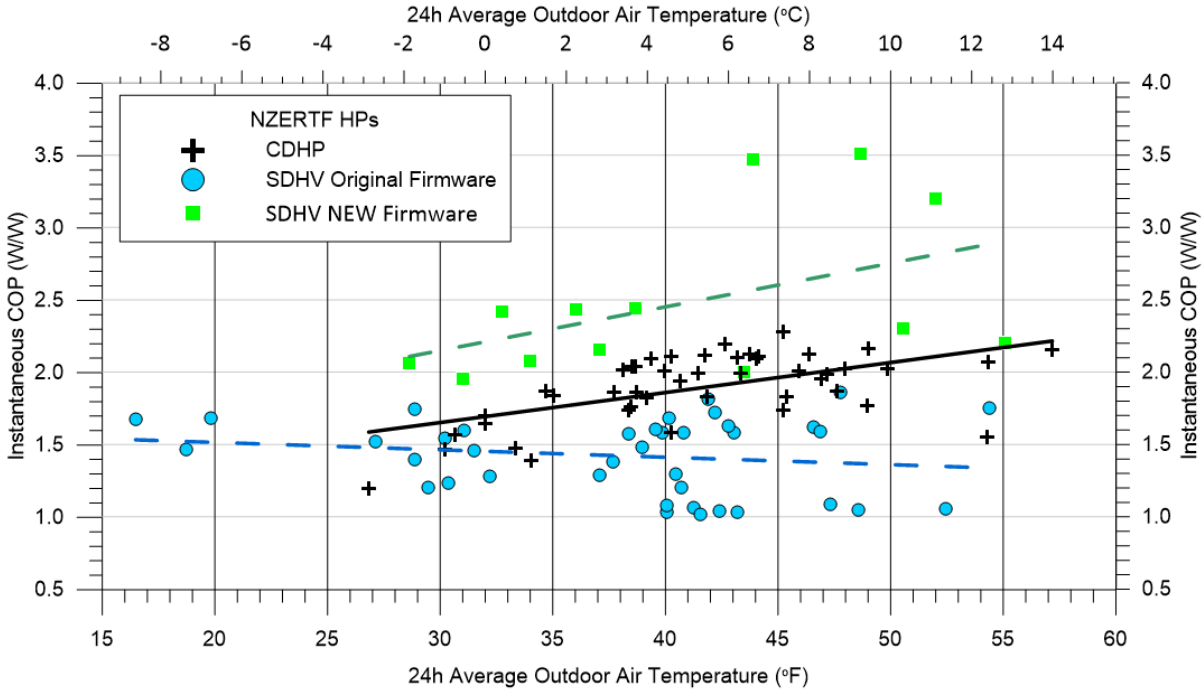

Figure 88: Heating COP as a function of daily average outdoor air temperature.

This figure illustrates the large improvement in heating COP due to a change in the SDHV firmware. This figure also shows that the SDHV system experienced the coldest heating days during the test period, but this did not reduce its COP as compared with the CDHP.

7.4.1 Defrost Performance

The conventional system and the SDHV system performed defrost operations to remove the buildup of frost on the outdoor heat exchangers. The CDHP defrost control was set to defrost every 90 minutes, as needed. Observations of the CDHP defrost showed that the defrost operation would occur every 90 minutes of accumulated compressor run time when the outdoor temperature was below 35°F. The SDHV system takes a different approach to the traditional reverse cycle defrost. When it senses frosting conditions, the unit employs hot-gas bypass to the outdoor heat exchanger while allowing the indoor unit to remain operating. If the control detects that the defrost parameter is not resolved by hot-gas bypass, then the system resorts to a full reverse-cycle defrost. The SDHV system uses no auxiliary electrical resistive heating elements in the air stream.

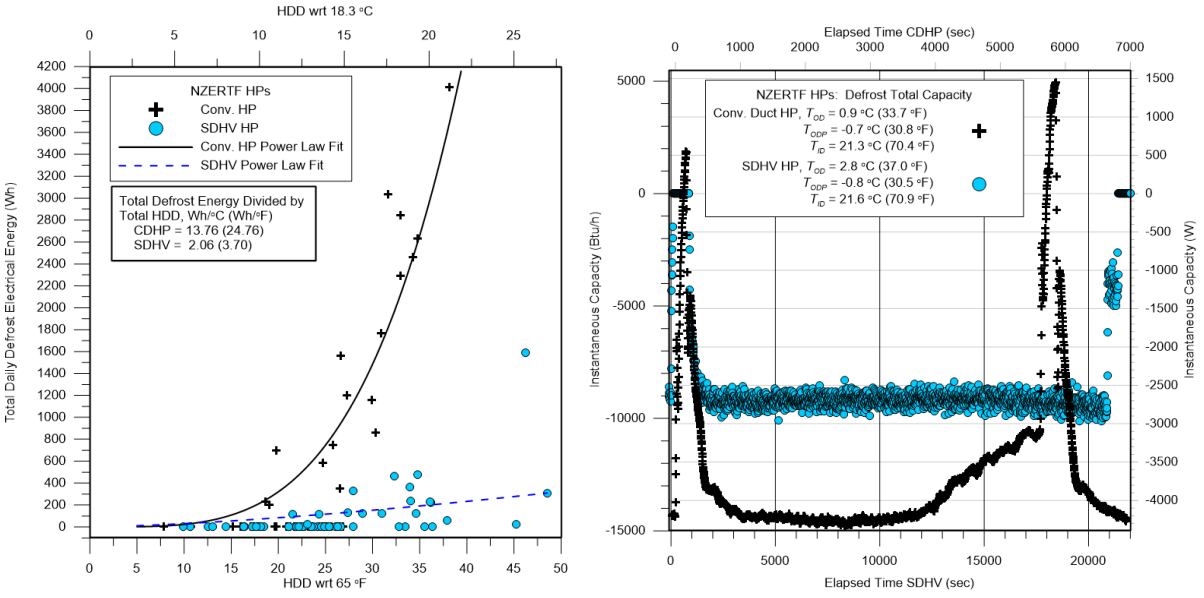

Figure 89: Heating daily defrost energy use (left) and example defrost heating capacity (right)

The SDHV system used an average of (624 ± 254) Wh less defrost energy per day than the CDHP (Figure 89 left). To demonstrate how the two systems perform defrosts, Figure 89 right shows a heating capacity plot that begins at the start of a defrost and ends at the end of a second defrost. The two systems perform a defrost, run at a steady state for a while, then defrost again. The timescales are not equivalent because the steady state run time between defrosts is very different for these examples. The top axis is the timescale for the CDHP, about 7,000 seconds (1 hour, 57 minutes), and the bottom axis is the timescale for the SDHV HP, about 22,000 seconds (6 hours, 6 minutes).

The CDHP defrost begins when the heating capacity before defrosting is 4,195 W (14,314 Btu h^{-1}). Figure 90 left shows a combined plot of heating capacity, resistive heat power, indoor (ID) blower power, and outdoor (OD) coil temperature during the CDHP defrost from 0 to 195 seconds. Heating capacity is shown as a negative value to differentiate it from cooling capacity. At the initiation of defrost, the outdoor fan is turned off as the refrigerant reversing valve is energized, like in cooling mode operation. About 15 seconds pass before electric resistive heat engages (5,000 W), and the indoor blower ramps up airflow rate; thus, the blower power demand moves up to approximately 400 W. A few seconds after the resistive heat turns on and the indoor blower ramps up, the outdoor coil temperature starts to increase. The outdoor coil temperature reaches a peak of 26.8°C (80.2°F) before the reversing valve switches back to heating mode (170 seconds). Resistive heat remains energized after the reversing valve switches to heating mode until turning off at 195 seconds as normal heating resumes. The 5 kW nominal supplementary resistive heat is not enough to prevent cold blow during defrost; the heating capacity goes positive, indicating a cooling effect upon the house, from 105 to 175 seconds. This defrost consumed 278 Wh of electrical energy.

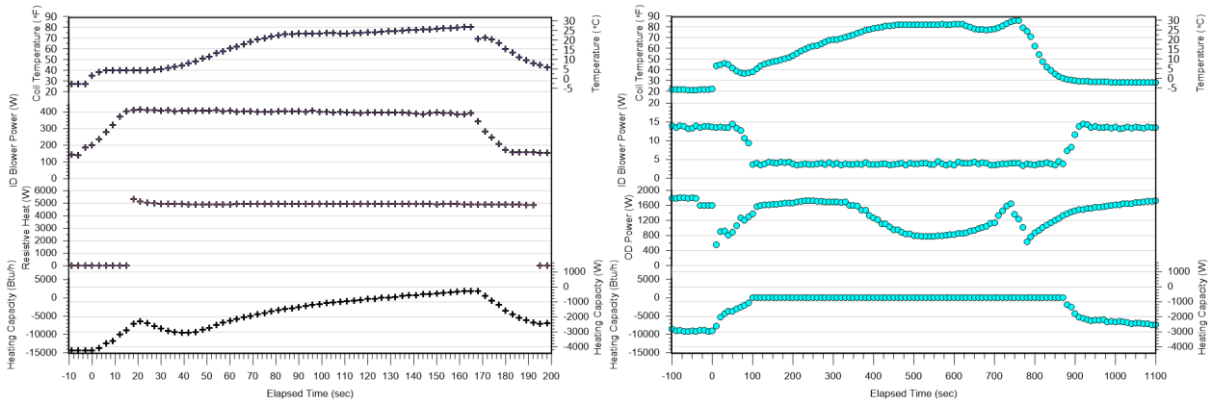

Figure 90: CDHP defrost characteristics (left) and SDHV defrost characteristics (right)

The SDHV defrost begins when the heating capacity before defrosting is 2,696 W (9,200 Btu h^{-1}). Figure 90 right shows a combined plot of heating capacity, resistive heat power, ID blower power, and OD coil temperature during the SDHV defrost from 0 to 760 seconds. Heating capacity is shown as a negative value to differentiate it from cooling capacity. At the initiation of defrost, the outdoor fan is turned off as the refrigerant reversing valve is energized, like in cooling mode operation. After about 100 seconds, the indoor blower ramps all the way off, and the outdoor coil temperature starts to increase. The outdoor coil temperature reaches a peak of 29.7°C (85.5°F) before the reversing valve switches back to heating mode (760 seconds). The cold blow effect seen for the CDHP during defrost is absent here. The heating capacity never goes positive since the indoor blower energizes at 860 seconds to resume normal heating operation. This defrost consumed 265 Wh of electrical energy.

Figure 4.52 looks at the frosting interval for both systems in more detail; heating capacities are shown as negative numbers. Before the previous defrost (not shown in the figure), the SDHV had a heating capacity of (2,700 ± 166) W ([9,215 ± 568] Btu h^{-1}) and total power demand of (1,766 ± 70) W. After defrost and once at a steady state again (Figure 4.52), the heating capacity was (2,709 ± 145) W ([9,244 ± 496] Btu h^{-1}) as power dropped to (1,695 ± 86) W while maintaining capacity.

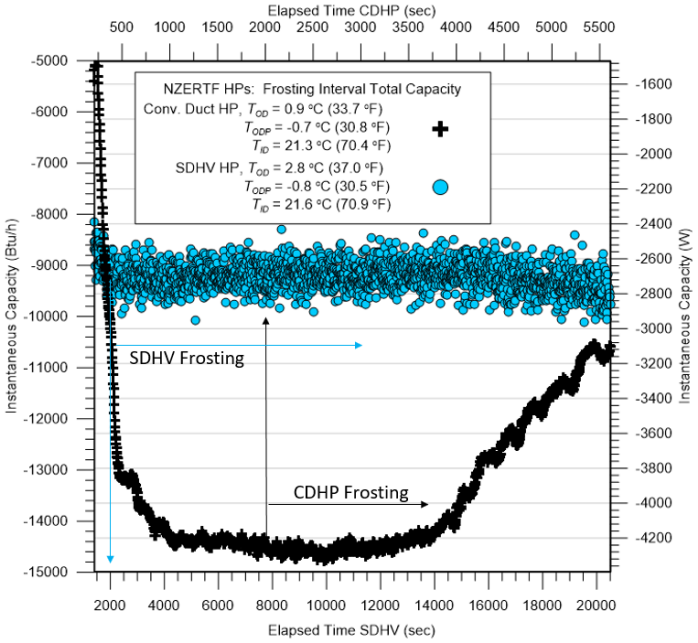

Figure 91: Frosting interval heating capacity.

During frosting (i.e., the end of defrost to the start of the next defrost), the capacity was maintained at (2,703 ± 148) W ([9,222 ± 504] Btu h^{-1}), and the power demand averaged (1,672 ± 88) W. One minute before the initiation of the next defrost, the heating capacity averaged (2,684 ± 156) W ([9,159 ± 532] Btu h^{-1}) with the total power demand averaging (1,636 ± 8) W. During frosting, the average heating capacity decreased by less than 1%, and the average total power demand decreased by 3.5%.

Before the previous defrost, the CDHP had a heating capacity of (4,194 ± 19) W ([14,310 ± 64] Btu h^{-1}) and a total power demand of (2,003 ± 424) W (Figure 52). After defrost and once at a steady state again (1,100–3,750 seconds), the heating capacity was (4,244 ± 69) W ([14,480 ± 234] Btu h^{-1}) and power demand was (2,011 ± 52) W. One minute before the initiation of the next defrost, the heating capacity averaged (3,144 ± 47) W ([10,729 ± 162] Btu h^{-1}) with the total power demand averaging (1,925 ± 10) W. During the last part of the frosting interval (3,750–5,610 seconds), the capacity dropped at an average of 36.2 W (123.4 Btu h^{-1}) each minute. The average heating capacity dropped by 26% during the frosting interval and before the next defrost began.

7.5 Conclusions of the NZERTF Field Experience

The objective of this study was to determine whether the high-velocity system could provide comparable energy use efficiency to the conventional system. The results of this study showed that the SDHV system meets the required loads and has slightly greater efficiency; the average cooling COP was (0.396 ± 0.113) higher, and the average heating COP was statistically equal. This near-equal performance was realized despite the fact that the SEER and HSPF ratings of the SDHV were 11 and 8% lower than the CDHP, respectively. New firmware was provided to improve the heating performance at the end of the heating season; this greatly improved the heating performance of the high-velocity system. The improvement was produced due to lowered condensing temperatures, which produced lower compressor power demand. Its average heating COP went from (1.8 ± 0.9) to (2.5 ± 1.1) at a 95% confidence level. The new firmware heating COP averaged (1.05 ± 0.23) higher than the old firmware over comparable temperature conditions.

The frosting and defrosting characteristics of these two systems were totally different. The SDHV avoided rapid capacity losses due to frosting by using the hot-gas bypass to reduce the frosting effect on capacity. The SDHV used no electric resistance backup heat, yet it provided comfortable conditions without cold blow during defrost. The CDHP showed a steady decrease in heating capacity during frosting with comparable drops in supply air temperature. The CDHP defrosted with a full reverse cycle while applying electric resistance heat to prevent cold blow.

Although the two systems used comparable amounts of energy during the heating season to remove frost from the outdoor heat exchanger, the SDHV frosting/defrosting controls provided a more consistent supply of air temperatures and avoided electric resistance heat installation. The better frosting defrost temperatures of the SDHV were produced at the cost of more system complexity due to the added hot-gas bypass valving.
The SDHV generally operated at very low airflow rates with total external static pressures (ESP) ranging from 37 to 63 Pa (0.15 to 0.25 in. WG). Although this ductwork was a high-pressure system designed for 2,039 m^3h^{-1} (1,200 cfm), due to its variable capacity and low airflows at low load, the system operated in the static pressure range of a well-designed conventional duct system. The CDHP operated most of the time at low compressor speeds with ESP in ranging from 50 to 125 Pa (0.2 to 0.5 in. WG). These results raise the question of whether a conventional, multispeed, or variable-speed HP with an ECM blower could work well with this kind of high-velocity duct system. Potential future work will include the investigation of a hybrid system that uses round duct trunk lines with an optimized version of the SDHV flexible take-offs and supplies. The round duct is much easier to join and seal than rectangular ducting, and less raw material is used to produce a given flow area with round duct.

7.6 NIST NZERTF Future Research and Investigations

The net-zero home on the NIST campus provides a unique opportunity to test new appliances, HVAC systems, and all associated controls/strategies. Several different aspects of low-energy homes will be investigated in the coming years. Some of these studies will include:

- air-distribution and HVAC zoning for low energy homes,
- a collaboration with ORNL to verify aspects of the Energy Plus software using NZERTF;
- performance testing of a ground-source CO_2-based air-conditioning system;
- performance testing of a combined HP and water-heating appliance;
- an indoor air quality collaboration and study with Boston University and NTNU/SINTEF to develop and exercise coupled residential building models;
- performance testing of a residential CO_2 HP-based water heating system; and
- CONTAM on a Chip, which is hardware implementation, integration into HVAC system.

8 Conclusions prototype heat pumps for nZEB

Prototype heat pumps, which have been developed and lab and/or field tested in IEA HPT Annex 49 refer to highly integrated units, either in the sense that multiple building service functions can be provide by the prototype, or in the sense of a compact design, which is even located directly in the building façade and can be operated autarkic as in the case of the Austrian development.
Furthermore, both personal services like in the case of the Roving Comforter (RoCo) by the University of Maryland providing cool air for the occupant's comfort or a room-wise space cooling by the façade integrated unit are developed.
On the other hand the long-term development of central highly integrated unit with multi-functional use, which has been a dedicated development for nZEB application, has passed field tests and is either on the market or undergoing a value engineering for cost reduction.
Most of the prototypes developed are also dedicated to cooling operation, a building functions with growing demand in the coming decades also in central and even northern Europe. In fact there is also a kind of shift in building load. By the high performance building envelope in nZEB space heating load are significantly reduced and DHW load area in the same range, in larger building even higher. Moreover, due to rising outdoor air temperatures and increasing indoor comfort requirement, space cooling will get more promninent also in residential application. Swiss testing of solar unglazed absorber during nighttime operation is hence also intended to integrate a highly efficient freecooling or a back-up recooling function in system configurations with source storage, which are currently only used for space heating and DHW application. In the southern state of the USA, though, not only space cooling, but also dehumidification has always been a necessity.
The high performance building envelope of nZEB enables low loads and thereby compact and highly integrated designs, which are well adapted. These designs appeared the first time as so-called compact units in the beginning of the years 2000 as heating systems for passive houses and may experience a renaissance. Currently, there is also a challenge of the worldwide initiative Mission Innovation to develop compact heating and cooling as so-called comfort and climate box. Compact designs have the advantage of little space demand. The control system can be internally optimised to the components. The use of the same component for multiple purpose, e.g. in space heating and cooling mode, and thereby longer running times justifies higher investment in high quality components, which may also have better performance values. Moreover, the vicinity of component in the unit facilitate the recovery of waste energy for other functions, either directly in simultaneous operation of by integrated storages.
A further features has been added to the design requirements of these units, which results from the renewable production on-site in nZEB and refers to the smartness of the units. Thus, using self-generated electricity for the operation may have cost benefits and may contribute to grid supportive operation, if energy flexibility can be provided by the unit. However, as a results of the evaluation of the façade integrated COOLSKIN unit, the battery is still too expensive and not economic. In fact, at current market conditions, it is hard to amortise investment into demand response capability, e.g. by larger thermal or storage or electrical battery integration.

9 Acknowledgment

IEA HPT Annex 49 is a co-operative research project on heat pump application in nearly Zero Energy Buildings in the framework of the Heat Pumping Technologies (HPT) Technology Collaboration Programme (TCP) of the International Energy Agency (IEA). This report is based on the contributions of all participants in the Annex 49 and the constructive and co-operative discussions during the project as well as the contributed results are highly appreciated.

The support and funding of the IEA HPT Annex 49 by the Swiss Federal Office of Energy (SFOE) is highly appreciated and gratitude is expressed to the programme managers of the SFOE heat pump research Dr. Carina Alles and Stephan Renz for advice and support in the IEA HPT Annex 49 and the Swiss national contributions.

The project COOLSKIN (FFG Project-Nr. 848871) was funded by the Austrian Climate and Energy Fund and was carried out as part of the Energy Research Programme 2014.

For the IHP section: Jeff Munk, Anthony Gehl, Ayyoub Momen, Bo Shen, Moonis Ally, Keith Rice (ret.), and Ed Vineyard (ret.) of ORNL; and Isaac Mahderekal of Intellichoice Energy.

For the Personal Cooling system section: Mohammad Heidarinejad, Daniel Alejandro Dalgo, Nicholas W. Mattise, Shengwei Zhu, Daniel Dalgo, and Shinsuke Kato of University of Maryland. We also gratefully acknowledge the support from the sponsors of the Center for Environmental Energy Engineering (CEEE) and Center for Sustainability in the Built Environment (City@UMD) at the University of Maryland.

For the NZERTF section: We would like to acknowledge the support and hard work of our Engineering Technician staff at the National Institute of Standards and Technology in Gaithersburg, Maryland, who were invaluable in obtaining the data used in this report. We thank Mr. Arthur Ellison, Mr. John Wamsley, and Mr. Luis Luyo.

The authors gratefully acknowledge Antonio Bouza of DOE BTO for his support of the US participation in IEA HPT Annex 49, the assembly of this report, and the ORNL technical activities summarized herein under Contract No. DE-AC05-00OR22725 with UT-Battelle LLC.

10 Abbreviations

Abbreviation	Meaning	Remark
AC	Alternating Current	
ACCA	Air conditioning Contractors of America	
A-HP	Air heat pump	
AHRI	US Air-Conditioning, Heating, and Refrigeration Institute	
AHU	Air handling unit	
ANOVA	Analysis of variance	
ANSI	American National Standards Institute	
AS	Air source	
ASHP	Air source heat pump	
ASHRAE	American society of heating refrigerating and air-conditioning engineers	
BIPV	Building integrated Photovoltaic	
BMS	Building Management systems	
BPM	Beats per minute	
BTO	Building technology office	Office of DOE
CDD	Cooling Degree Days	
CDHP	Conventionally ducted heat pump	
CEEE	Center of Environmental Energy Engineering	University of Maryland
CENG	compressed expanded natural graphite	
CFD	Computational fluid dynamics	
CM	Climate Master	
CND	Condenser	
COP	Coefficient Of Performance	
DAS	Data acquisition systems	
DC	Direct Current	
DH	dehumidification	
DHW	Domestic hot water	
DOE	US Department of Energy	
DS	Desuperheater	
DWH	Dedicated water heating	
ECM	electronically commutated motors	
EER	Energy Efficiency Ratio	
EF	Energy factor	
ESP	External static pressure	
EWT	entering water temperature	
GHP	Gas engine-driven heat pumps	
GHX	Ground heat exchanger	
GS	Ground source	
GW	Ground water	
HDD	Heat degree days	
HP	Heat pump	
HPT	Heat Pumping Technologies	IEA TCP
HPWH	heat pump water heater	
HS	Human Subject	
HSPF	Heating seasonal performance factor	
HVAC	Heating, Ventilation and Air-conditioning	
HW	Hot water	
HX	Heat exchanger	
ID	identification	
ID	indoor	
IEA	International Energy Agency	
IHP	Integrated Heat Pump	
ISO	International Standardisation Organisation	

Abbreviation	Meaning	Remark
IWT	Institute of thermal engineering	Institut für Wärmetechnik, TU Graz
MD	Maryland	
MPC	Model predictive control	
MPP	Maximum power point	
NIST	National Institute of Standards and Technology	
NREL	National Renewable Energy Laboratory	
nZE	nearly Zero Energy	
nZEB	nearly Zero Energy Building	
NZEB	Net Zero Energy Building	
NZERTF	Net Zero Energy Residential Testing Facility	
OAT	Outdoor air temperature	
OD	Outdoor air	
OD	outdoor	
ORNL	Oak Ridge National Laboratory	
PCHX	Phase Change Heat Exchanger	
PCM	Phase Change Material	
PE	Primary energy	
PID	Proportional Integral Differential	
PPD	predicted percent dissatisfied	
PV	Photovoltaic	
PV	Photovoltaic	
PV/T	photovoltaic/thermal	
PV/T	photovoltaic/thermal	
PVC	PV control	
RE	Renewable energy	
RH	Relative Humidity	
RoCo	Roving Comforter	
RTD	resistance temperature detectors	
RTU	rooftop HP unit	
SC	Space cooling	
SCHV	Small duct high velocity	
SCOP	Seasonal Coefficient of Performance	
SCR	fraction of PV self-consumption	
SEER	Seasonal Energy Efficiency Ratio	
SIA	Swiss Society of Engineers and Architects	Schweizerischer Ingenieur- und Architektenverein
SPF	Seasonal performance factor	
SSR	solar fraction (self-sufficiency ratio)	
SWG	Southwest Gas Corp	
TABS	Thermally activated building system	
TCF	technology commercialization fund	
TN	Tennessee	
TOU	time-of-use	
VCC	vapor compression cycle	
VS	Variable Speed	
VSD	Variable Speed Drive	
WSHP	Water source heat pump	

11 Literature

Austrian Standards Institute. 2006. "ÖNORM EN ISO 7730:2005."

Dott, R., T. Afjei, A. Genkinger, A. Dalibard, D. Carbonell, R. Consul, A. Heinz, M. Haller, A. Witzig, and J. Facão. 2013. Models of sub-components and validation for the IEA SHC Task 44/HPP Annex 38 Part C: heat pump models. International Energy Agency, A technical report of subtask C Deliverable C 2.

Heimrath, R., W. Lerch, T. Mach, T. Ramschak, and F. Fink. 2018. Hohe solare Deckungsgrade durch thermisch aktivierte Bauteile im urbanen Umfeld - solSPONGEhigh; Projektbericht im Rahmen des Programms Haus der Zukunft, im Auftrag des Bundesministeriums für Verkehr, Innovation und Technologie. Berichte aus Energie- und Umweltforschung 20/2018.

Hengel, F., A. Heinz, and R. Rieberer. 2014. "ANALYSIS OF AN AIR SOURCE HEAT PUMP SYSTEM WITH SPEED CONTROLLED COMPRESSOR AND VAPOR INJECTION." 11th IEA Heat Pump Conference. 1-15.

Meteotest. 2015. "Meteonorm, Global Meteorological Database for Engineers, Planner and Educations, Software and Data on CD-Rom." Bern, Schweiz.

SIA. 2015. SIA 2024:2015, Raumnutzungsdaten für Energie- und Gebäudetechnik. Swiss Society of Engineers and Architects.

Solar Energy Lab. 2017. "A Transient System Simulation Program - Trnsys, Version 17.2.004." University of Wisconsin.

TRNSYS 17. 2014. "TRNSYS 17: a Transient System Simulation Program, Volume 4: Mathematical Reference." Solar Energy Laboratory, University of Wisconsin-Madison.

Baxter, V., T. Grubbs, R. Campbell, W. V. Payne, and R. Radermacher, 2018. "State-of-the-Art Analysis of Nearly Zero Energy Buildings: Country report IEA HPT Annex 49 Task 1 USA," ORNL/TM-2018/981, October.

The National Institute of Building Sciences, A Common Definition for Zero Energy Buildings, U.S. Department of Energy, DOE/EE-1247, September 2015.

New Buildings Institute, "2016 List of Zero Net Energy Buildings," 2016. [Online]. Available: https://newbuildings.org/wp-content/uploads/2016/10/GTZ_2016_List.pdf.

United States Environmental Protection Agency, "ENERGY STAR," [Online]. Available: http://www.energystar.gov. [Accessed December 2017].

U.S. Energy Star Homes Program, "ENERGY STAR Qualified Homes, Version 3 Savings & Cost Estimate summary," June 2013. [Online]. Available: http://energystar.gov/ia/partners/bldrs_lenders_raters/downloads/EstimatedCostandSavings.pdf?1665-0032. [Accessed December 2017].

U.S. ENERGY STAR Program, "About ENERGY STAR," [Online]. Available: https://www.energystar.gov/about/origins_mission/energy_star_overview/about_energy_star_residential_sector. [Accessed December 2017].

U.S. ENERGY STAR Program, "2016 ENERGY STAR Certified New Homes Market Share," [Online]. Available: https://www.energystar.gov/newhomes/2016_energy_star_certified_new_homes_market_share. [Accessed December 2017].

California Public Utilities Commission, "Zero Net Energy - Action Plan: Commercial Building Sector 2010-2012".

Deru, M., K. Field, D. Studer, K. Benne, B. Griffith, P. Torcellini, B. Liu, M. Halverson, D. Winiarski, M. Yazdanian, J. Huang, D. Crawley. U.S. Department of Energy Commercial Reference Building Models of the National Building Stock. NREL; 2011.

ASHRAE Standard 90.1-2019: Energy Standard for Buildings except Low-Rise Residential Buildings, American Society of Heating, Refrigeration Air Conditioning Engineers, Inc., Atlanta, GA, 2004.

ASHRAE Standard 169-2006: Weather Data for Building Design Standards, American Society of Heating, Refrigerating, and air-conditioning Engineers, Inc., Atlanta, GA, 2006.

Du, Y., Battery powered portable vapor compression cycle system with PCM condenser, Mechanical Engineering, University of Maryland, 2016.

Heidarinejad, M., D. Alejandro Dalgo, N. W. Mattise, and J. Srebric, Personalized cooling as an energy efficiency technology for city energy footprint reduction, Journal of Cleaner Production, Volume 171, 2018, Pages 491-505, ISSN 0959-6526

Heidarinejad, M., M. Dahlhausen, S. McMahon, C. Pyke, and J. Srebric, Cluster analysis of simulated energy use for LEED certified U.S. office buildings, Energy Buildings, 85 (0) (2014) 86-97.

Zhu, S., Dalgo, D., Srebric, J., and Kato, S. 2017. "Cooling Efficiency of a Spot-type Personalized Ventilation," Building and Environment, 121(2017): 35-48.

Wemhoener, C. (Ed.). 2016. IEA HPT Annex 40 - Heat pump concepts for nearly Zero Energy Buildings, Final report Part 3, Report no. HPP-AN40-3, IEA Heat Pumping Technologies TCP, Borås.

Murphy, R.W., V. D. Baxter, C. K. Rice, and W. G. Craddick. 2007a. "Ground-Source Integrated Heat Pump for Near Zero Energy Houses: Technology Status Report." ORNL/TM-2007/177, December.

Murphy, R.W., V. D. Baxter, C. K. Rice, and W. G. Craddick. 2007b. "Air-Source Integrated Heat Pump for Near Zero Energy Houses: Technology Status Report." ORNL/TM-2007/112, July.

Baxter, V., J. Munk, and A. Gehl, 2016. "Field Demonstration of Ground-Source Integrated Heat Pump - Final Report. ORNL/TM-2016/474, September.

Air-conditioning, Heating, and Refrigeration Institute, 1998, ANSI/AHRI/ASHRAE/ISO Standard 13256-1, "Water-to-Air and Brine-to-Air Heat Pumps - Testing and Rating for Performance."

ClimateMaster, 2019, Trilogy Q-mode (QE) Series IOM; Installation, Operation, and Maintenance Instructions, October.

AHRI, Performance Rating of Unitary Air-Conditioning and Air-Source Heat Pump Equipment, 2017, Air-Conditioning Heating and Refrigeration Institute, 2111 Wilson Blvd., Suite 500,Arlington, VA 22201 USA. http://www.ahrinet.org/App_Content/ahri/files/STANDARDS/AHRI/AHRI_Standard_210-240_2017_add1.pdf

Battocletti, E. C. and W. E. Glassley, 2013. "Measuring the Costs and Benefits of Nationwide Geothermal Heat Pump Deployment," prepared for the USDOE Geothermal Technologies Program, February.

Ingram website: http://ingramswaterandair.com/commercial-units-commercial-package-heat-pump-c-45_170_173.html, accessed August 29, 2016

Vineyard, E., R. Wetherington, M. Bhandari, and J. Munk, 2015. "Field Demonstration of Gas Heat Pump Rooftop Unit with Waste Heat Recovery for Water Heating." Oak Ridge National Laboratory, September.

Cunningham, R., 2015. "In the Loop," Rural Electric Magazine October 5 web edition, http://remagazine.coop/in-the-loop/, accessed August 31, 2016.

Baxter, V., V. Payne, J. Ling, and R. Radermacher, 2015. "Heat Pump Concepts for nZEB - Technology developments, design tools, and testing of heat pump systems for nZEB in the USA: Country report IEA HPT Annex 40 Task 2, Task 3 and Task 4 of the USA," ORNL/TM-2015/560, December.

Baxter, V., C. K. Rice, J. Munk, M. Ally, and B. Shen, 2015. "Advanced Variable Speed Air Source Integrated Heat Pump (AS-IHP) Development- Final Report," ORNL/TM-215/525, September.

Baxter, V., C. K. Rice, J. Munk, M. Ally, B. Shen, and R. B. Uselton, 2017. "Air-Source Integrated Heat Pump System Development - Final Report," ORNL/TM-2017/305, July.

DOE/BTO Building America Program 2013. "Website for Building America Analysis Spreadsheets: DHW Event Schedule Generator," http://energy.gov/eere/buildings/building-america-analysis-spreadsheets (last accessed on September 24, 2015).

Hendron, R. and C. Engebrecht 2010. "Building America House Simulation Protocols," NREL REPORT: TP-550-49426, October.

Munk, J. D., C. Halford, and R. Jackson, 2013. "Component and System Level Research of Variable-Capacity Heat Pumps," ORNL/TM-2013/36, June.

ASHRAE, 2013. ASHRAE Handbook: Fundamentals.

National Oceanic and Atmospheric Administration (NOAA) NOAA Online Weather Data. Accessed August 3, 2015, and August 14, 2015. http://w2.weather.gov/climate/xmacis.php?wfo=mrx.

Uselton, R., 2014. Dedicated Dehumidifier and Water Heater, United States Patent 8,689,574 B2, April 1.

Lennox Industries Inc., 2014. "Lennox XP-25 2 to 5 Ton Heat Pump Product Specifications," Bulletin 210659, May.

Munk, J. D., V. D. Baxter, A. C. Gehl, M. R. Ally, B. Shen, C. K. Rice, and R. B. Uselton, 2017. "Prototype Air-Source Integrated Heat Pump Field Evaluation Results." Paper O.1.4.1 in Proceedings of the 12th IEA Heat Pump Conference, Rotterdam, The Netherlands, May 15-18, 2017.

NOAA. NOAA Online Weather Data. Accessed December 22, 2016. http://w2.weather.gov/climate/xmacis.php?wfo=mrx.

Zaltash, A., Vineyard, E.A., Linkous, R.L., Geoghegan. P., Wetherington, R., Mahderekal, I., 2008. "Laboratory evaluation: Performance of a 10 RT gas engine-driven heat pump (GHP)", ASHRAE Transactions, Vol 213.

Nextaire, no date. Multi-zone gas heat pump technical specifications Model 132.6.00.P.H.A.

Momen, A., A. Abu-Heiba, and E. A. Vineyard, 2015. "Multi-Function Gas Fired Heat Pump," ORNL/TM-2015/701, November.

US Department of Energy, 2019. "Technology Commercialization Fund." https://www.energy.gov/technologytransitions/services/technology-commercialization-fund (accessed 8-November.

Kim, H., K. Nguyen, A. McGuinness, and T.V. Dai, 2019, Characterization of residential air distribution system performance for thermal comfort, NIST GCR 19-021, National Institute of Standards and Technology. https://doi.org/10.6028/NIST.GCR.19-021

Fanney, A. H., W. V. Payne, T. Ullah, L. Ng, M. Boyd, F. Omar, M. Davis, H. Skye, B. Dougherty, B. Polidoro, W. Healy, and E. Pettit, 2015, Net-Zero and Beyond! Design and Performance of NIST's Net-Zero Energy Residential Test Facility, Energy and Buildings, 101, 95-109. https://www.sciencedirect.com/science/article/pii/S0378778815003655

ASHRAE Std. 62.2-2010, Ventilation and Acceptable Indoor Air Quality in Residential Buildings- (ANSI Approved), American Society of Heating, Refrigerating and Air-Conditioning Engineers, 1791 Tullie Circle, N.E., Atlanta, GA 30329.

Building America Program, 2019, Building America Publication and Product Library, https://www1.eere.energy.gov/library/default.aspx?page=2&spid=2.

Poerschke, A. and A. Rudd, 2016, Performance analysis of a modular small-diameter air distribution system. https://www.osti.gov/biblio/1240364

Besant, R. W. and Y. Asiedu, 2000, Sizing and balancing air duct systems, ASHRAE Journal. https://www.semanticscholar.org/paper/Sizing-and-balancing-air-duct-systems-Besant-Asiedu/56fe8e48450bb084dd00518246bf09d7d7d1586c.

Tsal, R. J., H.F. Behls, and R. Mangel, 1988, T-Method duct design, part I: optimization theory, ASHRAE Transactions, Vol. 94-2, Ottawa.

Caldas, L. G. and L.K. Norford, 2003, Genetic algorithms for optimization of building envelopes and the design and control of HVAC systems, ASME Transactions, Vol. 125, 343-51. https://doi.org/10.1115/1.1591803

Jorens, S., I. Verhaert, and K. Sorensen, 2018, Design optimization of air distribution systems in non-residential buildings, Energy & Bldgs., 175, 48-56. https://doi.org/10.1016/j.enbuild.2018.07.018

Martin, E., Withers, C., McIlvaine, J., Chasar, D., and Beal, D. 2018, Evaluating Moisture Control of Variable Capacity Heat Pumps in Mechanically Ventilated, Low-Load Homes in Climate Zone 2A, Cocoa, FL; Florida Solar Energy Center (FSEC). DOE/EE-1702. https://www.osti.gov/biblio/1421385-evaluating-moisture-control-variable-capacity-heat-pumps-mechanically-ventilated-low-load-homes-climate-zone .

Balke, Elizabeth, Gregory Nellis, Sanford Klein, Harrison Skye, Vance Payne and Tania Ullah, 2018 Detailed energy model of the National Institute of Standards and Technology Net-Zero Energy Residential Test Facility: Development, modification, and validation, Science and Technology for the Built Environment, 24:7, 700-713. https://doi.org/10.1080/23744731.2017.1381828

ACCA, 2012a, Manual J: Residential Load Calculation, 8th Edition, Version 2, Air Conditioning Contractors of America, 2800 Shirlington Rd, Suite 300, Arlington, VA USA 22206.

ACCA, 2012b, Manual D: Residential Duct Systems, 2nd Edition, Air Conditioning Contractors of America, 2800 Shirlington Rd, Suite 300, Arlington, VA USA 22206.

Cummings, J. B., and C. R. Withers Jr., 2014, Making the Case for Oversizing Variable-Capacity Heat Pumps, Florida Solar Energy Center, FSEC-PF-459-14, presented at 2014

ACEEE Summer Study on Energy Efficiency in Buildings. http://fsec.ucf.edu/en/publications/pdf/FSEC-PF-459-14.pdf.

Shirey III, D. B., H.I. Henderson, and R.A. Raustad, 2006, Understanding the dehumidification performance of air-conditioning equipment at part-load conditions, FSEC-CR-1537-05, Florida Solar Energy Center, DOE/NETL Proj. No. DE-FC26-01NT41253. https://doi.org/10.2172/881342

Davis, M., W.M. Healy, M. Boyd, L.C. Ng, W.V. Payne, H.M. Skye, and T. Ullah, 2014, Monitoring Techniques for the Net-Zero Energy Residential Test Facility, NIST Technical Note 1854. https://doi.org/10.6028/NIST.TN.1854.

Bouchelle, M. P., D.S. Parker, M.T. Anello, and K.M. Richardson, 2000, Factors influencing space heat and heat pump efficiency from a large-scale residential monitoring study, Proceedings of 2000 summer study on energy efficiency in buildings, ACEEE. http://www.fsec.ucf.edu/en/publications/html/FSEC-PF-362-01/

www.heatpumpingtechnologies.org

Heat Pump Centre
c/o RISE - Research Institutes of Sweden
PO Box 857
SE-501 15 BORÅS
Sweden
Tel: +46 10 516 5512
E-mail: hpc@heatpumpcentre.org

www.heatpumpingtechnologies.org

Report no. HPT-AN49-5